Kinetic Analysis of Human DNA Ligase III

by

Justin R. McNally

A dissertation submitted in partial fulfillment
of the requirements for the degree of
Doctor of Philosophy
(Biological Chemistry)
in the University of Michigan
2019

Doctoral Committee:

Associate Professor Patrick J. O'Brien, Chair
Associate Professor Bruce A. Palfey
Associate Professor JoAnn M. Sekiguchi
Associate Professor Raymond C. Trievel
Professor Thomas E. Wilson

Justin R. McNally

jrmcnall@umich.edu

ORCID iD: 0000-0003-2694-2410

Table of Contents

List of Tables

List of Figures

Abstract

DNA ligases catalyze the final step in DNA replication, repair and recombination pathways using a conserved three-step mechanism to generate a single phosphodiester bond. Humans have three *LIG* genes that encode the DNA ligase proteins; LIG1, LIG3 and LIG4. In the nucleus, LIG1 and LIG4 repair single- and double-strand DNA breaks, respectively. LIG3 repairs both single- and double-strand DNA breaks in mitochondria and the nucleus. In the mitochondria, LIG3 performs all the ligation events required for organellar viability. In the nucleus, LIG3 has been implicated in the error-prone alternative end-joining pathway, where it can generate a variety of chromosomal anomalies. Elucidating the biological functions of the LIG3 isozymes has been hampered by a lack of available biochemical information describing the specificity of these proteins. My thesis work describes the mechanistic framework needed for understanding the specificity of the different LIG3 isoforms, providing insight into the biological roles of the DNA ligases in DNA metabolism. Biochemical analysis of the nuclear LIG3 isozymes indicated the two enzymes were kinetically indistinguishable, suggesting their differing C-termini do not influence catalytic efficiency. When compared to LIG1, LIG3 binds Mg^{2+} ions 10-fold weaker, but has a 7-fold greater specificity toward the nicked DNA substrate. This increased catalytic efficiency has been attributed to the DNA binding property of the LIG3 N-terminal zinc finger domain. We determined that the zinc finger domain and a previously uncharacterized disordered linker region contribute equally to the catalytic efficiency of LIG3. To elucidate the activities of the ligases for double-strand break ligation, I report the first systematic kinetic analysis of LIG1- and LIG3-

catalyzed ligation of double strand breaks to elucidate their unique properties. LIG3 efficiently joined various DNA substrates under all tested conditions. In contrast, LIG1-catalyzed double-strand break ligation was highly sensitive to Mg^{2+} concentrations and molecular crowding. LIG1 activity rivaled that of LIG3 under optimal conditions but had a preference for 3' overhang over 5' overhang and blunt-ended DNA structures. Notably, LIG1 (but not LIG3) accumulated abortive ligation products under physiological conditions. Recently, the erroneous ligation activities attributed to LIG3 have implicated the enzyme as a driver of cancer progression. Moreover, LIG3 is overexpressed in cancers that require enzyme's activity for survival, making LIG3 an attractive pharmacological target. To discover novel LIG3 inhibitors that may be useful therapeutics, I developed a fluorescence-based ligation assay that reports on DNA ligation in real-time that was validated by the kinetic characterization of LIG1- and LIG3-catalyzed ligation. I adapted this assay to a discontinuous format to conduct a high-throughput screen of small-molecule libraries. Potent and selective ligase inhibitors targeting the ligases will be useful for better understanding their roles in biology, and ligase inhibitors may one day be an effective cancer therapy.

Chapter 1

Introduction to the human DNA ligases

The human genome is continuously under stress from endogenous and exogenous DNA damaging agents. Many DNA repair pathways have evolved to reverse the damage caused by these agents in order to maintain the genome. With the exception of direct repair pathways, all DNA repair pathways generate DNA breaks that must be repaired by DNA ligation. Unsuccessful ligation of these DNA breaks can lead to genomic rearrangements and mutagenesis, causing various diseases, including cancer. Humans possess three genes encoding DNA ligase proteins, DNA ligase I (LIG1), III (LIG3) and IV (LIG4). These enzymes are essential for joining breaks in the DNA phosphodiester backbone whether they are formed by DNA repair processes or generated as a result of spontaneous damage. Understanding the biochemistry of these ligases is crucial to elucidating their individual roles in DNA metabolism and understanding how these enzymes contribute to disease.

Conserved catalytic mechanism of the DNA ligases

Human DNA LIG1, LIG3 and LIG4 utilize a conserved three-step chemical mechanism to repair breaks in the DNA phosphodiester backbone (Figure 1.1). The DNA ligases first interact with ATP to become adenylylated on the active-site lysine. To do so, the catalytic lysine reacts with the alpha phosphate of ATP in the presence of Mg^{2+}, resulting in a covalent enzyme-AMP intermediate with the concomitant loss of inorganic pyrophosphate (PP_i). Upon the formation of an enzyme-substrate complex, the AMP moiety is transferred to the terminal 5' phosphate of the DNA in a Mg^{2+} dependent manner, generating a 5'-5' adenylylated DNA intermediate (Ap-DNA). To complete the final step of ligation, the 3'-hydroxyl performs a nucleophilic attack on the 5'

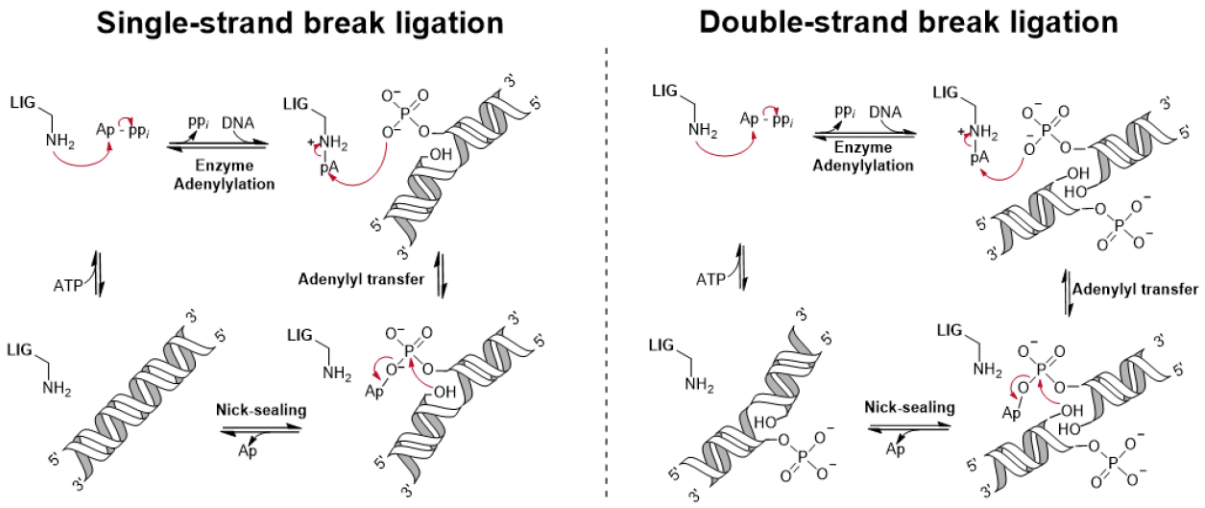

Figure 1.1. Conserved chemical mechanism of the human DNA ligases. *Left*, mechanism of single-strand DNA break (nicked DNA) ligation. One round of the three chemical ligation steps is necessary to generate a fully repaired DNA product. *Right*, mechanism for double-strand DNA ligation as exemplified using blunt-ended DNA. The first round of catalysis (DNA end-joining) requires the ligase to interact with two independent DNA molecules, and position the DNA ends such that the 3'-hydroxyl can efficiently attack the 5'-phosphate during the nick-sealing step of catalysis. The second round of catalysis is identical to that of the nicked DNA ligation mechanism *left.*

phosphate, resulting in the release of the AMP leaving group, completing the ligation reaction with the creation of a new phosphodiester bond (1). DNA molecules containing a single-strand break (SSB) require a single round of catalysis to completely repair the DNA strand (Figure 1.1, *left*).

The human DNA ligases are also capable of performing double-strand DNA break (DSB) ligation. DSB ligation requires the adenylylated ligase to coordinate and productively position the ends of two DNA molecules for catalysis. Following the first ligation event (joining of the two DNA molecules), a second ligation is required to completely restore the integrity of the DNA molecule (blunt-end substrate example provided in Figure 1.1, *right*). In the presence of DNA breaks with cohesive-end homology sufficient in length to stably anneal, the DNA ligases would likely join the two DNA molecules via a mechanism similar to that of nicked DNA ligation. Interestingly, the ligases do not catalyze this three step mechanism with perfect efficiency. Human LIG1 has been shown to dissociate from the Ap-DNA intermediate, resulting in abortive ligation. This abortive ligation is exacerbated under conditions of insufficient Mg^{2+} (2, 3). Abortive ligation intermediates are considered dead-end ligation products because the re-adenylylated enzyme is incapable of binding the aborted DNA species. Biochemical analysis of LIG1 clinical mutants indicate that naturally occurring mutations within the *LIG1* gene indicate the encoded enzymes generate appreciable abortive ligation intermediates under physiological conditions (4). To date, LIG1 abortive ligation has only been observed with nicked DNA substrates; however, in Chapter 4 we show that LIG1 can generate terminal adenylylated-DNA adducts while performing DSB ligation. The abortive ligation products produced by LIG1 can be directly repaired by the enzyme aprataxin, an Ap-DNA hydrolase that efficiently removes the adenylyl group from the DNA molecule to regenerate the ligation substrate (5, 6).

Conserved three-domain architecture of the human DNA ligases

The human DNA ligases belong to the nucleotidyltransferase protein superfamily. The ligases possess a structurally conserved three-domain architecture composed of a DNA-binding domain (DBD), nucleotidyltransferase domain (NTase) and oligonucleotide-binding domain (OB-Fold). Despite the ligases sharing only 22-23% sequence identity among these three domains (7), they share a high degree of structural conservation (Figure 1.2) (8-10). Crystal structures of the DNA-bound enzymes revealed that each of the enzymes completely encircle nicked DNA substrates, positioning the break within the NTase domain. The complete encirclement of DNA by the ligases is not absolutely required for catalytic activity. Removal of the DBD causes a reduction in nicked DNA ligation rates and increases abortive ligation (8, 11). The ligation rates of LIG1 and LIG3 lacking the DBD can be partially restored by the addition of the DBD *in trans*. The DBD contributes to catalysis by stabilizing the enzyme•substrate complex through non-specific electrostatic interactions along the minor groove of the DNA substrate, spanning upstream and downstream of the DNA break (8, 9, 11).

The NTase domains of the DNA ligases house their catalytic lysine residues (K568, K421 and K273 for LIG1, LIG3 and LIG4, respectively). This domain also contains the ATP nucleotide binding pocket and numerous acidic residues responsible for divalent metal ion coordination (presumably Mg^{2+}) (8). Interestingly, numerous crystal structures and biochemical studies of the human DNA ligases have been unsuccessful in identifying the metal cofactor binding sites. Efforts are ongoing to better understand how the ligases bind and utilize these cofactor(s).

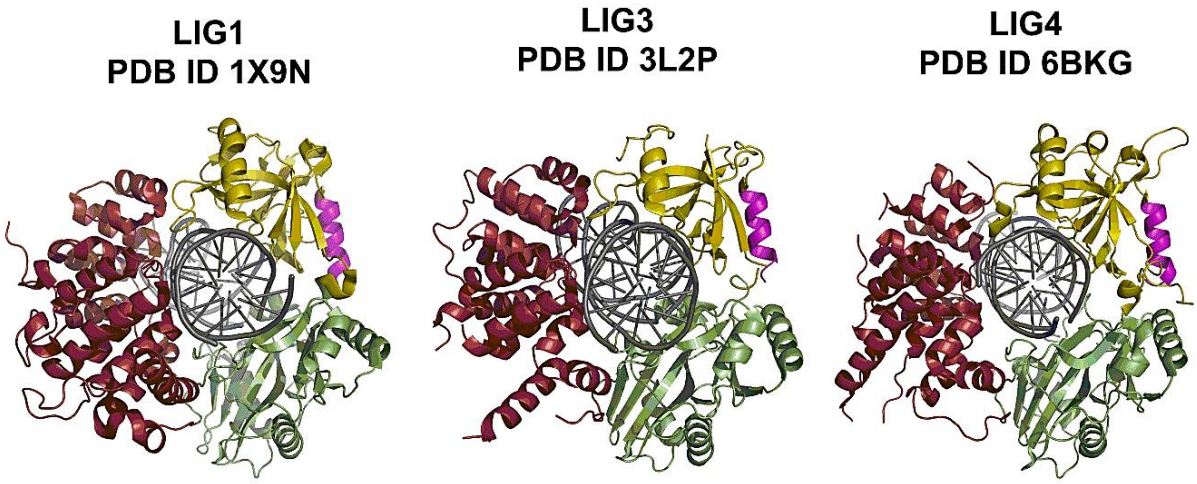

Figure 1.2. Structural conservation among the human DNA ligases. A, DNA LIG1, LIG3 and LIG4 possess a high degree of structural conservation among their DNA-binding (DBD, *Red*), nucleotidyltransferase (NTase, *green*) and oligonucleotide-binding (OB-fold, *yellow*) domains. Illustrated in *purple* is motif VI of the OB-fold, a conserved region required for enzyme adenylylation. PDB identifiers are indicated below respective enzyme labels. Images generated using PyMol software. Each of the enzymes have been crystallized in the presence of nicked DNA species.

The OB-fold has been shown to adopt two conformations, the first contributes to enzyme adenylylation, and the second stabilizes the enzyme•DNA substrate complex by interaction with DNA. Structural studies of the homologous *Chlorella* virus mRNA capping enzyme, and the human DNA ligases have highlighted the importance of these two conformational states (8-10, 12). In the first conformation, the alpha helix of motif VI is in close proximity to the nucleotide binding pocket of the NTase domain where it assists in enzyme adenylylation (motif VI, colored

purple in Figure 1.2) (8, 13). Motif VI is essential for DNA ligase activity, for its removal abolishes self-adenylylation (13). In the second conformation the OB-fold domain undergoes a rotation that causes motif VI to face outward from the enzyme, becoming solvent exposed (Figure 1.2). In this rotated state, the OB-fold contributes to DNA binding and encirclement of the DNA substrate. In the DNA-encircled state, motif VI is not needed for the DNA dependent steps of catalysis (8-10). Thus, the three domains shared among the ligases (DBD, NTase and OB-fold domains) each contribute to the ligation reactions catalyzed by these enzymes.

Unique N- and C-termini of the human DNA ligases.

The human DNA ligases have different N- and C-termini flanking their conserved catalytic regions (Figure 1.3). The N- and C termini play important roles in cellular localization, protein-protein interactions and substrate specificity (14).

Human DNA ligase I. The *LIG1* gene encodes a polypeptide possessing an unstructured N-terminal region of roughly 260 residues that are important for nuclear localization and protein-protein interactions. LIG1 interacts with the proliferating cell nuclear antigen (PCNA) through a PCNA binding motif, an interaction required for LIG1 localization to sites of DNA replication (15, 16). The N-terminal region of LIG1, prone to proteolysis/fragmentation in biochemical assays, does not contribute to the kinetic parameters of nicked DNA ligation and is thus commonly removed for *in vitro* biochemical analysis (2).

Human DNA ligase III. The *LIG3* gene encodes four unique LIG3 isozymes (Figure 1.3). Mitochondrial and nuclear isoforms are synthesized from alternative translation initiation sites, generating the essential mitochondrial isoform, and the seemingly dispensable nuclear isoform (17-22). Translation from the first of the two methionine start codons generate polypeptides

containing a mitochondrial leader sequence (MLS), whereas synthesis from the second methionine start codon generate shorter nuclear LIG3 isoforms lacking the MLS (23). In addition to the mitochondrial and nuclear isoforms of LIG3, two alternatively spliced isoforms have also been identified. Alternative splicing of the mRNA transcript results in the formation of a germ-line specific isoform (LIG3β) and an isoform found in all cell types (LIG3α) (23-26). The BRCA1 C-terminal (BRCT) domain, specific to LIG3α, interacts with X-ray repair cross-complementing protein 1 (XRCC1) in the cytoplasm and nucleus (27-31). LIG3β lacks the BRCT domain and is suggested to function independently of XRCC1 (25, 26, 28). Using an alternative exon during splicing generates an identifiable nuclear localization sequence (NLS) at the C-terminus of LIG3β. Since LIG3α lacks an NLS, it is postulated that LIG3α is targeted to the nucleus by the LIG3α•XRCC1 interaction since XRCC1 has an identifiable NLS (14, 32). Interestingly, it seems that MLS-LIG3α preferentially localizes to the mitochondria, even though the protein likely interacts with XRCC1 in the cytoplasm (33). Upon translocation into the mitochondria, the N-terminal MLS is removed, and the LIG3α•XRCC1 interaction must be disrupted, for XRCC1 has not been detected in the mitochondria (33, 34).

All LIG3 isozymes have an N-terminal zinc finger (ZnF) domain that is not present in LIG1 or LIG4. This domain is highly homologous to the poly (ADP-ribose) polymerase-1 (PARP1) ZnF domains, in which a single Zn^{2+} ion is coordinated by three cysteine and one histidine (C_2HC) residues (35-37). The solution structure of the LIG3 ZnF domain was reported in 2004, providing structural information of the ~100 amino acid domain (35). The role of the ZnF domain during LIG3-catalyzed ligation has been of interest for roughly two decades prior to the writing of this thesis, and has been shown to contribute to DNA binding and substrate specificity of LIG3 under a variety of *in vitro* conditions (9, 11, 36-39).

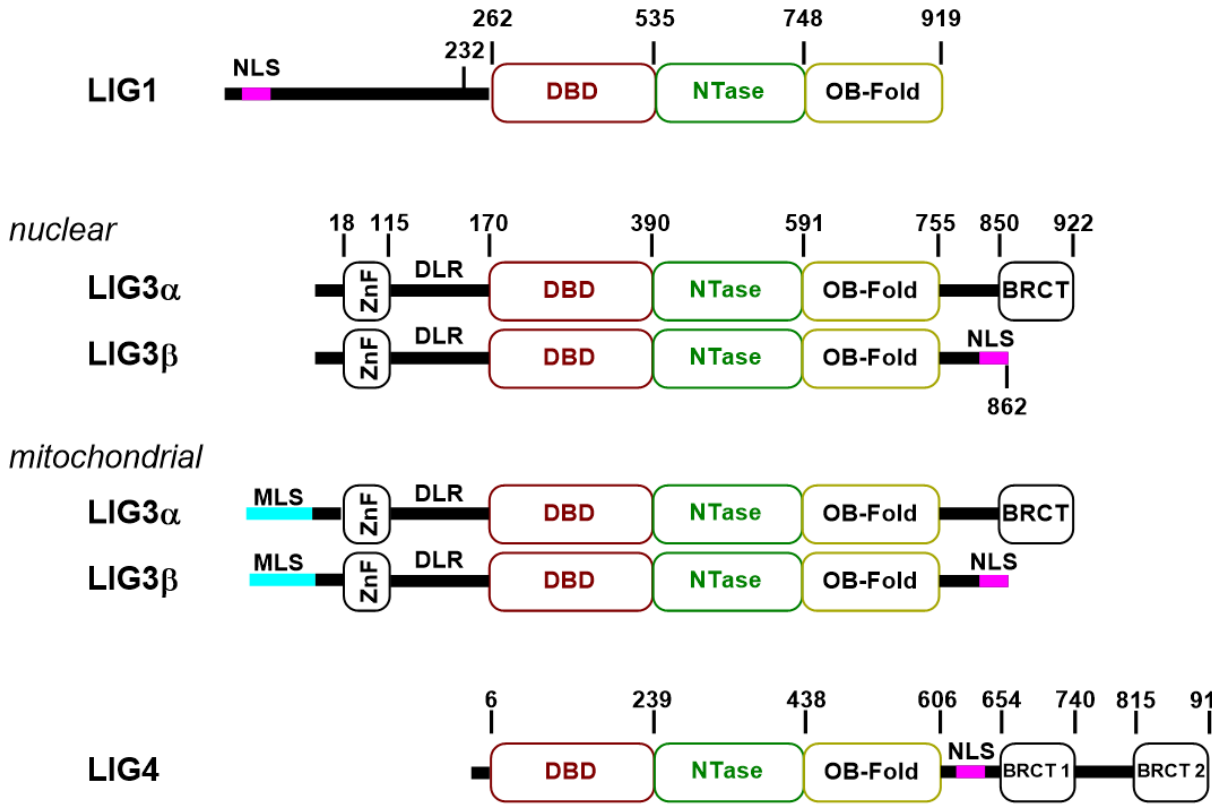

Figure 1.3. The differential N- and C-termini of the human DNA ligase gene products. DNA LIG1, LIG3 and LIG4 possess a high degree of structural conservation among their DBD (Red), NTase (*green*) and OB-fold (*yellow*) domains. Residue 232 of LIG1 indicates N-terminal truncation utilized in structural and biochemical assays. LIG3 possesses a unique zinc finger (ZnF) domain upstream of a disordered linker region (DLR). LIG3α isoform and LIG4 have BRCA1 C-terminal (BRCT) domains. Mitochondrial LIG3 alternative translation initiation isoforms possess an N-terminal mitochondrial leader sequence (MLS). LIG1, LIG3β and LIG4 have identifiable nuclear localization signal (NLS) sequences. Numbers represent identified domain boundaries.

Human DNA ligase IV. The *LIG4* gene encodes a polypeptide that is localized to the nucleus via a nuclear localization sequence located between the enzyme's OB-fold and BRCT1 domains. The C-terminal tandem BRCT domains of LIG4 have been suggested to each interact with Ku70/Ku80 heterodimers during nonhomologous end-joining (NHEJ) and V(D)J recombination (40). Similar to LIG3α•XRCC1, LIG4 constitutively interacts with XRCC4 in the cell. However, the LIG4•XRCC4 interaction is not mediated through BRCT domains (as seen with LIG3•XRCC1), but through the linker region joining the BRCT 1 and BRCT 2 domains (41). The activity of LIG4 seems to be dependent on the presence of these interacting proteins, without which, the enzyme may complete only a single round of ligation before becoming inactive since the enzyme is inefficient at self-adenylylation (42).

Biochemistry aids our understanding of LIG1 and LIG3 biological activities

DNA LIG1 is essential for embryonic development in mice and is widely referenced as the replicative DNA ligase (14, 43, 44). Recent cell based experiments, however, indicate the enzyme is not essential for DNA replication (17, 18, 45). The dependence of LIG1 activity for embryogenesis, but not cultured cell viability, suggests the activity attributed to LIG1 cannot be performed by the other human DNA ligases. In humans, mutations identified within the *LIG1* gene cause a wide range of phenotypes, including immunodeficiencies, varying degrees of growth retardation, and neurological defects (4, 46, 47). The mechanism(s) by which these mutations to LIG1 cause the described phenotypes are poorly understood and may or may not be linked to DNA replication. Biochemical analysis of these LIG1 clinical mutants suggest the proteins have altered DNA and metal cofactor binding properties, causing the enzymes to accumulate appreciable abortive ligation products (4). Reducing the efficiency of LIG1 could compromise the enzymes

ability to join the SSBs required for Okazaki fragment joining and the DNA repair pathways. It is becoming increasingly clear that the abortive ligation behavior attributed to LIG1 correlates with the enzyme's requirement for Mg^{2+} cofactor(s) since wild-type LIG1 accumulates abortive ligation products during SSB ligation under Mg^{2+} starved conditions (Chapter 2) (2, 3). Expanding upon this, I investigated the biochemical properties of LIG1 catalyzed end-joining using various structures of DSB. I found that human DNA LIG1 can efficiently catalyze the end-joining reaction; however, the enzyme is prone to accumulating abortive end-joining intermediates at low (physiological) Mg^{2+} levels. Interestingly, the accumulation of these 5'-adenylylated end-joining products was abolished at high (non-physiological) Mg^{2+} concentrations. Investigations into the end-joining characteristics of the LIG1 clinical mutants may prove fruitful for understanding the mechanisms by which these mutations lead to disease.

As observed for LIG1, LIG3 is also essential for embryonic development in mice (48). The cause of compromised embryogenesis in mice lacking LIG3 is likely genomic instability of the mitochondrial genome since LIG3 is the only ligase targeted to the organelle (19, 20, 49). However, Puebla-Osorio *et al*. invite the possibility that compromised embryogenesis may be caused by an accumulation of unrepaired DNA damage and/or abnormal sister chromatid exchange as has been seen in cells lacking LIG3 (48). LIG3 is dispensable for cell viability, but it is not clear whether nuclear LIG3 is needed for embryonic development (17-22). Interestingly, mutations within the *LIG3* gene that influence human health have not been identified, highlighting the biological necessity of the enzyme.

Originally believed to be expressed exclusively in vertebrates, the *LIG3* gene is now estimated to exist in roughly 30% of Eukarya (1, 7, 14). Since LIG3 has an inconsistent presence in Eukarya, many of the genetically tractable model organisms do not possess the *LIG3* gene,

complicating the process of determining LIG3 specific cellular functions and differentiating the roles of the DNA ligases in DNA metabolism (33). Eukaryotes lacking the *LIG3* gene utilize LIG1 homologs to perform the necessary ligation reaction in the nucleus and mitochondria (14). It is becoming increasingly clear that LIG1 and LIG3 have overlapping roles in the cell since LIG3 supports DNA replication and repair in the absence of LIG1 in mouse (43, 45, 50) and chicken cells (21). It is currently unknown how LIG3 is recruited to the replication fork during DNA replication. It is possible that LIG3 is recruited to the replication fork via XRCC1, since XRCC1 has been shown to co-localize and interact with PCNA in HeLa cells during the S-phase of the cell cycle (51). Likewise, little is known about the overlapping roles the ligases play in the base and nucleotide excision repair pathways since LIG1 and LIG3 can both perform the ligation events required for their completion (14, 52). Together, LIG1 and LIG3 are both capable of catalyzing the repair of single-strand breaks during DNA replication and repair.

To gain a better understanding of LIG1-, LIG3α- and LIG3β-catalyzed SSB ligation, I performed a systematic kinetic analysis of the recombinant proteins (Chapter 2) (2, 3). This comparative study indicated that LIG1 and LIG3 differ most in their Mg^{2+} binding affinity and $K_{M,\ DNA}$ values. Previous investigations by the Caldecott and Ellenberger groups provided compelling evidence that the LIG3 ZnF domain contributes to the DNA binding affinity of the enzyme (9, 11, 36-39). However, the degree by which the ZnF domain contributes to the kinetic parameters of LIG3-catalyzed SSB ligation remains in question. We designed N-terminal truncation constructs and point mutation in the ZnF domain to investigate the influence of the ZnF domain on the substrate and cofactor dependences of LIG3 (Chapter 3). This systematic analysis of substrate and cofactor dependences indicates that the ZnF domain does not contribute to the ATP dependence of LIG3; however, the removal of the domain increased Mg^{2+} affinity. Consistent with previous

observations, the ZnF domain contributed to the catalytic efficiency ($k_{cat}/K_{M, DNA}$) for nicked DNA substrates. Strikingly, we discovered that a previously uncharacterized disordered linker region (DLR) tethering the ZnF domain to the DBD contributes to LIG3 steady-state kinetic parameters. In our hands, the DLR increases LIG3 catalytic efficiency to an equal degree as the ZnF domain, suggesting this linker is important for DNA binding. The discovery of the DLR's contribution to LIG3 SSB ligation efficiency suggest the DNA interacting mechanisms of the LIG3 N-terminus are more complex than the current "jack knife" model proposed by Cotner *et al*. (9, 11). The 'jack knife" model predicts that the ZnF domain and DBD first interact with a nicked DNA substrate as if they are a single DNA binding module (ZnF-DBD). Following this interaction, the NTase and OB-Fold domains bind to, and encircle the DNA substrate, forcing the ZnF domain to disengage the DNA. To investigate whether the ZnF disengages a DNA substrate upon ligase binding, small-angle X-ray scattering experiments suggested the ZnF and DLR no longer interact with the DNA molecule after LIG3 has encircled it. These studies also suggest the DLR serves no function in addition to tethering the ZnF to the DBD (9). Conversely, my studies suggest that the DLR plays an important role in either DNA binding and/or stabilization of the enzyme•substrate complex via intramolecular interactions with the three-domain ligase core. Additional experimentation is required to better understand how the N-terminus of LIG3 is contributing to ligation efficiency.

In addition to catalyzing the ligation of SSBs, LIG3 is capable of catalyzing DNA end-joining (EJ) reactions (9, 11, 38, 39, 53). While the majority of DSBs are repaired via the LIG4-dependent nonhomologous end-joining (NHEJ) and/or homologous recombination pathways, the minor and relatively poorly understood LIG3-dependent alternative-EJ (alt-EJ) pathway is highly error-prone (42, 54). The alt-EJ pathway is capable of generating telomere fusions, reciprocal chromosomal translocations and DNA deletions and has gained interest because these

chromosomal anomalies drive cancer progression (54-58). Cells deficient in NHEJ and/or homologous recombination activity become increasingly dependent on alt-EJ pathways (59-62). Upon removal of LIG3 or alt-EJ factors, these erroneous ligation behaviors occur less frequently (55), suggesting the LIG3-dependent alt-EJ pathway is responsible for this deleterious behavior. In addition to the *in vivo* work investigating LIG3 DSB ligation characteristics, numerous biochemical studies indicate LIG3 can catalyze EJ reactions *in vitro* (9, 11, 38, 39, 53, 54). Guided by these biochemical studies, the Tomkinson and Ellenberger groups proposed that the combined DNA binding properties of the ZnF domain and DBD function as a single DNA interacting module that is capable of binding DNA ends. They also suggest the NTase and OB-Fold domains serve as a second DNA end binding module. The idea of LIG3 having two DNA binding models suggests the enzyme should be able to bridge two DNA molecules (9, 38). If LIG3 does interact with DNA ends as proposed (using two independent DNA-interacting modules), this may explain why LIG3 is more proficient in end-joining than the other DNA ligases under *in vitro* conditions. To broaden our understanding of LIG3 catalyzed EJ, we investigated the kinetic parameters of LIG3β on blunt-end and overhang containing substrates (Chapter 4). This analysis enabled the direct comparison of LIG1 and LIG3 activities. We report that LIG3 joined all of the tested substrates with similar efficiencies. Furthermore, we were able to determine the single-turnover rate constants for the sequential ligation events required to completely repair the DSB.

In addition to the erroneous ligation activity attributed to LIG3 and the alt-EJ pathway, elevated levels of LIG3 are needed for cancer cell survival (63-66). Targeted inhibition of LIG3 and disruption of abnormal DNA repair within cancerous cells may be an attractive mechanism for anti-cancer therapy. In order to pursue LIG3 as a valid target, an efficient method for screening small-molecule inhibitors of the DNA ligases must be employed. We designed and validated a

real-time fluorescence based assay that reports on DNA ligation activity. The robustness of this method suggests it may be utilized to efficiently determine the steady-state parameters of various DNA ligases. The assay may be easily adjusted for discontinuous use, enabling efficient high-throughput screening of small-molecule libraries (Chapter 5).

Conclusions

This thesis provides the first kinetic analysis of human DNA LIG3α and LIG3β on nicked DNA substrates. This systematic characterization enabled a direct comparative analysis of the LIG3 isoforms to LIG1. The LIG3 isoforms (enzymatically identical to each other) had markedly greater catalytic efficiencies on nicked DNA substrates than LIG1, presumably due to the N-terminal DNA binding ZnF domain. Interestingly, while investigating the role of the N-terminal region (consisting of the ZnF domain and DLR) in nicked DNA ligation, we identified a previously unidentified function of the LIG3 DLR. The ZnF domain and DLR independently increased the catalytic efficiency of LIG3-catalyzed nicked DNA ligation. We report, for the first time, the biochemistry of LIG1 catalyzed end-joining and compare this activity to that of LIG3. Since LIG3 may be a promising pharmacological target, we designed and validated a real-time ligation assay that is amendable to high throughput screening of small-molecule libraries to identify ligase inhibitors. Discovery of ligase specific inhibitors may provide tools to better define the biological roles of the human ligases, and lead to innovative therapeutic approaches to treat certain cancers.

References

1. Tomkinson AE, Vijayakumar S, Pascal JM, & Ellenberger T (2006) DNA Ligases: Structure, Reaction Mechanism, and Function. *Chem. Rev.* 106(2):687-699.

2. Taylor MR, Conrad JA, Wahl D, & O'Brien PJ (2011) Kinetic Mechanism of Human DNA Ligase I Reveals Magnesium-dependent Changes in the Rate-limiting Step That Compromise Ligation Efficiency. *J. Biol. Chem.* 286(26):23054-23062.

3. McNally JR & O'Brien PJ (2017) Kinetic analyses of single-stranded break repair by human DNA ligase III isoforms reveal biochemical differences from DNA ligase I. *J. Biol. Chem.* 292(38):15870-15879.

4. Maffucci P, *et al.* (2018) Biallelic mutations in DNA ligase 1 underlie a spectrum of immune deficiencies. *J. Clin. Invest.* 128(12):5489-5504.

5. Rass U, Ahel I, & West SC (2007) Actions of aprataxin in multiple DNA repair pathways. *J. Biol. Chem.* 282(13):9469-9474.

6. Ahel I, *et al.* (2006) The neurodegenerative disease protein aprataxin resolves abortive DNA ligation intermediates. *Nature* 443(7112):713-716.

7. Simsek D & Jasin M (2011) DNA ligase III: A spotty presence in eukaryotes, but an essential function where tested. *Cell Cycle* 10(21):3636-3644.

8. Pascal JM, O'Brien PJ, Tomkinson AE, & Ellenberger T (2004) Human DNA ligase I completely encircles and partially unwinds nicked DNA. *Nature* 432(7016):473-478.

9. Cotner-Gohara E, *et al.* (2010) Human DNA Ligase III Recognizes DNA Ends by Dynamic Switching between Two DNA-Bound States. *Biochemistry* 49(29):6165-6176.

10. Kaminski AM, *et al.* (2018) Structures of DNA-bound human ligase IV catalytic core reveal insights into substrate binding and catalysis. *Nat Commun* 9(1):2642.

11. Cotner-Gohara E, Kim I-K, Tomkinson AE, & Ellenberger T (2008) Two DNA-binding and Nick Recognition Modules in Human DNA Ligase III. *J. Biol. Chem.* 283(16):10764-10772.

12. Hakansson K, Doherty AJ, Shuman S, & Wigley DB (1997) X-ray crystallography reveals a large conformational change during guanyl transfer by mRNA capping enzymes. *Cell* 89(4):545-553.

13. Sriskanda V & Shuman S (1998) Mutational analysis of Chlorella virus DNA ligase: catalytic roles of domain I and motif VI. *Nucleic Acids Res.* 26(20):4618-4625.

14. Ellenberger T & Tomkinson AE (2008) Eukaryotic DNA Ligases: Structural and Functional Insights. *Annu. Rev. Biochem.* 77(1):313-338.

15. Song W, *et al.* (2007) A conserved physical and functional interaction between the cell cycle checkpoint clamp loader and DNA ligase I of eukaryotes. *J. Biol. Chem.* 282(31):22721-22730.

16. Montecucco A, *et al.* (1998) DNA ligase I is recruited to sites of DNA replication by an interaction with proliferating cell nuclear antigen: identification of a common targeting mechanism for the assembly of replication factories. *EMBO J.* 17(13):3786-3795.

17. Masani S, Han L, Meek K, & Yu K (2016) Redundant function of DNA ligase 1 and 3 in alternative end-joining during immunoglobulin class switch recombination. *Proc. Natl. Acad. Sci. U. S. A.* 113(5):1261-1266.

18. Lu G, *et al.* (2016) Ligase I and ligase III mediate the DNA double-strand break ligation in alternative end-joining. *Proc. Natl. Acad. Sci. U. S. A.* 113(5):1256-1260.

19. Simsek D, *et al.* (2011) Crucial role for DNA ligase III in mitochondria but not in Xrcc1-dependent repair. *Nature* 471(7337):245-248.

20. Gao Y, *et al.* (2011) DNA Ligase III is critical for mtDNA integrity but not Xrcc1-mediated nuclear DNA repair. *Nature* 471(7337):240-244.

21. Arakawa H, *et al.* (2012) Functional redundancy between DNA ligases I and III in DNA replication in vertebrate cells. *Nucleic Acids Res.* 40(6):2599-2610.

22. Lakshmipathy U & Campbell C (1999) The Human DNA Ligase III Gene Encodes Nuclear and Mitochondrial Proteins. *Mol. Cell. Biol.* 19(5):3869-3876.

23. Chen J, *et al.* (1995) Mammalian DNA ligase III: molecular cloning, chromosomal localization, and expression in spermatocytes undergoing meiotic recombination. *Mol. Cell. Biol.* 15(10):5412-5422.

24. Wei YF, *et al.* (1995) Molecular cloning and expression of human cDNAs encoding a novel DNA ligase IV and DNA ligase III, an enzyme active in DNA repair and recombination. *Mol. Cell. Biol.* 15(6):3206-3216.

25. Perez-Jannotti RM, Klein SM, & Bogenhagen DF (2001) Two Forms of Mitochondrial DNA Ligase III Are Produced inXenopus laevis Oocytes. *J. Biol. Chem.* 276(52):48978-48987.

26. Mackey ZB, *et al.* (1997) An alternative splicing event which occurs in mouse pachytene spermatocytes generates a form of DNA ligase III with distinct biochemical properties that may function in meiotic recombination. *Mol. Cell. Biol.* 17(2):989-998.

27. Taylor RM, Wickstead B, Cronin S, & Caldecott KW (1998) Role of a BRCT domain in the interaction of DNA ligase III-α with the DNA repair protein XRCC1. *Curr. Biol.* 8(15):877-880.

28. Nash RA, Caldecott KW, Barnes DE, & Lindahl T (1997) XRCC1 Protein Interacts with One of Two Distinct Forms of DNA Ligase III. *Biochemistry* 36(17):5207-5211.

29. Caldecott KW, Aoufouchi S, Johnson P, & Shall S (1996) XRCC1 Polypeptide Interacts with DNA Polymerase β and Possibly Poly (ADP-Ribose) Polymerase, and DNA Ligase III Is a Novel Molecular 'Nick-Sensor' In Vitro. *Nucleic Acids Res.* 24(22):4387-4394.

30. Caldecott KW, Tucker JD, Stanker LH, & Thompson LH (1995) Characterization of the XRCC1-DNA ligase III complex in vitro and its absence from mutant hamster cells. *Nucleic Acids Res.* 23(23):4836-4843.

31. Caldecott KW, McKeown CK, Tucker JD, Ljungquist S, & Thompson LH (1994) An interaction between the mammalian DNA repair protein XRCC1 and DNA ligase III. *Mol. Cell. Biol.* 14(1):68-76.

32. Masson M, *et al.* (1998) XRCC1 Is Specifically Associated with Poly(ADP-Ribose) Polymerase and Negatively Regulates Its Activity following DNA Damage. *Mol. Cell. Biol.* 18(6):3563-3571.

33. Tomkinson AE & Sallmyr A (2013) Structure and function of the DNA ligases encoded by the mammalian LIG3 gene. *Gene* 531(2):150-157.

34. Lakshmipathy U & Campbell C (2000) Mitochondrial DNA ligase III function is independent of Xrcc1. *Nucleic Acids Res.* 28(20):3880-3886.

35. Kulczyk AW, Yang J-C, & Neuhaus D (2004) Solution Structure and DNA Binding of the Zinc-finger Domain from DNA Ligase IIIα. *J. Mol. Biol.* 341(3):723-738.

36. Taylor RM, Whitehouse J, Caldecott KW, Cappelli E, & Frosina G (1998) Role of the DNA ligase III zinc finger in polynucleotide binding and ligation. *Nucleic Acids Res.* 26(21):4804-4810.

37. Mackey ZB, *et al.* (1999) DNA Ligase III Is Recruited to DNA Strand Breaks by a Zinc Finger Motif Homologous to That of Poly(ADP-ribose) Polymerase Identification of Two Functionally Distinct DNA Binding Regions Within DNA Ligase III. *J. Biol. Chem.* 274(31):21679-21687.

38. Kukshal V, *et al.* (2015) Human DNA ligase III bridges two DNA ends to promote specific intermolecular DNA end joining. *Nucleic Acids Res.* 43(14):7021-7031.

39. Taylor RM, Whitehouse CJ, & Caldecott KW (2000) The DNA ligase III zinc finger stimulates binding to DNA secondary structure and promotes end joining. *Nucleic Acids Res.* 28(18):3558-3563.

40. Costantini S, Woodbine L, Andreoli L, Jeggo PA, & Vindigni A (2007) Interaction of the Ku heterodimer with the DNA ligase IV/Xrcc4 complex and its regulation by DNA-PK. *DNA Repair (Amst)* 6(6):712-722.

41. Sibanda BL, *et al.* (2001) Crystal structure of an Xrcc4-DNA ligase IV complex. *Nat. Struct. Biol.* 8(12):1015-1019.

42. Pannunzio NR, Watanabe G, & Lieber MR (2018) Nonhomologous DNA end-joining for repair of DNA double-strand breaks. *J. Biol. Chem.* 293(27):10512-10523.

43. Bentley D, *et al.* (1996) DNA ligase I is required for fetal liver erythropoiesis but is not essential for mammalian cell viability. *Nat. Genet.* 13(4):489-491.

44. Petrini JH, Xiao Y, & Weaver DT (1995) DNA ligase I mediates essential functions in mammalian cells. *Mol. Cell. Biol.* 15(8):4303-4308.

45. Han L, Masani S, Hsieh CL, & Yu K (2014) DNA ligase I is not essential for mammalian cell viability. *Cell Rep* 7(2):316-320.

46. Barnes DE, Tomkinson AE, Lehmann AR, Webster AD, & Lindahl T (1992) Mutations in the DNA ligase I gene of an individual with immunodeficiencies and cellular hypersensitivity to DNA-damaging agents. *Cell* 69(3):495-503.

47. Willis AE & Lindahl T (1987) DNA ligase I deficiency in Bloom's syndrome. *Nature* 325(6102):355-357.

48. Puebla-Osorio N, Lacey DB, Alt FW, & Zhu C (2006) Early Embryonic Lethality Due to Targeted Inactivation of DNA Ligase III. *Mol. Cell. Biol.* 26(10):3935-3941.

49. Shokolenko IN, *et al.* (2013) Mitochondrial DNA Ligase is Dispensable for the Viability of Cultured Cells, but Essential for mtDNA Maintenance. *J. Biol. Chem.*

50. Bentley DJ, *et al.* (2002) DNA ligase I null mouse cells show normal DNA repair activity but altered DNA replication and reduced genome stability. *J. Cell Sci.* 115(Pt 7):1551-1561.

51. Fan J, Otterlei M, Wong HK, Tomkinson AE, & Wilson DM, 3rd (2004) XRCC1 co-localizes and physically interacts with PCNA. *Nucleic Acids Res.* 32(7):2193-2201.

52. Krokan HE & Bjoras M (2013) Base excision repair. *Cold Spring Harb. Perspect. Biol.* 5(4):a012583.

53. Bauer RJ, *et al.* (2017) Comparative analysis of the end-joining activity of several DNA ligases. *PLoS One* 12(12):e0190062.

54. Sallmyr A & Tomkinson AE (2018) Repair of DNA double-strand breaks by mammalian alternative end-joining pathways. *J. Biol. Chem.* 293(27):10536-10546.

55. Simsek D, *et al.* (2011) DNA Ligase III Promotes Alternative Nonhomologous End-Joining during Chromosomal Translocation Formation. *PLoS Genetics* 7(6).

56. Badie S, *et al.* (2015) BRCA1 and CtIP promote alternative non-homologous end-joining at uncapped telomeres. *EMBO J.* 34(6):828.

57. Jones RE, *et al.* (2014) Escape from telomere-driven crisis is DNA ligase III dependent. *Cell Rep* 8(4):1063-1076.

58. Boboila C, *et al.* (2012) Robust chromosomal DNA repair via alternative end-joining in the absence of X-ray repair cross-complementing protein 1 (XRCC1). *Proc. Natl. Acad. Sci. U. S. A.* 109(7):2473-2478.

59. Simsek D & Jasin M (2010) Alternative end-joining is suppressed by the canonical NHEJ component Xrcc4-ligase IV during chromosomal translocation formation. *Nat. Struct. Mol. Biol.* 17(4):410-416.

60. Mateos-Gomez PA, *et al.* (2015) Mammalian polymerase theta promotes alternative NHEJ and suppresses recombination. *Nature* 518(7538):254-257.

61. Corneo B, *et al.* (2007) Rag mutations reveal robust alternative end joining. *Nature* 449(7161):483-486.

62. Xie A, Kwok A, & Scully R (2009) Role of mammalian Mre11 in classical and alternative nonhomologous end joining. *Nat. Struct. Mol. Biol.* 16(8):814-818.

63. Newman EA, *et al.* (2015) Alternative NHEJ Pathway Components Are Therapeutic Targets in High-Risk Neuroblastoma. *Mol. Cancer Res.* 13(3):470-482.

64. Tomkinson AE, Howes TR, & Wiest NE (2013) DNA ligases as therapeutic targets. *Transl Cancer Res* 2(3).

65. Tobin LA, *et al.* (2013) Targeting abnormal DNA double-strand break repair in tyrosine kinase inhibitor-resistant chronic myeloid leukemias. *Oncogene* 32(14):1784-1793.

66. Tobin LA, *et al.* (2012) Targeting abnormal DNA repair in therapy-resistant breast cancers. *Mol. Cancer Res.* 10(1):96-107.

Chapter 2

Kinetic Analyses of Single-Strand Break Repair by Human DNA Ligase III Isoforms Reveal Biochemical Differences from DNA Ligase I[1,2]

Introduction

Human DNA Ligases I (LIG1), III (LIG3) and IV (LIG4) catalyze the ultimate steps in DNA replication and repair pathways. All three of the *LIG* genes are required for mouse embryonic development (1-5), and clinical mutations have been identified in both *LIG1* and *LIG4* genes that cause immunodeficiencies (6-8). LIG1 is believed to be the primary nuclear replicative DNA ligase, however recent studies indicate that LIG1 and nuclear LIG3 have overlapping functions (9-12). The LIG3 proteins are translated from two start sites to generate mitochondrial and nuclear isoforms, the latter of which is suggested to be dispensable (10,11,13-16). Two alternative splice isoforms of LIG3 are known that differ in their C-terminal regions. The major LIG3 isoform (LIG3α) contains a C-terminal BRCT domain that has been shown to interact with XRCC1 (17-21). Alternative splicing in male germ cells (22,23) gives rise to a shorter isoform (LIG3β) that

[1]Reproduced with permission from McNally JR & O'Brien PJ (2017) Kinetic analyses of single-stranded break repair by human DNA ligase III isoforms reveal biochemical differences from DNA ligase I. *J. Biol. Chem.* 292(38):15870-15879. © 2017 by The American Society for Biochemistry and Molecular Biology, Inc. Published in the U.S.A. [2]I performed the experiments, Patrick O'Brien and I designed the study, analyzed the data, and wrote the manuscript.

lacks the BRCT domain (Figure 2.1A). Although the beneficial roles of nuclear LIG3 isoforms are not clear, LIG3 has been implicated in error-prone alternative end joining which can lead to chromosomal translocations (11,24) and telomere fusions (25,26). Furthermore, elevated levels of LIG3 have been detected in cancer, making LIG3 a candidate for anticancer therapeutics (27-30). Crystal structures of the human DNA ligases (31,32) show a conserved catalytic core made up of three distinct domains that encircle the substrate (Figure 2.1B). However, the N- and C-terminal extensions differ significantly and these regions of the protein are likely to contribute to physiological differences between the ligases (Figures 2.1A). LIG1 has an unstructured N-terminal region that facilitates protein-protein interactions (31,34), but this region is dispensable for ligase activity *in vitro* (31,33). LIG3 also has an N-terminal extension containing a unique zinc-finger (ZnF) domain that has been implicated in DNA binding (32,35-40). Furthermore, this ZnF domain has been hypothesized to be a 'nick sensor' responsible for increasing LIG3 specificity and affinity toward DNA substrates containing a single-strand DNA break (19,32,35,38). The C-terminal extension of LIG3α contains a BRCT domain that is constitutively bound to XRCC1 in the nucleus. As, XRCC1 is not found in the mitochondria, it is of interest to characterize the biochemical properties of LIG3α in the absence of XRCC1 (41).

The human DNA ligases employ a conserved three-step chemical mechanism (Figure 2.1C) to harness the energy of ATP to catalyze the formation of a phosphodiester bond between adjacent 3′-hydroxyl and 5′-phosphate groups in DNA (42). During the first chemical step of ligation (step 1), ligase catalyzes the transfer of AMP from ATP to the active site lysine forming an adenylylated enzyme intermediate and releasing inorganic pyrophosphate. The adenylylated enzyme binds to a DNA substrate containing a single-strand break, and during the second chemical step, catalyzes the transfer of the AMP group to the 5′-phosphate at the break (nick), thereby

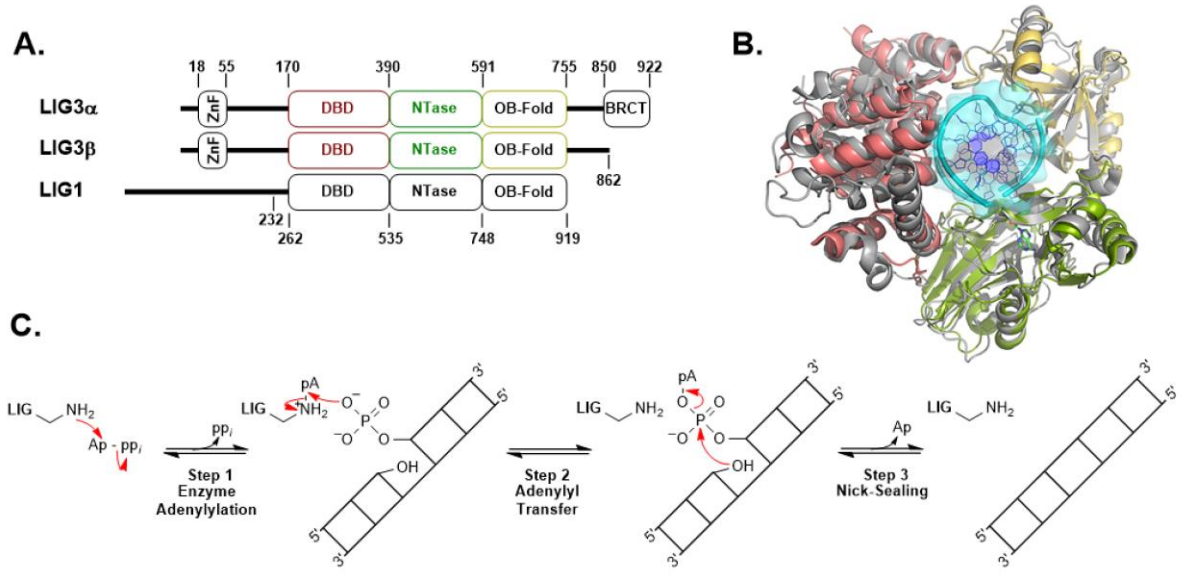

Figure 2.1. Conserved structure and mechanism of human DNA ligases. *A*, schematic representation of human DNA LIG3α, LIG3β and LIG1. Numbers indicate domain boundaries of the enzymes. LIG3α contains a C-terminal BRCT domain. The LIG1 Δ232 truncation mutant used throughout this study is catalytically identical to full length LIG1 (33). LIG3 isoforms and LIG1 possess conserved DNA binding (DBD), nucleotidyltransferase (NTase) and oligonucleotide-binding (OB-fold) domains. *B*, superimposition of LIG1 (grey) and LIG3 (color coded; DBD, red; NTase, green; OB-fold, yellow) structures 1X9N and 3L2P, respectively (31,32). *C*, mechanism of ATP-dependent DNA ligases.

generating an adenylylated DNA intermediate. During step 3, the 3′-hydroxyl at the nick attacks the adenylylated 5′-phosphate to generate a new phosphodiester bond and release AMP (Figure 2.1C). All three of these chemical steps are dependent on divalent metal ions (presumably Mg^{2+}), and previous work has supported a two metal ion mechanism for step 1 (enzyme adenylylation) catalyzed by human LIG1 (33).

As a starting point for understanding the biochemical differences between LIG1 and LIG3, we describe the kinetic and thermodynamic framework for LIG3-catalyzed ligation of a single-strand break. LIG3α and LIG3β exhibit similar kinetic parameters under all tested conditions,

indicating that the C-terminal BRCT domain of LIG3α does not directly contribute to ligation of nicked DNA substrates. Comparison of the biochemical properties of LIG3 and LIG1 reveals similar rates of the three chemical steps under conditions of saturating Mg^{2+}, but LIG3 has a higher k_{cat}/K_M value for nicked DNA and does not release adenylylated DNA intermediates as readily as LIG1. Unexpectedly, we found that LIG3 does not bind Mg^{2+} as tightly as LIG1, and this weaker binding by LIG3 is most pronounced in the nick-sealing step of catalysis. The apparent Mg^{2+} affinity of ~6 mM required for the stimulation of steady-state ligation catalyzed by LIG3 suggests that LIG3 activity can be regulated by the availability of free Mg^{2+} which is typically between 0.2 and 1 mM in the nucleus and cytosol (43). Intriguingly, mitochondrial Mg^{2+} concentration has been reported to be 10-fold greater than cytosolic Mg^{+2} levels (44), which could contribute to higher LIG3 activity in the mitochondria where it is the sole DNA ligase. This kinetic and thermodynamic framework for LIG3 identifies the different biochemical properties that distinguish it from LIG1, and it will enable future studies investigating the roles of isoform-specific accessory proteins and their contributions to ligase activity.

Results

Purity, stability and adenylylation state of the LIG3 isoforms

Recombinant human DNA LIG3α and LIG3β were purified to homogeneity over four chromatographic steps; phosphocellulose, NTA-Ni^{2+}, Cibacron Blue, and gel filtration (Figure 2.2A). LIG3α and LIG3β eluted at the same salt concentration from the Cibacron Blue (HiTrap Blue) column but eluted at different volumes with gel filtration, consistent with the greater molecular weight of LIG3α. Prior to detailed kinetic studies, the stabilities of LIG3α and LIG3β were investigated at 4 °C and 37 °C using a gel-based DNA ligation assay (Figure A.1). Both

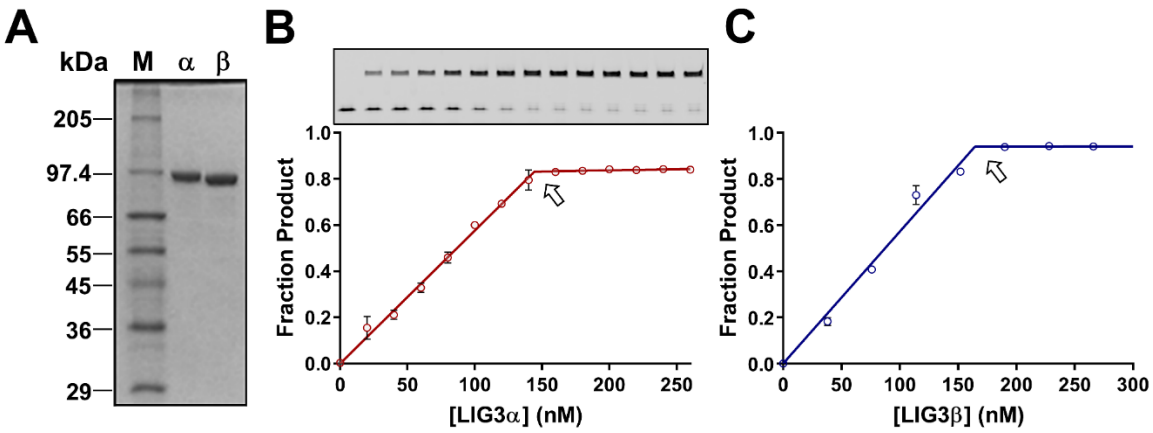

Figure 2.2. Purity and active site titrations of LIG3 isoforms. *A*, 12% SDS-PAGE coomassie stained gel containing 0.5 µg of purified LIG3α and LIG3β with molecular weights of 102.7 and 95.9 kDa (M, protein sizing standards; α, Lig3α; β, Lig3β). *B and C,* representative active site titrations of LIG3α and LIG3β isoform, inset gel shows product (upper bands) and substrate (lower bands). In the absence of ATP, the adenylylated enzyme is limited to a single turnover ligation. Reactions contained 150 nM 28-mer nicked DNA substrate and 20 mM Mg^{2+} (see Methods for details). The equivalence point of the titration (denoted by arrow) indicates the concentration of adenylylated enzyme (data points are the mean ± SD; n=2).

LIG3α and LIG3β maintain activity when stored at 4 °C for more than one month (Figure A.2A). LIG3β is quite stable at 37 °C ($t_{1/2}$ >> 4 hours), however LIG3α is significantly less stable at this temperature ($t_{1/2}$ = 2 hours; Figure A.2B). These findings are consistent with previous reports suggesting LIG3α is less stable than LIG3β (45). Nevertheless, the stability studies established that both LIG3 isoforms are sufficiently stable for rigorous biochemical analysis.

Consistent with a previous report from the Ellenberger lab, we obtained a mixture of adenylylated and deadenylylated recombinant LIG3 from our initial four-step purification scheme (36). Adenylylated enzyme (E-AMP) can be quantified by performing ligation reactions in the absence of ATP, because the number of ligated DNA molecules corresponds to the number of active E-AMP molecules (Figures 2.2B and 2.2C). To assess the adenylylation status of our initial

LIG3 preparations, enzyme samples were preincubated with ATP and $MgCl_2$ to fully adenylylate any deadenylylated enzyme species prior to the addition of the DNA substrate (Figure 2.3A). Under these conditions a pre-steady-state burst was observed followed by a slower steady-state

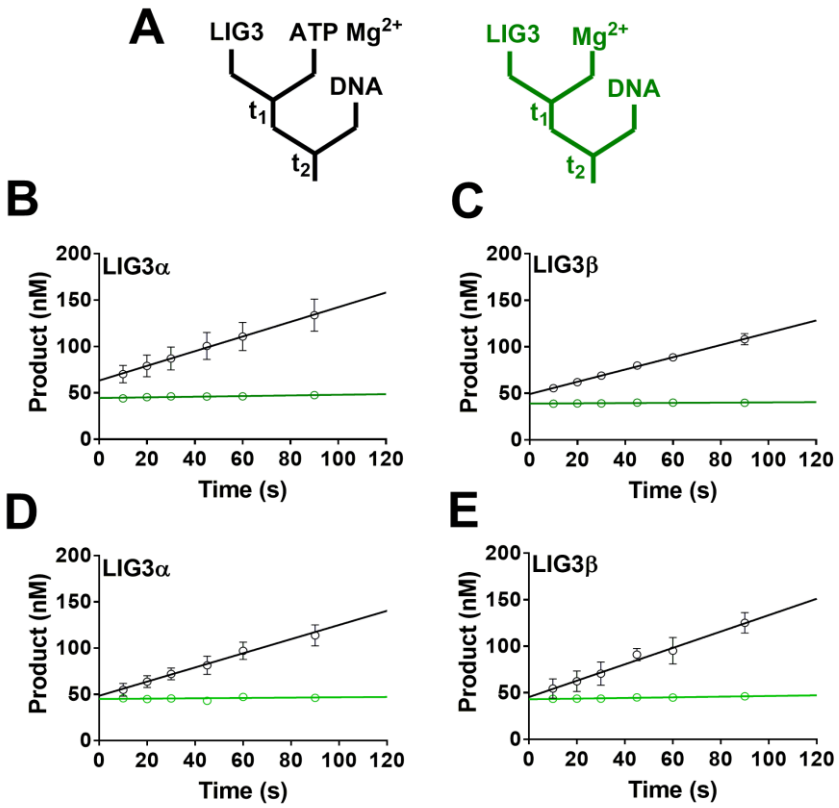

Figure 2.3. Adenylylation state of purified LIG3 isoforms. *A*, schematics for burst experiments. The left (black) scheme indicates that LIG3 was incubated in the presence of ATP and Mg^{2+} to ensure complete enzyme adenylylation prior to the addition of DNA. The scheme to the right (green) displays reaction conditions in which no ATP was added to the reaction solution. Colors of the diagrams correspond to the colors of the linear fits in *B – E*. *B and C*, burst kinetics indicate LIG3α and LIG3β are 73% and 81% adenylylated, respectively. *D and E*, burst kinetics of LIG3α and LIG3β, respectively, after the addition of an adenylylation step during protein purification generates 100% adenylylated protein. Burst experiments after preincubation of LIG3 with ATP and Mg^{2+} did not increase burst amplitude. All experiments contained an estimated 50 nM enzyme, 200 nM DNA and 20 mM Mg^{2+} in the presence and absence of 0.5 μM ATP. Each experiment was completed in triplicate (mean ± SD).

phase (Figures 2.3B-2.3E). Comparison of the burst amplitude with the amplitude of ligation in the absence of ATP allowed us to determine that the preparations of LIG3α and LIG3β were 73% and 81% adenylylated, respectively (Figures 2.3B and 2.3C). The heterogeneity in adenylylation status of the purified ligases was remedied in future purification protocols by treating LIG3 fractions with excess ATP and $MgCl_2$ prior to the final gel filtration step of purification (Figures 2.3D and 2.3E). The LIG3 proteins used in all subsequent experiments were purified using the improved protocol that yields homogeneous adenylylated enzyme.

Substrate dependence of the LIG3 isoforms

Steady-state conditions were used to investigate the substrate dependence of both LIG3 isoforms. The ATP concentration dependencies for multiple-turnover ligation were determined in the presence of saturating Mg^{2+} (20 mM) and saturating nicked DNA substrate (1 μM). The reaction progress curves generated at each ATP concentration were linear in all cases (Figure 2.4A), and the initial rates were plotted as a function of ATP concentration (Figure 2.4B). Fitting the Michaelis-Menten equation (Eq. 2.1) to the ATP dependence data yielded almost identical k_{cat} and $K_{M,ATP}$ values for LIG3α and LIG3β (Table 2.1). These K_M values are roughly three-fold higher than the previously reported value for LIG1 that was obtained under similar reaction conditions (33).

We next examined the concentration dependencies of the nicked DNA substrate, keeping fixed saturating concentrations of ATP (1 mM) and Mg^{2+} (20 mM). Under the standard conditions of 150 mM ionic strength, LIG3β saturated at a very low concentration of DNA ($K_M \leq 5$ nM; Figure A.3). It was not possible to test lower concentrations of DNA using the gel-based fluorescence assay, and therefore the salt concentration was increased to 300 mM (using NaCl) to

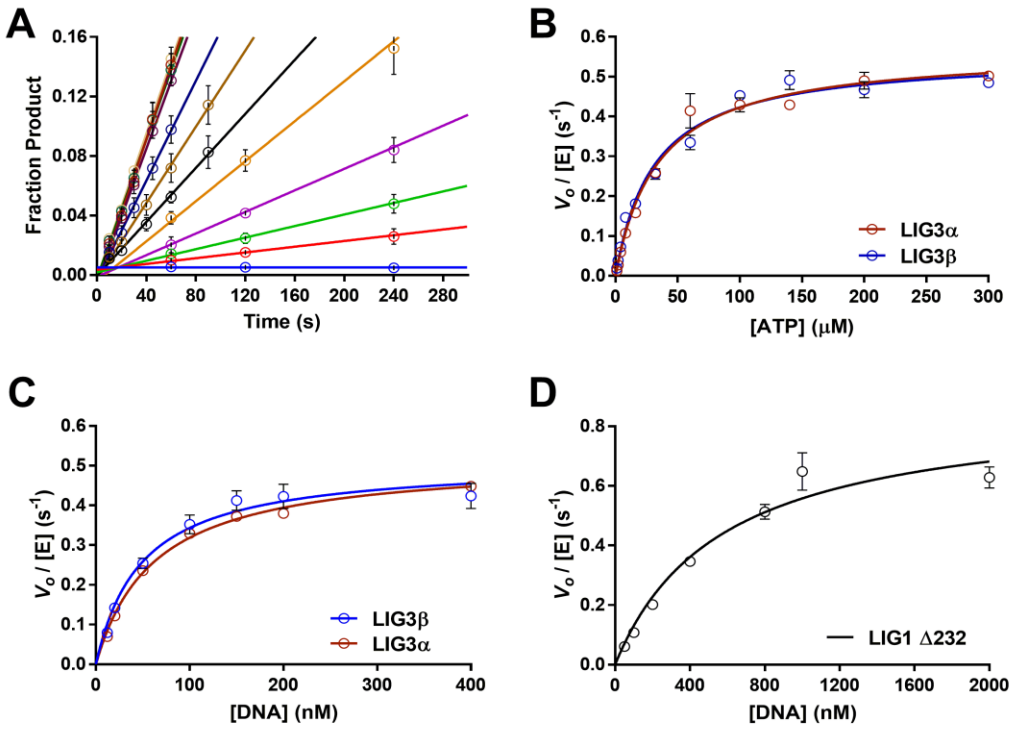

Figure 2.4. Substrate dependence of LIG3α, LIG3β and LIG1. *A*, representative ATP concentration dependence of LIG3β used to determine initial velocities under multiple-turnover conditions. Reactions performed at each ATP concentration (0 – 300 μM) were fit using linear regression to determine initial rates. *B*, ATP dependence was measured under multiple-turnover conditions in the presence of saturating DNA (1 μM) and Mg^{2+} (20 mM). Initial velocities are plotted as a function of ATP concentration and fit using the Michaelis-Menten equation yielding $k_{cat,\,ATP}$ values of 0.57 ± 0.02 s^{-1} and 0.55 ± 0.02 s^{-1} for LIG3α and LIG3β, respectively. The respective $K_{M,\,ATP}$ values are 34 ± 4 μM and 31 ± 3 μM. *C*, DNA dependence was measured at 300 mM ionic strength with 1 mM ATP and 20 mM Mg^{2+}. LIG3α and LIG3β have $k_{cat,\,DNA}$ values of 0.52 ± 0.02 s^{-1} and 0.51 ± 0.03 s^{-1}, and $K_{M,\,DNA}$ values of 62 ± 6 nM and 49 ± 8 nM, respectively. *D*, LIG1 DNA concentration dependence was measured under the same condition as for LIG3 in panel C. The $k_{cat,\,DNA}$ value for LIG1 is 0.87 ± 0.10 s^{-1} and the $K_{M,\,DNA}$ value is 570 ± 170 nM. Each experiment was completed in triplicate (mean ± SD).

weaken the protein-DNA interaction. At this higher salt condition, complete Michaelis-Menten curves were obtained for both of the LIG3 isoforms (Figure 2.4C). LIG3α and LIG3β have K_M values for DNA of ~60 nM and ~50 nM and catalytic efficiency (k_{cat}/K_M) values of 8.4×10^6 $M^{-1}s^{-1}$ and 1.0×10^7 $M^{-1}s^{-1}$, respectively (Table 2.1). The very similar rate constants observed for the two LIG3 isoforms indicate that the C-terminal BRCT domain of LIG3α does not directly affect the

ligation reaction. To compare the catalytic efficiency of LIG3 isoforms to that of LIG1, it was necessary to determine the DNA concentration dependence of LIG1 at the same higher ionic strength conditions (Figure 2.4D). LIG1 is approximately an order of magnitude less efficient than LIG3 under these conditions, with a $K_{M,\,DNA}$ value of 570 nM and a $k_{cat}/K_{M,\,DNA}$ value of 1.5×10^{6} $M^{-1}s^{-1}$ (Table 2.1). The higher catalytic efficiencies of the LIG3 isoforms are primarily due to the decreased $K_{M,\,DNA}$ values.

Mg^{2+} concentration dependence for multiple-turnover ligation

The preceding experiments were performed in the presence of a high concentration of Mg^{2+} (20 mM). This ensures that Mg^{2+}, which is an essential cofactor for DNA ligases, is saturating. Free Mg^{2+} levels in the cell are typically much lower and therefore it is important to investigate the Mg^{2+} dependence on ligation (43). The free Mg^{2+} concentration dependence for multiple-turnover ligation was determined in the presence of saturating ATP and nicked DNA substrate (1 mM ATP, 1 μM DNA). A hyperbolic one site-specific binding equation (Eq. 2.2) fit well to the data, providing the half-maximal concentration of free Mg^{2+} (K_{Mg}) required for ligase activity. Free Mg^{2+} concentrations were calculated using the K_d values for ATP•Mg^{2+} and ATP•$2Mg^{2+}$. It is likely that K_{Mg} is equal to the K_d for Mg^{2+} binding to the enzyme, because dissociation equilibrium constants in the millimolar range are typically indicative of fast dissociation rate constants. The observation that LIG3 is rapidly and efficiently quenched using EDTA on the millisecond timescale is consistent with fast dissociation of Mg^{2+}. The Mg^{2+} dependencies of LIG3α and LIG3β are essentially superimposable and the fits yield similar $k_{cat,\,Mg}$ and K_{Mg} values (Figure 2.5A, Table 2.1). It is striking that the affinity for Mg^{2+} (K_{Mg} ~6 mM) is about 10-fold weaker than was previously observed for LIG1 under similar conditions (Table 2.1).

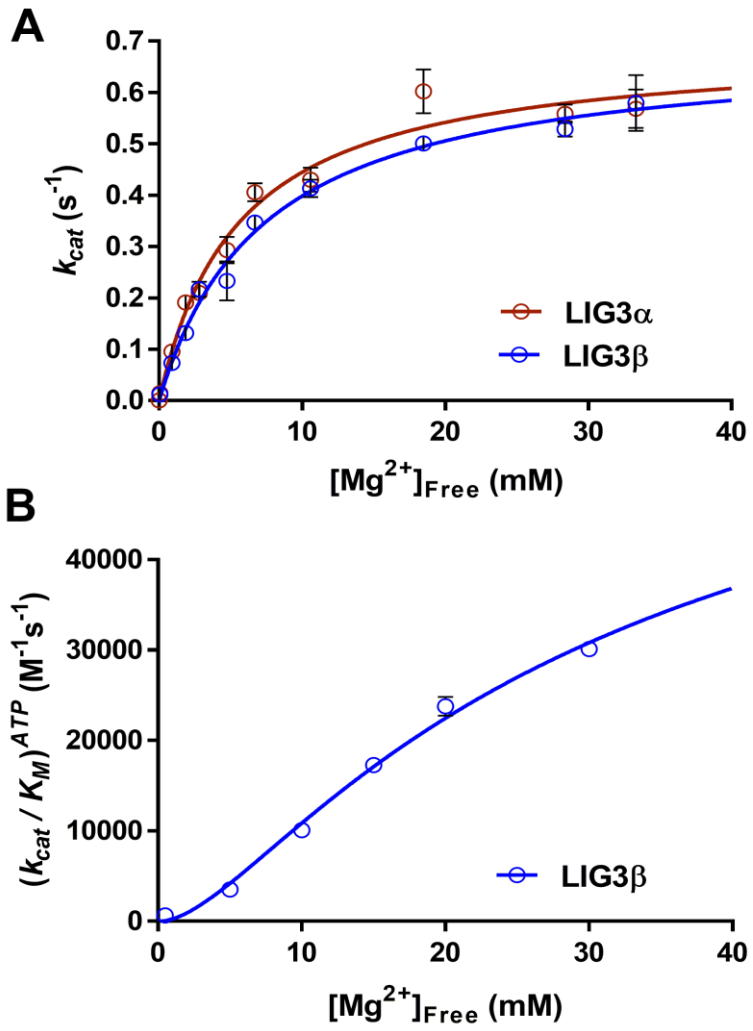

Figure 2.5. Magnesium dependence for multiple-turnover ligation. *A*, reactions contained 1 µM DNA, 1 mM ATP, and the concentration of free Mg^{2+} was varied between 0 and 35 mM. Data were fit using a hyperbolic one site-specific binding equation (Eq. 2.2) yielding maximal $k_{cat, Mg}$ values of 0.69 ± 0.04 s^{-1} and 0.69 ± 0.03 s^{-1}, and K_{Mg} values of 5.6 ± 0.9 mM and 7.4 ± 0.7 mM for LIG3α and LIG3β, respectively. *B*, Investigation of the Mg^{2+} concentration dependence of enzyme adenylylation. The Mg^{2+} concentration dependence was performed using subsaturating ATP concentrations (Figure A.4). The magnesium concentration dependence of $(k_{cat}/K_M)^{ATP}$ for LIG3β was fit using a two metal random binding model (Eq. 2.3). Each experiment was completed in at least triplicate (mean ± SD).

We next determined the catalytic efficiency $(k_{cat}/K_M)^{ATP}$ for LIG3β as a function of Mg^{2+} concentration, which monitors the steps up to and including enzyme adenylylation. This can be most conveniently accomplished by measuring the linear dependence of the reaction rate as a function of ATP concentration when ATP is subsaturating (Figure A.4). The Mg^{2+} dependence of $(k_{cat}/K_M)^{ATP}$ (Figure 2.5B) could not be fit well by a hyperbolic dependence on a single essential Mg^{2+}, but could be better fit by a two-metal ion, random binding model (Eq. 2.3). These data support a two-metal mechanism for the reaction of LIG3 with ATP, analogous to the two-metal ion mechanism proposed for LIG1 (33).

Table 2.1
Comparison of kinetic parameters for multiple turnover ligation by human DNA ligases.[a]

150 mM I	LIG3α	LIG3β	LIG1[b]	Relative LIG3α/LIG3β	Relative LIG1/LIG3β
$k_{cat,\ ATP}$ (s^{-1})	0.57 ± 0.02	0.55 ± 0.02	0.74 ± 0.09	1.0	1.3
$k_{cat,\ Mg}$ (s^{-1})	0.69 ± 0.04	0.69 ± 0.03	0.81 ± 0.10	1.0	1.2
$K_{M,\ ATP}$ (μM)	34 ± 4	31 ± 3	11 ± 3	1.1	0.35
K_{Mg} (mM)	5.6 ± 0.9	7.4 ± 0.7	0.71 ± 0.2	0.76	**0.10**
$k_{cat}/K_{M,\ ATP}$ ($M^{-1}s^{-1}$)	$1.7 \pm 0.2 \times 10^4$	$1.8 \pm 0.2 \times 10^4$	6.7×10^4	0.94	3.7
k_{cat}/K_{Mg} ($M^{-1}s^{-1}$)	120 ± 20	93 ± 10	$1.1 \pm 0.4 \times 10^3$	1.3	**12**
300 mM I	**LIG3α**	**LIG3β**	**LIG1**	**Relative LIG3α/LIG3β**	**Relative LIG1/LIG3β**
$k_{cat,\ DNA}$ (s^{-1})	0.52 ± 0.02	0.51 ± 0.03	0.87 ± 0.10	1.0	1.7
$K_{M,\ DNA}$ (nM)	62 ± 6	49 ± 8	570 ± 170	1.3	**12**
$k_{cat}/K_{M,\ DNA}$ ($M^{-1}s^{-1}$)	$8.4 \pm 0.9 \times 10^6$	$1.0 \pm 0.2 \times 10^7$	$1.5 \pm 0.5 \times 10^6$	0.84	**0.15**

[a]Multiple-turnover parameters were obtained at 150 mM ionic strength (top), and 300 mM ionic strength (bottom). The ATP dependence was determined with 20 mM fixed concentration of Mg^{2+}, and the Mg^{2+} dependence was determined with 1 mM fixed concentration of ATP. [b]LIG1 values at 150 mM NaCl were previously published (33). Error is represented as one standard deviation from the mean (n≥3).

Single-turnover ligation kinetics

Although the LIG3 isoforms exhibited very similar steady-state kinetic parameters, it is possible that larger differences could exist for steps that are not rate-limiting. Therefore, we also performed single-turnover ligation experiments using excess amounts of saturating LIG3α and LIG3β. As previously observed for other DNA ligases, LIG3-catalyzed single-turnover ligation followed a two-step irreversible mechanism. Simultaneous fitting of the substrate, intermediate and product yielded the microscopic rate constants for adenylyl transfer ($k_{obs,\ transfer}$) and nick-sealing ($k_{obs,\ seal}$). At a high concentration of Mg^{2+} (20 mM), LIG3α and LIG3β exhibit almost identical microscopic rate constants for both steps (Figures 2.6A and 2.6B). Given the identical kinetic parameters for the two LIG3 isoforms, and the greater stability of LIG3 β, we chose to perform a comprehensive single-turnover kinetic analysis of LIG3β.

To determine the metal cofactor requirements for each chemical step of ligation, the Mg^{2+} binding affinities and microscopic rate constants were systematically under single-turnover conditions. The observed rate constants for adenylyl transfer (Figure 2.6C) and nick-sealing by LIG3β (Figure 2.6D) are plotted as a function of Mg^{2+} concentration. These data were fit by a hyperbolic dependence to yield the maximal $k_{transfer}$ and k_{seal} rate constants of 0.90 s^{-1} and 18 s^{-1}, respectively (Table 2.2). Using the net rate constants method (Eq. 2.5), the rate constant for enzyme adenylylation ($k_{adenylylation}$) was calculated to be 1.6 s^{-1} (Table 2.2). The rate constants at saturating Mg^{2+} for all three of the chemical steps catalyzed by LIG3β are strikingly similar to the kinetic parameters for LIG1 that were previously obtained under similar reaction conditions. The apparent affinity for Mg^{2+} in the adenylyl transfer step is only 2-fold weaker for LIG3 compared to LIG1 with K_{Mg} values of 0.3 and 0.15 mM, respectively. In contrast, the Mg^{2+} affinity for nick-sealing

is 7-fold weaker for LIG3 as compared to LIG1 with values of 18 mM and 2.6 mM, respectively (Table 2.2).

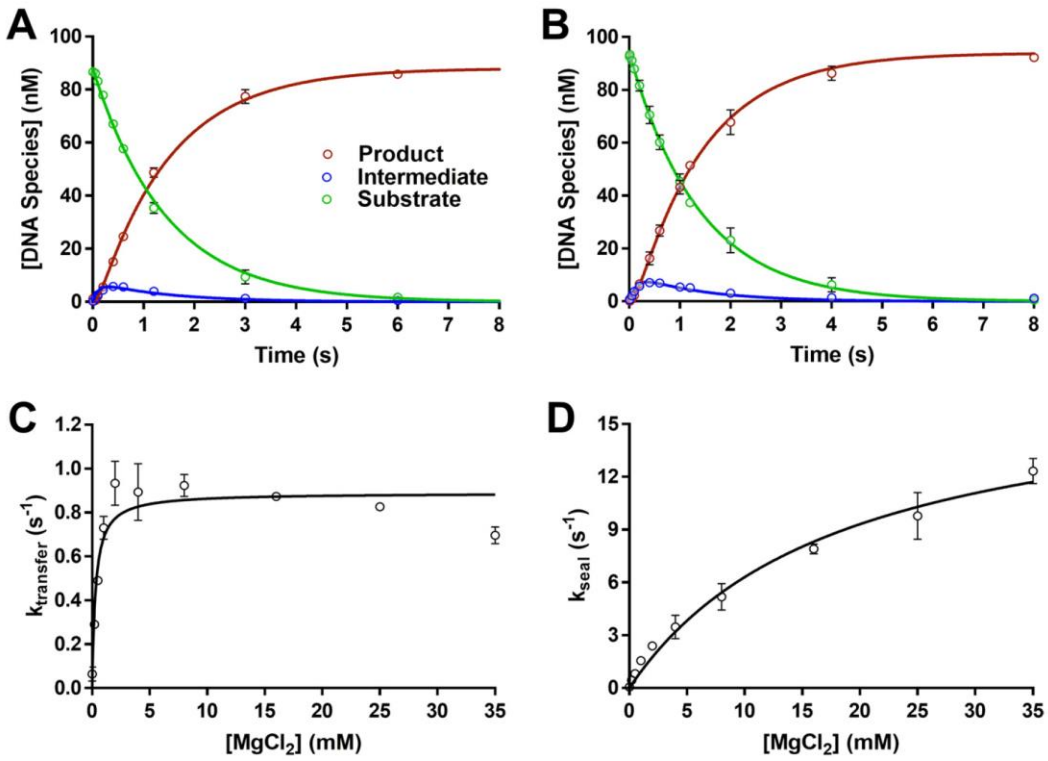

Figure 2.6. Single-turnover ligation kinetics. Representative single turnover kinetics of DNA LIG3α (A) and LIG3β (B) indicate the two enzymes behave similarly under single-turnover conditions at 20 mM Mg^{2+}. Data were fit using a two-step irreversible mechanism using the program Berkeley Madonna. The rate constants for adenylyl transfer are 0.7 s^{-1} and 0.8 s^{-1} and for nick sealing are 8.7 s^{-1} and 8.9 s^{-1} for LIG3α and LIG3β, respectively. Experiments contained 100 nM fluorescein labeled DNA, 600 nM enzyme and 20 mM $MgCl_2$ with no added ATP. *C*, Mg^{2+} concentration dependence for the adenylyl transfer step using LIG3β. *D*, Mg^{2+} concentration dependence of the nick-sealing step for LIG3β. Data were fit using a hyperbolic one site-specific binding equation (Eq. 2) yielding $k_{transfer}$ and k_{seal} values of 0.89 ± 0.03 s^{-1} and 19 ± 6 s^{-1}, respectively. The K_{Mg} values for adenylyl transfer and nick-sealing steps are 0.30 ± 0.06 mM and 18 ± 3 mM, respectively. Each experiment was completed in at least triplicate (mean ± SD).

Table 2.2
Comparison of single-turnover parameters of LIG3β and LIG1[a]

Kinetic parameter	LIG3β	LIG1[b]	Relative LIG1/LIG3β
$k_{adenylylation}$ (s^{-1})[c]	1.6 ± 0.2	1.3 ± 0.3	0.81
$k_{transfer}$ (s^{-1})	0.89 ± 0.03	2.6 ± 0.6	2.9
k_{seal} (s^{-1})	19 ± 6	12 ± 2	0.63
$K_{Mg,\ transfer}$ (mM)	0.30 ± 0.07	0.15 ± 0.06	0.50
$K_{Mg,\ seal}$ (mM)	18 ± 3	2.6 ± 0.9	**0.14**

[a]Single-turnover parameters were obtained at 150 mM ionic strength. All reactions contained 600 nM adenylylated enzyme and 100 nM nicked DNA substrate in the presence of 20 mM Mg^{2+} and absence of ATP.
[b]LIG1 values were previously reported for Δ232 LIG1 under similar experimental conditions (33). [c]The microscopic rate constant for enzyme adenylylation was calculated using a k_{cat} value of 0.55 s^{-1} with the net rate constants equation (Eq. 4). Error is represented as one standard deviation from the mean (n≥3).

Accumulation of adenylylated DNA intermediates

Previous study of LIG1 revealed that this ligase releases adenylylated DNA intermediates under conditions of low free Mg^{2+} concentration (33). LIG1 is quickly adenylylated and cannot rebind the intermediate, resulting in abortive ligation (Figure 2.7A). The propensity for abortive ligation under Mg^{2+}-starved conditions was attributed to differential affinity for Mg^{2+} in the adenylyl transfer and nick-sealing steps (33). As LIG3 shows a similar reduction in Mg^{2+} affinity for nick-sealing as compared to adenylyl transfer steps, we investigated whether LIG3 is also susceptible to abortive ligation on a nicked DNA substrate. Guided by the previous investigation of LIG1, multiple-turnover assays were conducted in the presence of low concentration of free Mg^{2+} (70-fold below K_{Mg}). Analogous ligation reactions using LIG1 were performed for direct comparison between the enzymes. The fraction abortive ligation was calculated for both LIG1 and LIG3β (Eq. 2.4; Figure 2.7B). Whereas 8% of attempted ligation events were aborted by LIG1, only 1% of ligation events were aborted by LIG3β. Thus, LIG3 appears to be less susceptible than LIG1 to abortive ligation of nicked DNA substrates.

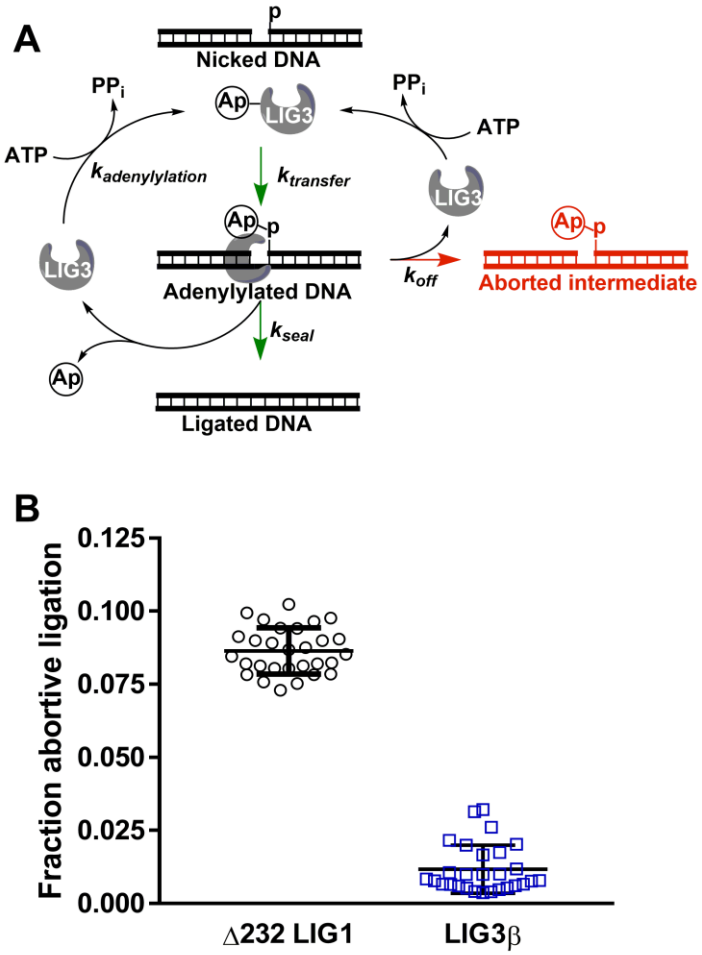

Figure 2.7. Accumulation of adenylylated DNA intermediate. *A,* abortive ligation mechanism observed under Mg^{2+}-starved conditions. Adenylylated ligase interacts with nicked DNA substrates, generating adenylylated DNA intermediate. The partitioning between the nick-sealing steps and abortive ligation is represented with k_{seal} and k_{off}, respectively. Following successful or abortive ligation, ligase becomes adenylylated, preventing the enzyme from rebinding the adenylylated DNA intermediate and completing the nick-sealing step. *B,* propensity of DNA ligases for abortive ligation. Free Mg^{2+} concentrations were 70-fold below K_{Mg} for LIG1 and LIG3β in all experiments. Abortive ligation data represents multiple time points obtained from multiple-turnover time courses conducted in quadruplicate (see methods for details). Error bars indicate one standard deviation from the mean.

Discussion

DNA ligases I and III contain three structurally conserved domains (DBD, NTase and OB-fold domains; Figure 2.1) that each contribute to substrate binding and ligation (32). Despite this high degree of structural homology, LIG1 and LIG3 share only 22% primary sequence identity across these three domains (Figure 2.1B). On the one hand, the high degree of structural homology might indicate similar biochemical activities, but on the other hand, there are numerous substitutions throughout the proteins, including the DNA-binding interfaces of the DBD and OB-fold domains that could lead to distinct biochemical properties. Outside of the core three-domain architecture of the ligases, the human ligases also have unique N- and C-terminal domains that likely influence their localization, protein-protein interactions, and substrate specificity. As a first step toward understanding the biochemical differences between the human DNA ligases, we have characterized recombinant human LIG3α and LIG3β under single- and multiple-turnover conditions and compared the kinetic framework to that of the previously studied human DNA LIG1. This analysis reveals similarities and differences that are relevant to understanding their unique biological functions. Furthermore, this information provides an essential starting point for future studies that explore the functional consequences of mutations in LIG3 as well as the regulatory effects of LIG3 interacting proteins, such as XRCC1.

Recombinant LIG3α was found to be less stable than LIG3β, with a half-life of roughly two hours, as compared to at least four hours for LIG3β in our assay conditions (Figure A.2). This is consistent with the previous findings by the Caldecott group that LIG3α exhibits limited stability *in vivo* and that interaction with XRCC1 is important for stability (45). It remains unclear whether mitochondrial LIG3α requires a mitochondrial-specific protein binding partner or whether it functions as a homodimer (41). Nevertheless, the stability of recombinant Lig3α was sufficient for

a complete *in vitro* kinetic characterization. We found that the two LIG3 isoforms are indistinguishable under all experimental conditions tested using a nicked DNA substrate (Table 2.1). This has implications for mitochondrial DNA ligation and establishes that the different C-termini of the LIG3 isoforms do not change the kinetics of single-strand break ligation.

We can also directly compare the kinetic parameters for the LIG3 isoforms to those of the previously studied LIG1. Comparison of the substrate dependencies of the enzymes under conditions of saturating Mg^{2+} demonstrates that these enzymes have very similar efficiencies for utilization of ATP. However, the LIG3 isoforms have higher catalytic efficiency than LIG1 toward nicked DNA substrates due to the reduced $K_{M,\ DNA}$ of the LIG3 isoforms. These findings are consistent with previous studies suggesting that the ZnF domain of LIG3 contributes to DNA binding during ligation of both single- and double-strand breaks (19,32,35,38). A "jackknife" model for nick recognition has been previously proposed for explaining how LIG3 uses two independent DNA binding domains to bind to a nick (32). Our studies do not directly test this model, but require that the proposed conformational changes upon nick recognition would have to be fast to obtain such similar kinetics for the LIG3 isoforms and LIG1, for LIG1 lacks a ZnF domain (Figure 2.1A). These overall similarities in the rates of the chemical steps at saturating Mg^{2+} concentration are consistent with the strong conservation of the active site architecture (Figure 2.1B).

Surprisingly, LIG3 requires a much higher concentration of Mg^{2+} cofactor to achieve maximal activity as compared to LIG1. The structural basis for this biochemical difference is unknown, but the observation of an approximate 10-fold reduction in K_{Mg} for steady-state ligation raises the possibility that this difference in Mg^{2+} affinity is biologically relevant. The free Mg^{2+} concentration in nuclei has been estimated to be between 0.2 – 2 mM, which would be

subsaturating for LIG3 and lead to suppressed catalytic activity (46). In contrast, recent studies have suggested that mitochondria have up to 10-fold higher concentration of free Mg^{2+} compared to the cytosol (44). We speculate that this difference in Mg^{2+} affinity could reflect an adaption to limit LIG3 activity in the nucleus where multiple ligases are present and yet allow for high catalytic activity in the mitochondria where it is the sole DNA ligase.

The weaker affinity of LIG3 for Mg^{2+} is most apparent in the adenylylation step and in the nick-sealing step of the reaction, while the adenylyl transfer step is more similar for LIG3 and LIG1 (Table 2.2). These differences in Mg^{2+} affinity in the different steps of the reaction leads to a greater buildup of adenylylated intermediate for LIG3 (Figure A.5) as compared to LIG1 at a physiological free Mg^{2+} concentration of 1 mM. Nevertheless, LIG3 is more efficient at ligation than LIG1 under conditions of low free Mg^{2+} and LIG3 is not susceptible to abortive ligation on a normal nick (Figure 2.7). As abortive ligation involves the release of adenylylated DNA intermediate, we can infer that LIG3 must have greater DNA binding affinity as compared to LIG1.

Conclusions

This study provides the foundational kinetic and thermodynamic framework for ligation of single-strand breaks catalyzed by the LIG3 isoforms. We suggest that the BRCT domain of LIG3α does not contribute to ligation of single-strand breaks, revealing nearly identical kinetic parameters for the LIG3 isoforms. The LIG3 isoforms differ from LIG1 in their substrate and Mg^{2+} dependencies, despite a high degree of structural similarity in the catalytic domain. The kinetic and thermodynamic framework presented here for LIG3 will facilitate future investigations of the functional differences between human DNA ligases and their variants.

Experimental procedures

Expression and purification of LIG3 isoforms

Full-length human DNA LIG3α and LIG3β cDNAs were cloned into a modified pET28 plasmid containing an N-terminal His_6-SUMO tag, and the open reading frames were confirmed by Sanger sequencing of both strands. The enzymes were expressed in *E. coli* C41 pRare 2 cells. Bacterial cultures were grown in LB and induced at an OD_{600} of 0.6 using 300 µM IPTG followed by an incubation at 16 °C for 24 hours at 230 RPM. Cells were harvested via centrifugation at 6,000 RFC for 20 minutes at 4 °C. Pellets were suspended in lysis buffer (50 mM Tris, pH 7.5, 300 mM NaCl, 3 mM EDTA, 10 mM BME, 10% glycerol, 1 mM benzamidine-HCl and 1 mM PMSF) and stored at -80 °C. Prior to purification, cells were thawed and lysed by three passages through a cell homogenizer. Lysates were clarified by centrifugation for 1 hour at 39,000 RFC at 4 °C and further clarified using a 0.45 µm filter. All purification steps were performed at 4 °C. The clarified lysate was loaded onto a cellulose phosphate column (Sigma) equilibrated with purification buffer (50 mM Tris, pH 7.5, 10% glycerol, 2 mM BME) containing 250 mM NaCl and 3 mM EDTA. The enzyme was eluted with purification buffer containing 2 M NaCl then loaded onto a HisTrap HP column (GE Healthcare) equilibrated with purification buffer containing 1 M NaCl and 20 mM imidazole. Loaded protein was washed using 200 mM NaCl and 20 mM imidazole and then eluted using a linear imidazole gradient of 20 to 600 mM. Ligase containing fractions were pooled and the His_6-SUMO tag digested using ubiquitin-like protease (ULP1) prior to loading onto a HiTrap Blue column (GE Healthcare) equilibrated with purification buffer containing 200 mM NaCl. The bound protein was eluted using a linear gradient of 200 mM – 2 M NaCl. Protein containing fractions were collected and concentrated using 30K MWCO Amicon Ultra concentrators. To ensure the purified protein was 100% adenylylated, 20 mM $MgCl_2$ and 1

mM ATP were added to the concentrated HiTrap Blue fractions and incubated for 30 minutes on ice. Purification buffer was exchanged with LIG3 storage buffer (50 mM NaMOPS, pH 7.5, 300 mM NaCl, 10% glycerol, 1 mM TCEP) over a Superdex S200 26/60 gel filtration column. Protein containing fractions were collected and concentrated to 40 mg/mL, snap frozen using liquid nitrogen, and stored at -80 °C. The purity of the ligase isoforms was greater than 95% as judged by SDS-PAGE (Figure 2.2A). Human DNA ligase I (LIG1) was prepared as previously described (33).

DNA substrates

Oligonucleotides were obtained from Integrated DNA Technologies (IDT) and purified using 15% polyacrylamide, 8 M urea DNA sequencing gels as previously described (33). The double stranded nicked DNA substrate used throughout this study was generated by annealing the following oligonucleotides: 5′-CCGAATCAGTCCGACGACGCATCAGCAC, 5′-GTGCTGATGCGTC and 5′P-GTCGGACTGATTCGG-FAM, where P indicates the presence of a 5′-phosphate, and FAM indicates the presence of 3′-fluorescein. The oligonucleotides were annealed at equimolar equivalents in annealing buffer (10 mM NaMES, pH 6.5, 50 mM NaCl) by heating the solution to 95 °C and cooling to 4 °C at a rate of 12 °C per minute.

Gel-based ligation assay

All single- and multiple-turnover reactions were performed at 37 °C, in standard reaction buffer (50 mM NaMOPS, pH 7.5, 10 % glycerol, 1 mM TCEP, 100 μg/mL BSA (MP Biomedicals)) at an ionic strength of 150 mM unless otherwise stated. Multiple-turnover ligation reactions were quenched at designated times into quench solution (90% formamide, 50 mM

EDTA, 0.006% bromophenol blue, 0.006% xylene cyanol). Single-turnover experiments were quenched using 0.2 M NaOH, followed by 2-fold dilution into the quench solution described above. Quenched samples were incubated at 95 °C for 3 minutes, snap cooled using ice water then loaded onto a 15% (w/v) polyacrylamide, 8 M urea, 1X TBE DNA denaturing gel. Gels were scanned using a Typhoon Trio^{+} imager (GE Healthcare) set to monitor excitation at 488 nm and emission through a 520 nm band-pass filter. DNA substrate, intermediate, and product bands were quantified using ImageQuant TL (GE Healthcare). Data were plotted and analyzed using GraphPad Prism.

Multiple-turnover kinetics

Steady-state reactions were performed in standard reaction buffer at 150 mM ionic strength unless otherwise stated. Multiple-turnover reaction volumes were 30 µL, from which 3 µL was quenched into 30 µL quench solution at designated times. Initial rates were determined by the linear rate of product formation within the first 10% of product formation. Results represent the average of least three independent experiments. Burst experiments contained an estimated 50 nM ligase and 200 nM DNA. LIG3 isoforms were preincubated in the absence and presence of 20-fold greater molar concentration of ATP in the presence of 20 mM Mg^{2+} for 1 hour on ice followed by 10 minutes at 37 °C. Following the enzyme adenylylation incubations, samples were diluted 500-fold to achieve reaction concentrations prior to mixing with DNA. Adenylylation state was determined by comparison between ATP treated and ATP omitted samples. Burst amplitudes are proportional to adenylylated enzyme concentration. The ATP concentration dependencies of the LIG3 isoforms were investigated using 5 nM enzyme in the presence of saturating Mg^{2+} (20 mM) and saturating 28mer DNA (1 µM) while adjusting ATP concentrations between 0 and 300 µM.

The initial rates (V_0/[E]) were plotted as a function of ATP concentration and fit using the Michaelis-Menten equation (Eq. 2.1). The free Mg^{2+} concentration dependence (0-35 mM) was investigated under both saturating and subsaturating ATP concentrations. Free Mg^{2+} concentrations were calculated using K_d values for ATP•Mg^{2+} and ATP•2Mg^{2+} of 12 μM and 17 mM as previously described (33,47). In the presence of saturating ATP (1 mM), the initial rates were fit by a hyperbolic curve (Eq. 2.2). In the presence of subsaturating ATP (0.5, 1, 2 μM), $(k_{cat}/K_M)^{ATP}$ values were generated and plotted as a function of Mg^{2+} concentrations revealing cooperative enzymatic behavior that best fit to a two-site random binding model (Eq. 2.3). The DNA concentration dependence for multiple-turnover ligation was obtained using standard reaction buffer at ionic strengths of 150 mM and 300 mM. DNA concentration dependencies of LIG1 and LIG3 were compared under the 300 mM ionic strength reaction conditions. Reactions contained 5 nM enzyme, 1 mM ATP, 20 mM Mg^{2+} and 0.02-1 μM nicked DNA substrate. Initial rates versus DNA concentration data were fit to the Michaelis-Menten equation (Eq. 2.1).

$$\frac{V_{init}}{[E]} = \frac{k_{cat} \times [S]}{(K_M + [S])} \qquad \text{(Eq. 2.1)}$$

$$\frac{V_{init}}{[E]} = \frac{k_{cat} \times [Mg^{2+}]}{(K_M + [Mg^{2+}])} \qquad \text{(Eq. 2.2)}$$

$$\left(\frac{k_{cat}}{K_M}\right)^{ATP} = \frac{\left(\frac{k_{cat}}{K_M}\right)^{ATP}_{Max}}{\frac{K_1 * K_2}{[Mg^{2+}]^2} + \frac{K_1 + K_2}{[Mg^{2+}]} + 1} \qquad \text{(Eq. 2.3)}$$

Quantifying adenylylated DNA intermediate

Ligation experiments were performed under multiple-turnover conditions (5 nM LIG1 or LIG3β, 200 nM nicked DNA) in standard reaction buffer. Using LIG1 as previously described (33), the accumulation of abortive ligation intermediates was observed when free Mg^{2+} concentration was 70-fold below its respective K_{Mg} value. Free Mg^{2+} concentrations were calculated as described above. Accumulation of abortive ligation intermediates was investigated using 1 mM Mg^{2+} and the ATP concentration was adjusted to achieve a free Mg^{2+} concentration that was 70-fold below the individually measured K_{Mg} values for LIG1 and LIG3. 2 mM ATP was required to achieve 10.5 μM free Mg^{2+} in the case of LIG1, whereas 1 mM ATP was needed to achieve 98 μM free Mg^{2+} in the LIG3β containing reactions. The fraction of aborted ligation events was calculated from the concentration of intermediate (I) and product (P) formed under the free Mg^{2+}-starved conditions at various points during the initial rates portion of the ligation reaction (Eq. 2.4).

$$Fraction\ abortive\ ligation = \frac{[I]}{([I]+[P])} \qquad \text{(Eq. 2.4)}$$

Single-turnover ligation kinetics

Single-turnover ligation kinetics were investigated using a KinTek RFQ-3 rapid mixing apparatus. Reaction times varied from 5 ms to 10 min. Experiments were performed by rapidly mixing equal volumes of 1.2 μM LIG3, and 200 nM nicked DNA substrate to generate 600 nM enzyme and 100 nM substrate. Enzyme and substrate concentrations were varied to ensure single-turnover conditions were saturating (data not shown). For experiments investigating the

magnesium dependence for adenylyl transfer and nick-sealing steps of catalysis, ionic strength was calculated using the Debye-Hückel theory of electrolytes and held constant at 150 mM using NaCl. Samples were allowed to equilibrate at 37 °C for at least 1 minute prior to each reaction. Reactions were allowed to age for predetermined times and the reactions stopped using 200 mM NaOH, because the aforementioned quench solution used for multiple-turnover ligation kinetics was not sufficient to stop catalysis at 5 ms after mixing (Figure A.6). NaOH quenched samples were diluted 2-fold in formamide quench solution and processed as previously described (33). The observed rates of adenylyl transfer and nick-sealing were plotted as a function of Mg^{2+} concentration and fit using a hyperbolic single-site binding equation (Eq. 2.2). The concentrations of total and free Mg^{2+} were assumed equal due to the absence of ATP in the single-turnover reactions. The value of $k_{adenylylation}$ was calculated using the net rate constant method (k_{cat} = 0.55 s^{-1}; Eq. 2.5).

$$\frac{1}{k_{cat}} = \frac{1}{k_{adenylylation}} + \frac{1}{k_{transfer}} + \frac{1}{k_{seal}} \qquad \text{(Eq. 2.5)}$$

References

1. Bentley, D., Selfridge, J., Millar, J. K., Samuel, K., Hole, N., Ansell, J. D., and Melton, D. W. (1996) DNA ligase I is required for fetal liver erythropoiesis but is not essential for mammalian cell viability. *Nat. Genet.* **13**, 489-491

2. Bentley, D. J., Harrison, C., Ketchen, A. M., Redhead, N. J., Samuel, K., Waterfall, M., Ansell, J. D., and Melton, D. W. (2002) DNA ligase I null mouse cells show normal DNA repair activity but altered DNA replication and reduced genome stability. *J. Cell Sci.* **115**, 1551-1561

3. Puebla-Osorio, N., Lacey, D. B., Alt, F. W., and Zhu, C. (2006) Early Embryonic Lethality Due to Targeted Inactivation of DNA Ligase III. *Mol. Cell. Biol.* **26**, 3935-3941

4. Barnes, D. E., Stamp, G., Rosewell, I., Denzel, A., and Lindahl, T. (1998) Targeted disruption of the gene encoding DNA ligase IV leads to lethality in embryonic mice. *Curr. Biol.* **8**, 1395-1398

5. Frank, K. M., Sekiguchi, J. M., Seidl, K. J., Swat, W., Rathbun, G. A., Cheng, H. L., Davidson, L., Kangaloo, L., and Alt, F. W. (1998) Late embryonic lethality and impaired V(D)J recombination in mice lacking DNA ligase IV. *Nature* **396**, 173-177

6. Barnes, D. E., Tomkinson, A. E., Lehmann, A. R., Webster, A. D., and Lindahl, T. (1992) Mutations in the DNA ligase I gene of an individual with immunodeficiencies and cellular hypersensitivity to DNA-damaging agents. *Cell* **69**, 495-503

7. O'Driscoll, M., Cerosaletti, K. M., Girard, P. M., Dai, Y., Stumm, M., Kysela, B., Hirsch, B., Gennery, A., Palmer, S. E., Seidel, J., Gatti, R. A., Varon, R., Oettinger, M. A., Neitzel, H., Jeggo, P. A., and Concannon, P. (2001) DNA ligase IV mutations identified in patients exhibiting developmental delay and immunodeficiency. *Mol. Cell* **8**, 1175-1185

8. Girard, P. M., Kysela, B., Harer, C. J., Doherty, A. J., and Jeggo, P. A. (2004) Analysis of DNA ligase IV mutations found in LIG4 syndrome patients: the impact of two linked polymorphisms. *Hum. Mol. Genet.* **13**, 2369-2376

9. Petrini, J. H., Xiao, Y., and Weaver, D. T. (1995) DNA ligase I mediates essential functions in mammalian cells. *Mol. Cell. Biol.* **15**, 4303-4308

10. Masani, S., Han, L., Meek, K., and Yu, K. (2016) Redundant function of DNA ligase 1 and 3 in alternative end-joining during immunoglobulin class switch recombination. *Proc. Natl. Acad. Sci. U. S. A.* **113**, 1261-1266

11. Lu, G., Duan, J., Shu, S., Wang, X., Gao, L., Guo, J., and Zhang, Y. (2016) Ligase I and ligase III mediate the DNA double-strand break ligation in alternative end-joining. *Proc. Natl. Acad. Sci. U. S. A.* **113**, 1256-1260

12. Han, L., Masani, S., Hsieh, C. L., and Yu, K. (2014) DNA ligase I is not essential for mammalian cell viability. *Cell Rep* **7**, 316-320

13. Simsek, D., Furda, A., Gao, Y., Artus, J., Brunet, E., Hadjantonakis, A.-K., Van Houten, B., Shuman, S., McKinnon, P. J., and Jasin, M. (2011) Crucial role for DNA ligase III in mitochondria but not in Xrcc1-dependent repair. *Nature* **471**, 245-248

14. Gao, Y., Katyal, S., Lee, Y., Zhao, J., Rehg, J. E., Russell, H. R., and McKinnon, P. J. (2011) DNA ligase III is critical for mtDNA integrity but not Xrcc1-mediated nuclear DNA repair. *Nature* **471**, 240-244

15. Arakawa, H., Bednar, T., Wang, M. L., Paul, K., Mladenov, E., Bencsik-Theilen, A. A., and Iliakis, G. (2012) Functional redundancy between DNA ligases I and III in DNA replication in vertebrate cells. *Nucleic Acids Res.* **40**, 2599-2610

16. Lakshmipathy, U., and Campbell, C. (1999) The Human DNA Ligase III Gene Encodes Nuclear and Mitochondrial Proteins. *Mol. Cell. Biol.* **19**, 3869-3876

17. Caldecott, K. W., McKeown, C. K., Tucker, J. D., Ljungquist, S., and Thompson, L. H. (1994) An interaction between the mammalian DNA repair protein XRCC1 and DNA ligase III. *Mol. Cell. Biol.* **14**, 68-76

18. Caldecott, K. W., Tucker, J. D., Stanker, L. H., and Thompson, L. H. (1995) Characterization of the XRCC1-DNA ligase III complex in vitro and its absence from mutant hamster cells. *Nucleic Acids Res.* **23**, 4836-4843

19. Caldecott, K. W., Aoufouchi, S., Johnson, P., and Shall, S. (1996) XRCC1 Polypeptide Interacts with DNA Polymerase β and Possibly Poly (ADP-Ribose) Polymerase, and DNA Ligase III Is a Novel Molecular 'Nick-Sensor' In Vitro. *Nucleic Acids Res.* **24**, 4387-4394

20. Nash, R. A., Caldecott, K. W., Barnes, D. E., and Lindahl, T. (1997) XRCC1 Protein Interacts with One of Two Distinct Forms of DNA Ligase III. *Biochemistry* **36**, 5207-5211

21. Taylor, R. M., Wickstead, B., Cronin, S., and Caldecott, K. W. (1998) Role of a BRCT domain in the interaction of DNA ligase III-α with the DNA repair protein XRCC1. *Curr. Biol.* **8**, 877-880

22. Perez-Jannotti, R. M., Klein, S. M., and Bogenhagen, D. F. (2001) Two Forms of Mitochondrial DNA Ligase III Are Produced inXenopus laevis Oocytes. *J. Biol. Chem.* **276**, 48978-48987

23. Mackey, Z. B., Ramos, W., Levin, D. S., Walter, C. A., McCarrey, J. R., and Tomkinson, A. E. (1997) An alternative splicing event which occurs in mouse pachytene spermatocytes generates a form of DNA ligase III with distinct biochemical properties that may function in meiotic recombination. *Mol. Cell. Biol.* **17**, 989-998

24. Simsek, D., Brunet, E., Wong, S. Y.-W., Katyal, S., Gao, Y., McKinnon, P. J., Lou, J., Zhang, L., Li, J., Rebar, E. J., Gregory, P. D., Holmes, M. C., and Jasin, M. (2011) DNA Ligase III Promotes Alternative Nonhomologous End-Joining during Chromosomal Translocation Formation. *PLoS Genetics* **7**

25. Badie, S., Carlos, A. R., Folio, C., Okamoto, K., Bouwman, P., Jonkers, J., and Tarsounas, M. (2015) BRCA1 and CtIP promote alternative non-homologous end-joining at uncapped telomeres. *EMBO J.* **34**, 828

26. Jones, R. E., Oh, S., Grimstead, J. W., Zimbric, J., Roger, L., Heppel, N. H., Ashelford, K. E., Liddiard, K., Hendrickson, E. A., and Baird, D. M. (2014) Escape from telomere-driven crisis is DNA ligase III dependent. *Cell Rep* **8**, 1063-1076

27. Newman, E. A., Lu, F., Bashllari, D., Wang, L., Opipari, A. W., and Castle, V. P. (2015) Alternative NHEJ Pathway Components Are Therapeutic Targets in High-Risk Neuroblastoma. *Mol. Cancer Res.* **13**, 470-482

28. Tomkinson, A. E., Howes, T. R., and Wiest, N. E. (2013) DNA ligases as therapeutic targets. *Transl Cancer Res* **2**

29. Tobin, L. A., Robert, C., Nagaria, P., Chumsri, S., Twaddell, W., Ioffe, O. B., Greco, G. E., Brodie, A. H., Tomkinson, A. E., and Rassool, F. V. (2012) Targeting abnormal DNA repair in therapy-resistant breast cancers. *Mol. Cancer Res.* **10**, 96-107

30. Tobin, L. A., Robert, C., Rapoport, A. P., Gojo, I., Baer, M. R., Tomkinson, A. E., and Rassool, F. V. (2013) Targeting abnormal DNA double-strand break repair in tyrosine kinase inhibitor-resistant chronic myeloid leukemias. *Oncogene* **32**, 1784-1793

31. Pascal, J. M., O'Brien, P. J., Tomkinson, A. E., and Ellenberger, T. (2004) Human DNA ligase I completely encircles and partially unwinds nicked DNA. *Nature* **432**, 473-478

32. Cotner-Gohara, E., Kim, I.-K., Hammel, M., Tainer, J. A., Tomkinson, A. E., and Ellenberger, T. (2010) Human DNA Ligase III Recognizes DNA Ends by Dynamic Switching between Two DNA-Bound States. *Biochemistry* **49**, 6165-6176

33. Taylor, M. R., Conrad, J. A., Wahl, D., and O'Brien, P. J. (2011) Kinetic Mechanism of Human DNA Ligase I Reveals Magnesium-dependent Changes in the Rate-limiting Step That Compromise Ligation Efficiency. *J. Biol. Chem.* **286**, 23054-23062

34. Ellenberger, T., and Tomkinson, A. E. (2008) Eukaryotic DNA Ligases: Structural and Functional Insights. *Annu. Rev. Biochem.* **77**, 313-338

35. Cotner-Gohara, E., Kim, I.-K., Tomkinson, A. E., and Ellenberger, T. (2008) Two DNA-binding and Nick Recognition Modules in Human DNA Ligase III. *J. Biol. Chem.* **283**, 10764-10772

36. Kukshal, V., Kim, I. K., Hura, G. L., Tomkinson, A. E., Tainer, J. A., and Ellenberger, T. (2015) Human DNA ligase III bridges two DNA ends to promote specific intermolecular DNA end joining. *Nucleic Acids Res.* **43**, 7021-7031

37. Taylor, R. M., Whitehouse, J., Caldecott, K. W., Cappelli, E., and Frosina, G. (1998) Role of the DNA ligase III zinc finger in polynucleotide binding and ligation. *Nucleic Acids Res.* **26**, 4804-4810

38. Mackey, Z. B., Niedergang, C., Murcia, J. M.-d., Leppard, J., Au, K., Chen, J., Murcia, G. d., and Tomkinson, A. E. (1999) DNA Ligase III Is Recruited to DNA Strand Breaks by a Zinc Finger Motif Homologous to That of Poly(ADP-ribose) Polymerase Identification of Two Functionally Distinct DNA Binding Regions Within DNA Ligase III. *J. Biol. Chem.* **274**, 21679-21687

39. Taylor, R. M., Whitehouse, C. J., and Caldecott, K. W. (2000) The DNA ligase III zinc finger stimulates binding to DNA secondary structure and promotes end joining. *Nucleic Acids Res.* **28**, 3558-3563

40. Tomkinson, A. E., and Sallmyr, A. (2013) Structure and function of the DNA ligases encoded by the mammalian LIG3 gene. *Gene* **531**, 150-157

41. Lakshmipathy, U., and Campbell, C. (2000) Mitochondrial DNA ligase III function is independent of Xrcc1. *Nucleic Acids Res.* **28**, 3880-3886

42. Tomkinson, A. E., Vijayakumar, S., Pascal, J. M., and Ellenberger, T. (2006) DNA Ligases: Structure, Reaction Mechanism, and Function. *Chem. Rev.* **106**, 687-699

43. Romani, A. M. (2011) Cellular magnesium homeostasis. *Arch. Biochem. Biophys.* **512**, 1-23

44. Gout, E., Rebeille, F., Douce, R., and Bligny, R. (2014) Interplay of Mg2+, ADP, and ATP in the cytosol and mitochondria: unravelling the role of Mg2+ in cell respiration. *Proc. Natl. Acad. Sci. U. S. A.* **111**, E4560-4567

45. Taylor, R. M., Moore, D. J., Whitehouse, J., Johnson, P., and Caldecott, K. W. (2000) A Cell Cycle-Specific Requirement for the XRCC1 BRCT II Domain during Mammalian DNA Strand Break Repair. *Mol. Cell. Biol.* **20**, 735-740

46. Gunther, T. (2006) Concentration, compartmentation and metabolic function of intracellular free Mg2+. *Magnes. Res.* **19**, 225-236

47. Cherepanov, A. V., and de Vries, S. (2003) Kinetics and thermodynamics of nick sealing by T4 DNA ligase. *Eur. J. Biochem.* **270**, 4315-4325

Appendix A

Additional figures to support Chapter 2

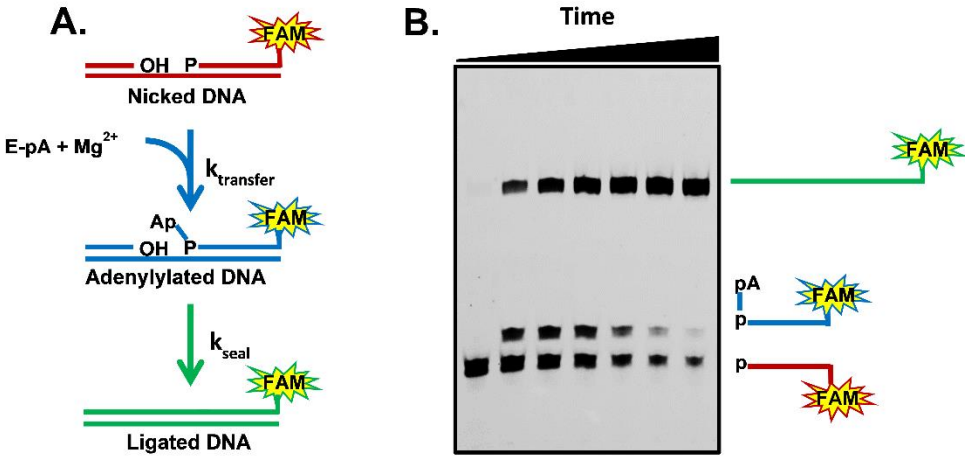

Figure A.1. Gel-based ligation assay. *A*, reaction schematic illustrating observable species of single turnover ligation. The 28-mer DNA substrate has a 3' positioned fluorescein label (FAM) allowing for the detection of all species. $k_{transfer}$ is the rate at which the adenylyl group is transferred from the enzyme to the 5'-phosphate at the nick. k_{seal} is the rate at which the 3'-hydroxyl at the nick attacks the neighboring 5'-phosphate resulting in the release of the adenylyl leaving group upon formation of the phosphodiester bond. *B*, representative 15 % polyacrylamide, 8 M urea DNA sequencing gel indicating substrate (red), intermediate (blue) and product (green) species in a single-turnover ligation experiment. For single-turnover experiments: Reactions contained 600 nM ligase, 100 nM of duplex 28-mer nicked DNA substrate, in standard reaction buffer at 150 mM ionic strength. For multiple-turnover experiments: Reactions contained 5 nM ligase and 1 μM duplex 28-mer nicked DNA substrate (unless otherwise stated) in the presence of 1 mM ATP and 20 mM Mg^{2+} (unless otherwise stated). Multiple-turnover experiments did not accumulate detectable intermediate (blue). Intermediate accumulation was quantified when investigating abortive properties of LIG1 and LIG3β.

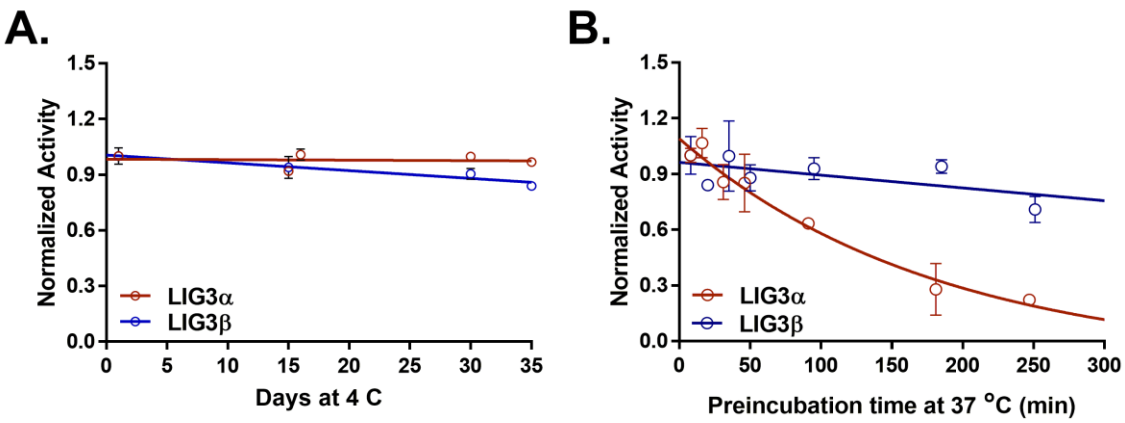

Figure A.2. Stability of LIG3 isoforms. *A*, stability of LIG3 isoforms when stored at 4 °C. *B*, LIG3 stability at 37 °C. Ligase activity was investigated by analyzing the initial velocities of samples stored at 4 or 37 °C. DNA ligases retain almost all activity over the course of a month when stored at 4 °C. However, at 37 °C, LIG3α has a half-life of two hours and the half-life of LIG3β is greater than four hours. LIG3 activity was measured after pre-incubating concentrated enzyme stocks (4 °C in storage buffer) or 5 nM enzyme (37 °C in reaction buffer) at various times followed by analyzing initial rates in the presence of 1 μM DNA. Initial velocities were normalized by dividing the initial rate of the pre-incubated enzyme at 37 °C, by the initial rate of enzyme under normal assaying procedures (1 minute pre-incubation at 37 °C). Normalized rates were plotted as a function of pre-incubation time and an exponential decay equation was fit to the data.

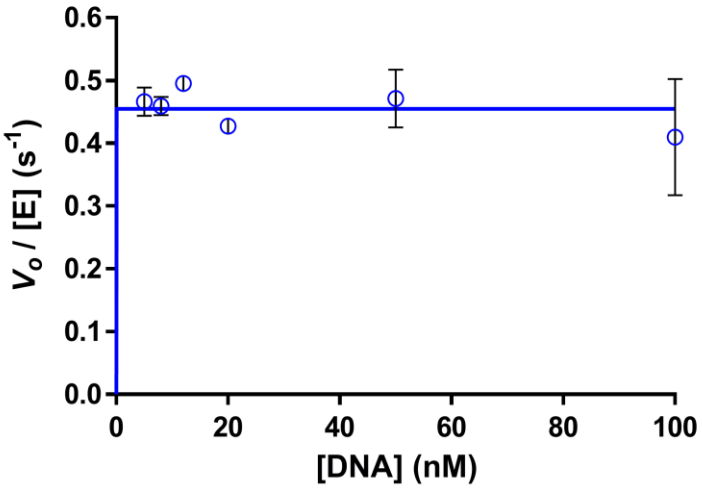

Figure A.3. DNA dependence for LIG3β at 150 mM ionic strength. DNA concentration dependence was measured for multiple-turnover ligation in the standard reaction buffer with saturating ATP (1 mM), saturating Mg^{2+} (20 mM), and 1 nM LIG3β. Ionic strength was adjusted to 150 mM using NaCl and reactions were performed at 37 ºC. These data reveal that the value for $K_{M,\,DNA}$ is less than 5 nM under these conditions and limitations in fluorescence detection prevented lower concentrations of DNA from being tested.

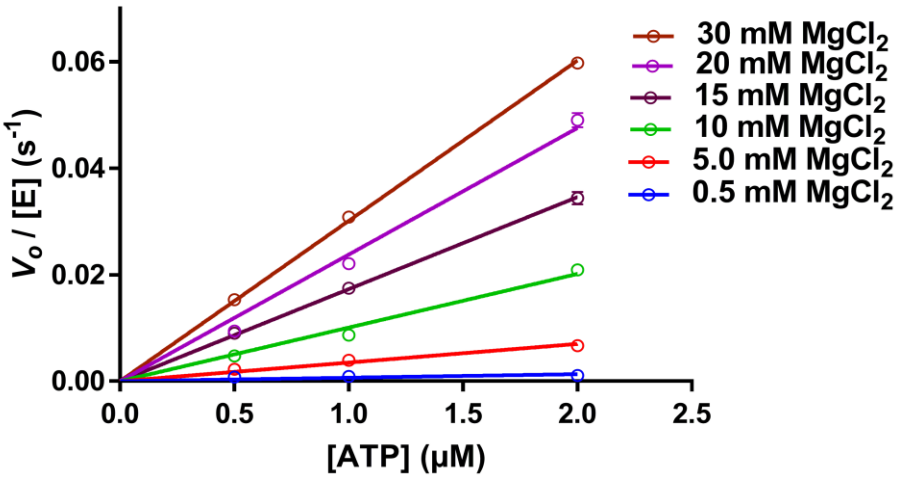

Figure A.4. Measurements of k_{cat}/K_M for utilization of ATP $(k_{cat}/K_M)^{ATP}$ by LIG3β. Reactions contained 5 nM LIG3β and 500 nM 28-mer nicked DNA substrate in standard reaction buffer containing 0.5, 1.0 and 2.0 μM ATP. The effect of Mg^{2+} at each ATP concentration was investigated using 0.5-30 mM Mg^{2+}. The linearity of the initial velocities as a function of ATP concentration suggests these reactions were subsaturating for ATP. The slopes provided by the linear fits are equal to the $(k_{cat}/K_M)^{ATP}$ in units of $\mu M^{-1}s^{-1}$. All of the reactions were performed in at least triplicate and the error bars represent one standard deviation from the mean (error bars in most cases are smaller than the symbols).

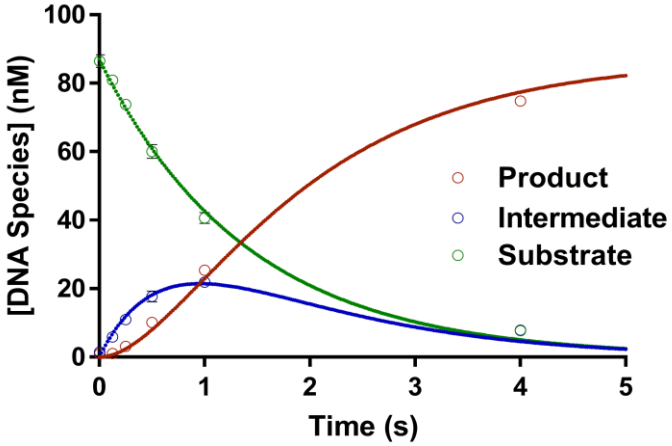

Figure A.5. Single-turnover ligation catalyzed by LIG3β at 1 mM Mg^{2+} concentration. Representative single turnover ligation with 600 nM enzyme and 100 nM DNA substrate under the standard reaction conditions with 1 mM $MgCl_2$. The time course was fit to a two-step irreversible model using Berkeley Madonna software. Reactions were performed in triplicate and the error bars represent one standard deviation from the mean.

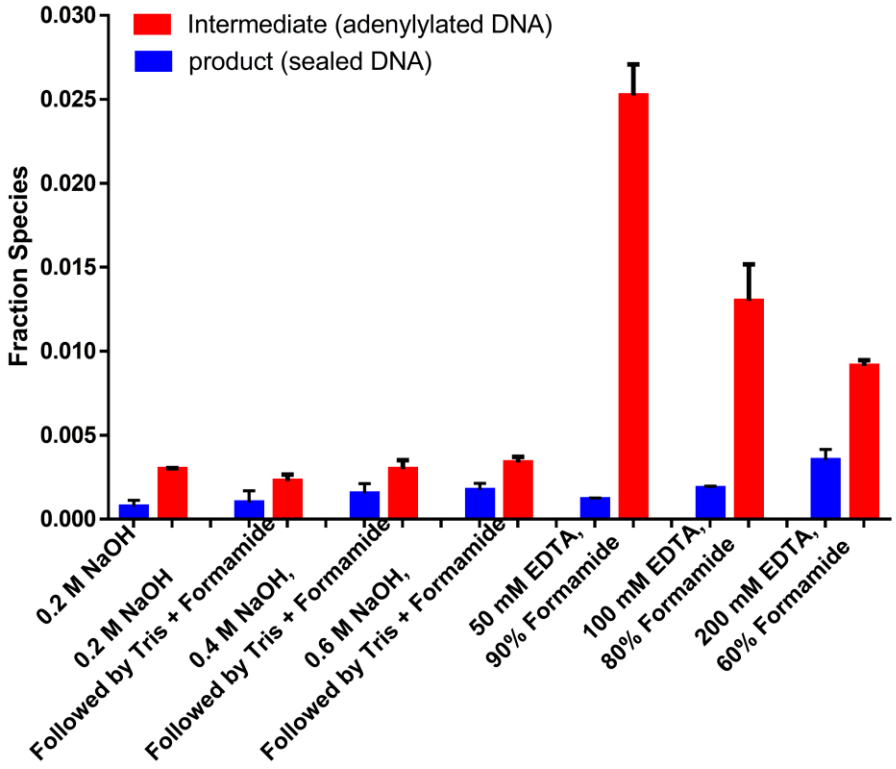

Figure A.6. Identification of an effective quench for single-turnover studies. Reactions contained 600 nM LIG3β, 100 nM nicked DNA substrate, 20 mM $MgCl_2$ in standard reaction buffer. Reactions were all quenched at 5 ms. Quench solutions of more than 0.2 M NaOH were sufficient to reproducibly stop ligase activity at 5 ms. After quenching reactions with varying NaOH concentrations, indicated samples quenched were neutralized using an equivalence of Tris buffer, pH 7.5 after 2 minutes at room temperature. The EDTA and formamide based quench solutions used for the multiple-turnover studies were unable to prevent accumulation of the adenylylated DNA intermediate, however increasing the concentration for EDTA from 50 to 200 mM led to a partial quench of the ligase-catalyzed reaction.

Chapter 3

The LIG3 N-terminus, in its entirety, contributes to single-strand DNA break ligation[3]

Introduction

The three human DNA ligase gene products, DNA ligases I (LIG1), III (LIG3) and IV (LIG4) are required for catalyzing the ultimate step of DNA replication, repair and recombination pathways. These enzymes contain a conserved, three domain catalytic region consisting of a DNA binding domain (DBD), nucleotidyltransferase domain (NTase), and oligonucleotide-binding domain (OB-fold) (Figure 3.1A). Each of the human DNA ligases have been crystallized in the presence of a nicked DNA substrate, revealing that they completely encircle a nicked DNA substrate through a high degree of structural conservation while possessing relatively low (22-23%) amino acid sequence identities (2-5). The three enzymes have a conserved ATP-dependent three-step chemical mechanism that is utilized to join adjacent DNA molecules by catalyzing the formation of a single phosphodiester bond (Figure 3.1B). Briefly, the ligases are first adenylylated on an active-site lysine by reaction with ATP thereby forming and releasing inorganic

[3]The work reported in Chapter 3 would not have been possible without the help of Anna K. Wu and Amanda M. Ames. I assisted Anna with the molecular biology experiments required to generate and confirm all of the N-terminal ZnF constructs (point and truncation mutants) used throughout this study. Amanda performed the enzyme stability experiments in Appendix C. I purified the proteins, characterized the enzymes and wrote the chapter.

pyrophosphate (PP_i). Upon interacting with the 5' terminal phosphate of DNA, the AMP from the active site lysine is transferred to the 5' phosphate, forming a 5'-5' adenylylated DNA (Ap-DNA) intermediate. The Ap-DNA species is short-lived as the 5' adenylylate is a suitable leaving group for the 3' hydroxyl nucleophilic attack of the 5' phosphate, forming the phosphodiester bond between the adjacent 3' hydroxyl and 5' phosphate. The transient kinetics reporting the rate constants and metal cofactor dependences of adenylyl transfer and nick-sealing catalyzed by human LIG1 and LIG3 were previously described (1, 6). Although these enzymes are similar in structure, their low amino acid sequence conservation leads to differential Mg^{2+} cofactor requirements for the chemical steps of ligation. LIG1 and LIG3 differ greatly in their nicked DNA ligation efficiencies; however, these observations are likely due to structural differences extending beyond their conserved three-domain structure.

Flanking their conserved domains, the human DNA ligases have different N- and C-termini that are important for their independent biological functions. These termini contain structured domains and unstructured functional regions that contribute to either substrate specificity, or biological activity via protein-protein interactions (7). The *LIG3* gene encodes four isozymes differing in their N- and C- termini. Two isozymes are synthesized from alternative translation initiation, generating the essential mitochondrial isoform, and the seemingly dispensable nuclear isoform (8-13). Two additional LIG3 isoforms are generated via alternative splicing of the mRNA transcript, resulting in the formation of a germ-line specific isoform (LIG3β) and an isoform present in all cell types (LIG3α) that differ in their C-termini (Figure 3.1A) (14-17). LIG3α possesses a BRCA1 C-terminal (BRCT) domain that interacts with X-Ray Repair Cross Complementing protein 1 (XRCC1) (18-22), whereas LIG3β lacks the BRCT domain (16, 17). Kinetic analysis of recombinant nuclear LIG3α and LIG3β indicate the isozymes are biochemically

indistinguishable when acting on a nicked DNA substrate (1), suggesting that LIG3β is a sufficient surrogate for understanding the contributions of the N-terminal region of LIG3 during single-strand DNA break ligation.

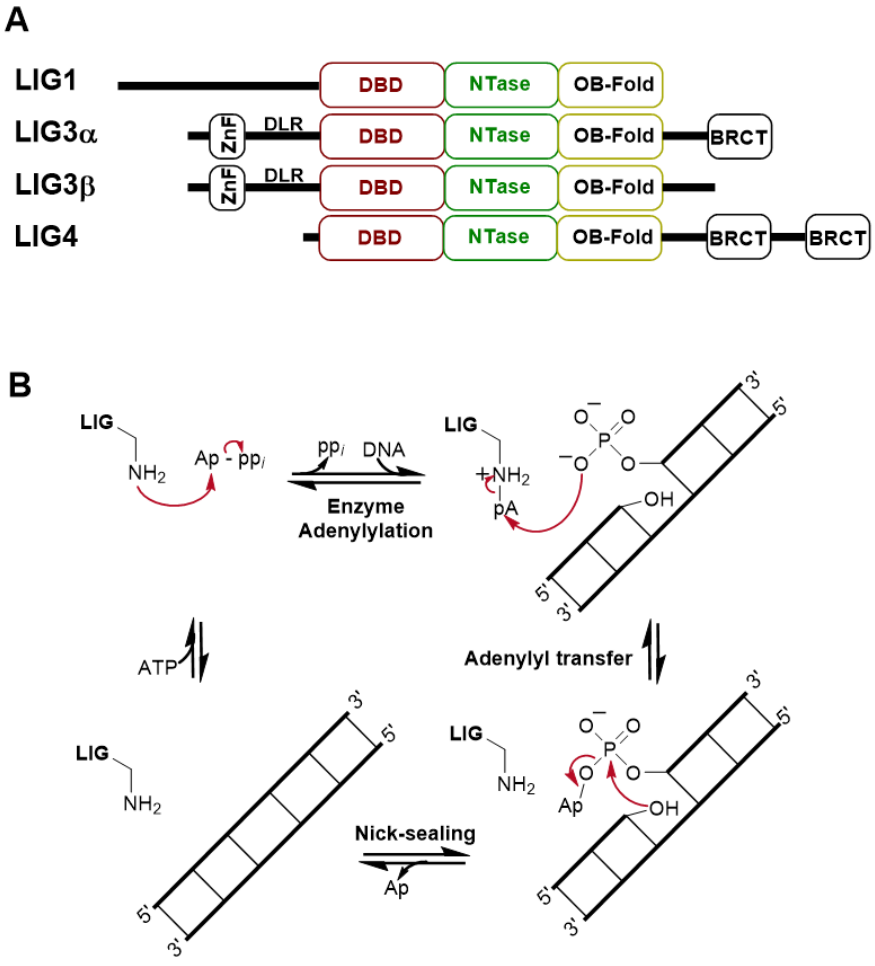

Figure 3.1. Structural and chemical properties of the human DNA ligases. A, Schematic representation of the human DNA ligases. The protein products of the three mammalian ligase genes have a conserved three-domain architecture consisting of a DNA binding domain (DBD, Nucleotidyltransferase domain (NTase), and oligonucleotide binding domain (OB-Fold). The LIG3 isoforms possess an N-terminal zinc finger (ZnF) domain that is tethered to the DBD via a disordered linker region (DLR). B, conserved chemical mechanism of the ATP-dependent mammalian DNA ligases illustrated using a nicked (single-strand break) containing DNA.

Since the mid 1990's, attempts to identify the function of the N-terminal ZnF domain during single- and double-strand break ligation have been ongoing. Interestingly, the degree by which the N-terminal ZnF domain contributes to LIG3β activity is dependent on the design of the protein construct and sensitive to experimental conditions. The ZnF domain was first described by the Caldecott group as a novel "nick sensor", but this description of the domain was quickly amended after the creation of alternative protein constructs that indicated the ZnF domain interacts nonspecifically with DNA secondary structure (20, 23, 24). Building upon these studies, the Tomkinson and Ellenberger groups investigated the role of the ZnF domain by comparing the full length LIG3β protein to the highly truncated crystallization construct lacking all residues upstream of the DBD (residues 1-169), effectively removing the ZnF domain and a disordered linker region (DLR) localized between the ZnF and DBD domains (Figure B.2) (3, 25). These studies indicate the N-terminus of LIG3 (referred to as the zinc finger within the studies) contributes to nicked DNA binding and is essential for the end-joining activity of LIG3 (3, 25). Due to experimental design, it is unclear whether these conclusions accurately reflect the role of the ZnF domain (residues 1-116), or if the results are due to a more complex DNA binding mechanism utilized by the entire N-terminus of LIG3 (residues 1-169). Building upon the observation that this N-terminal region strongly interacts with DNA (and the assumption that the DNA binding energy is specific to the ZnF domain – residues 1-116), it was proposed that the N-terminal region of LIG3 functions as an independent DNA interacting module requiring the ZnF and DBD domains, excluding any contribution by the DLR. In this model, the ZnF and DBD domains physically interact, forming a half-ring shaped assembly capable of interacting with single- and double-strand DNA breaks (3, 25, 26). Due to the assumption that the ZnF domain was solely responsible for the DNA binding energy of the N-terminus of LIG3, this model omitted the contribution of the DLR. The degree by

which the ZnF domain and/or the DLR contribute to DNA binding or LIG3-catalyzed ligation remains unresolved, requiring a systematic analysis of this region of the LIG3 protein.

To better define the role of the LIG3β N-terminus, we describe a systematic kinetic analysis of numerous LIG3 N-terminal variants under steady-state conditions. To do so, we mutagenized highly conserved residues localized to the DNA binding interface of the ZnF domain to determine the degree by which the DNA binding properties of the ZnF domain contribute to the kinetic parameters of LIG3-catalyzed nicked DNA ligation. Two N-terminal truncation mutants were also generated to investigate the kinetic parameters of LIG3 in the presence and absence of the N-terminal ZnF domain, and DLR (Figure 3.2). Mutagenesis of the ZnF domain, and truncations of the N-terminus had minimal effects on maximal ligation rates (k_{cat}). Modifications to the N-terminus of LIG3 had no effect on the ATP concentration dependence; however, the alterations did influence the dependence on Mg^{2+} and DNA concentration. Mutagenesis to the N-terminus of LIG3 increased Mg^{2+} binding affinity; whereas, the same mutants reported decreased nicked DNA ligation efficiencies when compared the full-length enzyme. Strikingly, removal of the DLR further reduced the ligation efficiency of LIG3, consistent with this region contributing to DNA binding as indicated by increased $K_{M,DNA}$ values. This kinetic analysis suggests the N-terminal region of LIG3, in its entirety, contributes to the ligation efficiency of nicked DNA substrates. These findings bring into the question the interpretation of previously reported findings, and reveal the degree by which the N-terminal region contributes to the kinetic parameters of LIG3 catalyzed single-strand DNA break ligation.

Results and discussion

Generation of LIG3 N-terminal mutants.

To determine the contributions of the N-terminal ZnF domain and the disordered linker region (DLR) to LIG3 activity, amino acid substitutions and N-terminal truncations were made to the LIG3β polypeptide. Four highly conserved residues (Lys12, Lys19, Arg31 and Trp50) were identified as candidates for mutagenesis via multiple sequence alignments of homologs possessing low primary sequence identity (Figure B.1). Superimposition of the LIG3 ZnF domain with the highly homologous PARP1 ZnF1 domain within the PARP1 ZnF•DNA cocrystal structure suggest that these residues are located within the DNA binding interface of the ZnF domain (Figure 3.2A and 3.2B). Of the four conserved residues, amino acid substitutions Arg31→Ala (R31A) and Trp50→Ala (W50A) were pursued to disrupt the ZnF domain's DNA binding affinity without perturbing the domain structure. Zn^{2+} coordinating residues were not considered for mutagenesis in order to preserve the structural Zn^{2+} binding site and the tertiary structure of the ZnF domain. To investigate the degree by which the ZnF domain, as a whole, contributes to the kinetic parameters of nicked DNA ligation by LIG3, the ZnF domain was removed using boundaries defined by the solution structure (Δ116 LIG3) (27). To investigate the contribution of the DLR located between the ZnF and DBD domains, a second truncation construct (Δ169) was generated based on the crystallization construct (Figure 3.2C) (3). The combination of point and truncation mutations enable a systematic mapping of the LIG3 N-terminus in respect to its kinetic contributions to single-strand break ligation.

The four mutants (R31A, W50A, Δ116, and Δ169) were expressed and purified as previously described (1). Each of the proteins were chromatographically identical to FL LIG3β

during purification with the exception of the Δ116 and Δ169 LIG3 truncation constructs. The Δ116 and Δ169 LIG3 mutants exhibited lower apparent molecular weights during gel filtration, and greater mobility when analyzed via SDS-PAGE than FL LIG3β. Each of the purified proteins were

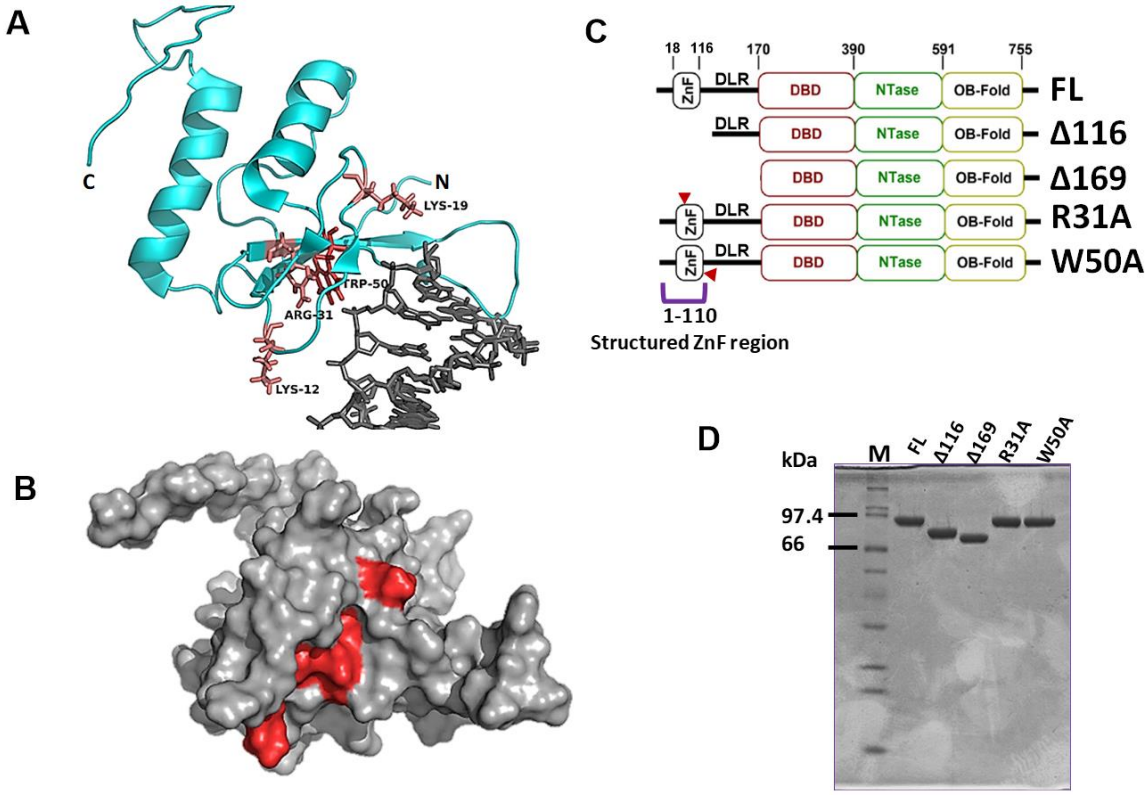

Figure 3.2. LIG3 mutagenesis. *A*, structural model of LIG3α ZnF•DNA interaction to illustrate location of mutagenized residues. The LIG3α ZnF domain shares high sequence and structural similarities with PARP ZnF1 domain. The LIG3 ZnF domain was superimposed onto PARP ZnF1•DNA cocrystal structure, followed by omission of PARP ZnF1 to reveal a plausible LIG3α ZnF•DNA complex (PDB IDs: 1UW0 (LIG3α ZnF) and 3OD8 (PARP ZnF1•DNA)). *B*, space-filling model of LIG3α ZnF domain to illustrate localization of proposed sites of mutagenesis. Images rendered in PyMol software. Residue selection was guided by extensive multiple sequence alignments of ZnF homologs distant ancestry (low sequence identity) (Figure B.1). *C*, gene schematics of the proteins expressed and purified for enzyme analysis. *D*, LIGβ isozymes were expressed and purified to greater than 95% purity as determined by SDS-PAGE analysis (1 µg of each protein loaded). Sigma wide range protein markers are indicated by *M*.

greater than 95% pure, as determined by SDS-PAGE analysis (Figure 3.2D). Active enzyme concentrations were determined and confirmed to be 100% adenylylated by burst analysis as previously described (data not shown) (1). All LIG3β mutants were stable in standard reaction conditions at 37 ̊C for at least 4 hours in the absence of DNA (Figure B.3). Based on these data, each of the LIG3β mutants were of sufficient quality and stability for kinetic analysis.

Influence of the N-terminal region on ATP and Mg^{2+} concentration dependences.

To gain a holistic understanding of how the LIG3 N-terminal region contributes to substrate and cofactor requirements, we investigated the ATP and Mg^{2+} concentration dependences for each of the LIG3β variants. Using a gel-based ligation assay (Figure B.4), ATP concentration dependences were determined using 5 nM enzyme, 400 nM DNA with saturating 20 mM $MgCl_2$ while varying ATP concentrations from 0-300 μM. Initial rates of product formation (Figure 3.3A) were plotted as a function of ATP concentration to determine k_{cat} and $K_{M,ATP}$ values for each of the LIG3 variants (Figure 3.3B, Table 3.1). Each of the proteins had similar $K_{M,ATP}$ values with small deviations in k_{cat}, suggesting the N-terminal region of LIG3 does not play a kinetically distinguishable role in enzyme adenylylation.

Investigation of the Mg^{2+} concentration dependences of the LIG3 variants revealed an unexpected 4-fold increase in Mg^{2+} affinity for the truncated LIG3β constructs, and 2-fold increase for the N-terminal point mutants when compared to FL LIG3β (Figure 3.3D , Table 3.1) (1). These data indicate that alterations to the ZnF domain and its affinity toward DNA influence the enzyme's Mg^{2+} affinity via some unknown mechanism. Importantly, these Mg^{2+} concentration dependences likely report on the dissociation constant (K_d) for Mg^{2+} (referred as K_{Mg}) since Mg^{2+} binding in the millimolar concentration range suggests fast dissociation rates. Rapid mixing

experiments using FL LIG3 confirmed the rapid dissociation of the metal cofactor, as EDTA effectively inactivates the enzyme on the millisecond timescale (1, 6). Together, these results indicate that the N-terminal region of LIG3 does not contribute to enzyme adenylylation, however, the ZnF domain contributes to the Mg^{2+} affinity of LIG3 by an unknown mechanism.

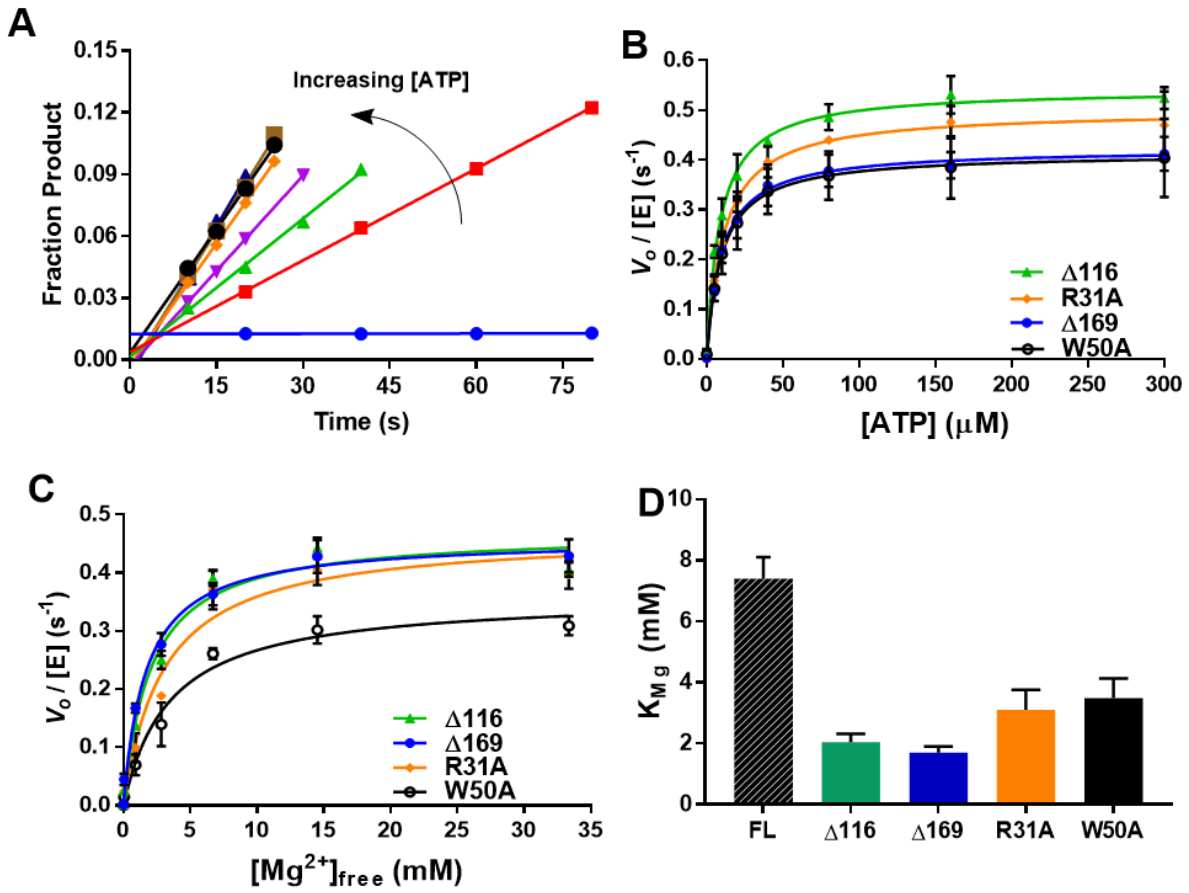

Figure 3.3. ATP and magnesium concentration dependences of LIG3 N-terminal mutants. A, Representative initial rates from Δ169 LIG3β ATP concentration dependences. Initial rates were determined by linear regression of the first 15% of product formation. B, Michaelis-Menten analysis of ATP concentration dependence on Δ169, Δ116, R31A and W50A LIG3β nicked DNA ligation. C, Mg^{2+} concentration dependences of the LIG3β ZnF mutants. D, comparison of K_{Mg} of the various LIG3β ZnF mutants. Full-length LIG3β (FL) data was previously reported (1). Representative time course is from a single experiment. Initial rates were determined by at least three independent experiments (mean, error bars represent one S.D.)

The N-terminal linker of LIG3 contributes to the efficiency of nicked DNA ligation.

It is currently unknown how much the LIG3 N-terminal ZnF domain actually contributes to nicked DNA ligation. To better understand the extent by which the N-terminal ZnF domain and DLR contribute to the nicked DNA ligation efficiency of LIG3, DNA concentration dependences were determined for each of the LIG3 mutants. To accurately determine $K_{M,\,DNA}$ values, conditions of 300 mM ionic strength (adjusted using NaCl) were chosen to enable a quantitative comparison of the mutant and full-length LIG3β constructs (1). Interestingly, the R31A, W50A and Δ116 LIG3 variants had similar $K_{M,\,DNA}$ values (Figure 3.4A, Table 3.1). The observed 3-fold increase in $K_{M,\,DNA}$ values among the LIG3 point and truncation mutants indicate the mutations made to the

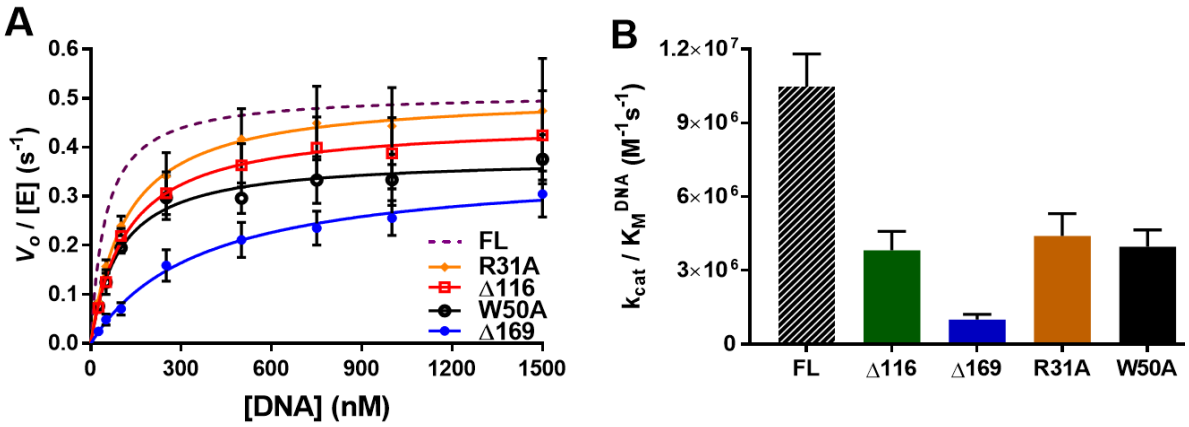

Figure 3.4. Catalytic efficiencies of LIG3β ZnF variants. A, Initial rates of Δ169 (*blue closed circles*), Δ116 (*red open squares*), R31A (*orange open diamonds*), and W50A (*black open circles*) were plotted as a function of nicked DNA concentration and fit well to the Michaelis-Menten equation (equation 3.1). For comparison to FL LIG3β, the *purple dashed line* represents the Michaelis-Menten fit described previously under identical reaction conditions (1). B, comparison of LIG3β catalytic efficiencies ($k_{cat}/K_{M,\,DNA}$) on nicked DNA substrates.

putative DNA binding interface of the ZnF domain effectively eliminated the DNA binding energy contributed by the domain. Strikingly, removal of the DLR (and ZnF domain) resulted in an additional 3-fold increase in $K_{M,\,DNA}$, when compared to the R31A and W50A mutants. Thus, the removal of the entire N-terminus of LIG3 (residues 1-169) resulted in a 7.3-fold increase in $K_{M,\,DNA}$ when compared to FL LIG3β (Table 3.1) (1). Interestingly, previous studies investigating the affinity of FL and Δ169 LIG3 proteins on nicked DNA substrates reported a 56-fold difference in DNA binding affinity (25). If this is indeed the case, then disruption of the LIG3 N-terminus has a much larger effect on K_d than K_M. Comparison of the previously reported catalytic efficiencies of LIG1 with the Δ169 LIG3β construct reveal very similar intrinsic ligation efficiencies of the conserved ligase cores (1.5×10^6 M^{-1} s^{-1} and 1.0×10^6 M^{-1} s^{-1} for LIG1 and Δ169 LIG3β, respectively) (Chapter 2) (1). Experiments investigating the DNA binding affinity of the LIG3 N-terminal variants would provide valuable mechanistic insight to how this region influences LIG3 activity. Alterations to the N-terminus of LIG3 primarily influenced K_M values, suggesting that the ZnF domain does not contribute to the rate-limiting step of steady-state nicked DNA ligation. These data indicate that the DLR, located between the ZnF and DBD domains, contributes to the catalytic efficiency of LIG3 by reducing $K_{M,\,DNA}$.

Table 3.1
Comparison of LIG3β N-terminal mutant kinetic parameters.[a]

	FL[b]	Δ116	Δ169	R31A	W50A	$\frac{\Delta 169}{FL}$	$\frac{\Delta 116}{FL}$	$\frac{\Delta 169}{\Delta 116}$
$*k_{cat,\ DNA}$ (s^{-1})	0.51 ± 0.03	0.45 ± 0.02	0.37 ± 0.03	0.51 ± 0.02	0.38 ± 0.01	0.73	0.88	0.82
$k_{cat,\ ATP}$ (s^{-1})	0.55 ± 0.02	0.54 ± 0.01	0.42 ± 0.01	0.50 ± 0.01	0.41 ± 0.01	0.76	0.98	0.77
$k_{cat,\ Mg}$ (s^{-1})	0.69 ± 0.03	0.47 ± 0.02	0.46 ± 0.01	0.47 ± 0.04	0.36 ± 0.02	0.67	0.68	0.98
$*K_{M,\ DNA}$ (nM)	49 ± 8	120 ± 20	360 ± 80	120 ± 20	100 ± 10	7.3	2.4	3.0
$K_{M,\ ATP}$ (μM)	31 ± 3	8.5 ± 0.6	10 ± 1	11 ± 1	10 ± 2	0.32	0.27	1.2
K_{Mg} (mM)	7.4 ± 0.7	2.0 ± 0.3	1.7 ± 0.2	3.0 ± 0.9	3.4 ± 0.7	0.23	0.27	0.85
$*k_{cat}/K_{M,\ DNA}$ ($M^{-1}s^{-1}$)	$1.0 \pm 0.2 \times 10^7$	$3.4 \pm 0.8 \times 10^6$	$1.0 \pm 0.2 \times 10^6$	$4.4 \pm 0.9 \times 10^6$	$3.9 \pm 0.7 \times 10^6$	0.1	0.34	0.29
$k_{cat}/K_{M,\ ATP}$ ($M^{-1}s^{-1}$)	$1.8 \pm 0.2 \times 10^4$	$6.3 \pm 0.5 \times 10^4$	$4.3 \pm 0.5 \times 10^4$	$4.4 \pm 0.5 \times 10^4$	$4.2 \pm 0.9 \times 10^4$	2.4	3.5	0.68
k_{cat}/K_{Mg} ($M^{-1}s^{-1}$)	93 ± 10	230 ± 30	270 ± 30	150 ± 50	100 ± 20	2.9	2.5	1.2

[a]Multiple-turnover parameters were determined at 150 and 300 mM (*) ionic strength. The ATP concentration dependences were conducted at fixed 20 mM $MgCl_2$, and Mg^{2+} concentration dependences were conducted at fixed 1 mM ATP. Mg^{2+} concentrations dependences were adjusted to reflect free Mg^{2+} concentrations in solution (Methods).
[b]FL LIG3β values were previously described (1).

Conclusions

To investigate the contribution of the LIG3β N-terminal ZnF domain during nicked DNA ligation, we describe a complete multiple-turnover kinetic analysis of several LIG3 N-terminal mutants. Highly conserved residues localized to the DNA binding interface of the ZnF domain were identified by multiple sequence and structural alignments. Targeted mutagenesis of the conserved residues along with N-terminal truncations to the LIG3 polypeptide allowed a kinetic analysis investigating the individual contributions of the ZnF domain and DLR. In our hands, the N-terminus of LIG3 did not influence maximal rates of ligation, nor did it influence ATP requirements for ligation. Disruption of DNA binding or deletion of the ZnF domain, in its entirety, increased the Mg^{2+} binding affinity of LIG3. Likewise, alterations to the N-terminus of LIG3 influenced K_M values for the nicked DNA substrate. Removal of the N-terminal ZnF domain resulted a 3-fold reduction in nicked DNA ligation efficiency, a reduction similarly observed with the alanine point mutations made within the putative DNA binding interface of the ZnF domain. These findings indicate the R31A and W50A amino acid substitutions effectively disrupted DNA binding by the ZnF domain. Strikingly, removal of the DLR (and ZnF domain) reduced catalytic efficiency by an additional 3-fold. These data indicate the DLR contributes to steady-state ligation to a similar extent as the ZnF domain by contributing to DNA binding (via an unknown mechanism). This kinetic analysis indicates that the N-terminal region, in its entirety, contributes to the efficiency of LIG3-catalyzed single-strand break ligation.

Materials and methods

Mutagenesis, expression and purification of LIG3 variants.

Full length LIG3α and LIG3β were cloned into a modified pET28 vector resulting in an N-terminal His_6-SUMO LIG3β fusion protein. Sanger sequencing was conducted to ensure the enzyme was mutation free. Conserved N-terminal ZnF residues were determined using NCBI blast with filters modified to enable acquisition of homologs with low sequence identity. Obtained sequences were compiled and subject to multiple sequence alignment using the Clustal Omega multiple sequence alignment tool (Figure B.1). Lys12, Lys19, Arg31 and Trp50 were targeted for mutagenesis. QuickChange primers were designed to change Lys and Arg residues to Ala, Met and Glu, and the Trp residue to Ala and Glu. QuickChange mutagenesis was performed using wild type FL LIG3α and LIG3β constructs described in Figure 3.2 using the primers described in Figure B.5. Sanger sequencing of the entire LIG3α and LIG3β open reading frames confirmed mutations. Open reading frame sequences were analyzed using DNASTAR Navigation software to confirm the absence of random mutations. LIG3β Ala mutants of Arg31 (R31A) and Trp50 (W50A) were chosen for enzymatic characterization. N-terminal LIG3α and LIG3β truncation mutants were designed using the ZnF domain structural boundaries determined by the solution structure of the ZnF domain, (residues 1-116) (27). The N-terminal boundary of the LIG3 DBD was determined by multiple sequence analysis, and confirmed by X-Ray crystallography (3, 5), resulting in the removal of residues 1-169. The only difference between Δ116 and Δ169 LIG3 constructs is the presence of a disordered linker region (DLR) 53 residues in length tethering the ZnF to the DBD domain of LIG3 (Figure B.2.). Truncated LIG3 DNA was amplified by PCR using the primers described in Figure B.5. The primers contained BamHI and SalI restriction sites enabling efficient

incorporation into the same modified pET28 vector used for FL LIG3 fusion proteins. R31A, W50A, Δ116 and Δ169 LIG3β were expressed and purified as previously described in Chapter 2 (1).

Oligonucleotide substrates used to monitor ligase activity.

Oligonucleotides were obtained from Integrated DNA Technologies and further purified using 15% DNA denaturing PAGE as previously described (6). The nicked DNA substrate used throughout this study was generated by annealing three oligonucleotides together in which an upstream 13mer and 5'phosphorylated fluorescein (FAM) labeled 15mer DNA were both annealed to a complementary 28mer template, generating a 28bp duplex DNA substrate with a centrally located nick. The sequences of the 13, 15 and 28mers are: 5' GTGCTGATGCGTC, 5'P-GTCGGACTGATTCGG-FAM and 5' CCGAATCAGTCCGACGACGCATCAGCAC, respectively, where P indicates 5' phosphorylation and FAM indicates the presence of a 3' fluorescein. The three oligonucleotides were annealed at equimolar equivalents in 10 mM NaMES, pH 6.5, 50 mM NaCl by cooling the solution from 95 ˚C to 4 ˚C at a rate of 12 ˚C min^{-1}.

Discontinuous gel-based ligation assay.

All reactions were performed at 37 ˚C in standard reaction buffer containing 50 mM NaMOPS, pH 7.5, 10% glycerol, 1 mM DTT, and 0.1 mg mL^{-1} BSA (MP Biomedicals) with ionic strength maintained at 150 mM unless otherwise stated. DNA, ATP, $MgCl_2$ and NaCl concentrations were adjusted on an experimental basis depending on the variable in question. Ligation reactions were stopped at predetermined times by transferring reaction solution into 1.5X quench solution (90% formamide, 50 mM EDTA, 0.006% bromophenol blue, 0.006%xylene

cyanol). Quenched samples were incubated at 95˚C for 3 minutes before snap cooling in ice water prior to loading onto a 15% polyacrylamide, 8 M urea, 1X TBE DNA-denaturing gel. Gels were scanned using a typhoon 5 imaging system (GE Healthcare) set to monitor emission at 525 (BP20) with excitation set to 488 nm (Figure B.3). Separated DNA species were quantified using ImageQuant TL (GE Healthcare) and plotted using GraphPad Prism.

Multiple-turnover ligation.

Reactions contained substrate in excess of enzyme concentration under all tested conditions. Reactions were 30 µL in volume; from which 3 µL was transferred to quench solution at predetermined times. Quenched samples were analyzed using the gel-based assay described above to determine initial rates. Initial rates were determined by linear regression of the first 10% of product formation, and then plotted as a function of the variable in question. Data presented within this study represent the average of at least 3 individual experiments unless otherwise stated within the figure legend. Active concentrations and adenylylation states of LIG3β mutants (R31A, W50A, Δ116, Δ169) were determined by burst analysis as previously described (1). ATP concentration dependences of the LIG3 variants were performed in standard reaction buffer containing 20 mM $MgCl_2$, with ionic strength at 150 mM using NaCl. Ionic strengths were calculated using the Debye-Hückel theory of electrolytes. Reactions contained 5 nM enzyme with 400 nM DNA substrate and ATP concentrations were varied from 0-300 µM. Initial rates at each ATP concentration were plotted as a function of ATP concentration. The data fit well to a Michaelis-Menten equation (equation 3.1). $MgCl_2$ concentration dependences (0-33 mM) were conducted in the presence of 5 nM enzyme, 400 nM DNA and saturating ATP (1 mM). Ionic strength was maintained at 150 mM using NaCl. Initial rates were plotted as a function of free

Mg^{2+} concentration and fit well to a hyperbolic curve (equation 3.2). Free Mg^{2+} was calculated based on the ATP•Mg^{2+} and ATP•2Mg^{2+} K_d values of 12 μM and 17 mM, respectively (1, 28). DNA concentration dependences were measured at 300 mM ionic strength with 5 nM enzyme, 1 mM ATP and 20 mM $MgCl_2$. Nicked DNA concentrations ranged from 0.025 – 1.5 μM. Initial rates plotted as a function of nicked DNA concentration fit well to the Michaelis-Menten equation (equation 3.1). Errors of calculated catalytic efficiencies were determined by propagation of error.

$$\frac{V_o}{[E]} = \frac{k_{cat}\times[S]}{(K_M+[S])} \qquad \text{(Eq. 3.1)}$$

$$\frac{V_{init}}{[E]} = \frac{k_{cat} \times [Mg^{2+}]}{\left(K_{Mg} + [Mg^{2+}]\right)} \qquad \text{(Eq. 3.2)}$$

References

1. McNally JR & O'Brien PJ (2017) Kinetic analyses of single-stranded break repair by human DNA ligase III isoforms reveal biochemical differences from DNA ligase I. *J. Biol. Chem.* 292(38):15870-15879.

2. Pascal JM, O'Brien PJ, Tomkinson AE, & Ellenberger T (2004) Human DNA ligase I completely encircles and partially unwinds nicked DNA. *Nature* 432(7016):473-478.

3. Cotner-Gohara E*, et al.* (2010) Human DNA Ligase III Recognizes DNA Ends by Dynamic Switching between Two DNA-Bound States. *Biochemistry* 49(29):6165-6176.

4. Kaminski AM*, et al.* (2018) Structures of DNA-bound human ligase IV catalytic core reveal insights into substrate binding and catalysis. *Nat Commun* 9(1):2642.

5. Simsek D & Jasin M (2011) DNA ligase III: A spotty presence in eukaryotes, but an essential function where tested. *Cell Cycle* 10(21):3636-3644.

6. Taylor MR, Conrad JA, Wahl D, & O'Brien PJ (2011) Kinetic Mechanism of Human DNA Ligase I Reveals Magnesium-dependent Changes in the Rate-limiting Step That Compromise Ligation Efficiency. *J. Biol. Chem.* 286(26):23054-23062.

7. Ellenberger T & Tomkinson AE (2008) Eukaryotic DNA Ligases: Structural and Functional Insights. *Annu. Rev. Biochem.* 77(1):313-338.

8. Masani S, Han L, Meek K, & Yu K (2016) Redundant function of DNA ligase 1 and 3 in alternative end-joining during immunoglobulin class switch recombination. *Proc. Natl. Acad. Sci. U. S. A.* 113(5):1261-1266.

9. Lu G*, et al.* (2016) Ligase I and ligase III mediate the DNA double-strand break ligation in alternative end-joining. *Proc. Natl. Acad. Sci. U. S. A.* 113(5):1256-1260.

10. Simsek D*, et al.* (2011) Crucial role for DNA ligase III in mitochondria but not in Xrcc1-dependent repair. *Nature* 471(7337):245-248.

11. Gao Y*, et al.* (2011) DNA Ligase III is critical for mtDNA integrity but not Xrcc1-mediated nuclear DNA repair. *Nature* 471(7337):240-244.

12. Arakawa H*, et al.* (2012) Functional redundancy between DNA ligases I and III in DNA replication in vertebrate cells. *Nucleic Acids Res.* 40(6):2599-2610.

13. Lakshmipathy U & Campbell C (1999) The Human DNA Ligase III Gene Encodes Nuclear and Mitochondrial Proteins. *Mol. Cell. Biol.* 19(5):3869-3876.

14. Chen J, *et al.* (1995) Mammalian DNA ligase III: molecular cloning, chromosomal localization, and expression in spermatocytes undergoing meiotic recombination. *Mol. Cell. Biol.* 15(10):5412-5422.

15. Wei YF, *et al.* (1995) Molecular cloning and expression of human cDNAs encoding a novel DNA ligase IV and DNA ligase III, an enzyme active in DNA repair and recombination. *Mol. Cell. Biol.* 15(6):3206-3216.

16. Perez-Jannotti RM, Klein SM, & Bogenhagen DF (2001) Two Forms of Mitochondrial DNA Ligase III Are Produced inXenopus laevis Oocytes. *J. Biol. Chem.* 276(52):48978-48987.

17. Mackey ZB, *et al.* (1997) An alternative splicing event which occurs in mouse pachytene spermatocytes generates a form of DNA ligase III with distinct biochemical properties that may function in meiotic recombination. *Mol. Cell. Biol.* 17(2):989-998.

18. Taylor RM, Wickstead B, Cronin S, & Caldecott KW (1998) Role of a BRCT domain in the interaction of DNA ligase III-α with the DNA repair protein XRCC1. *Curr. Biol.* 8(15):877-880.

19. Nash RA, Caldecott KW, Barnes DE, & Lindahl T (1997) XRCC1 Protein Interacts with One of Two Distinct Forms of DNA Ligase III. *Biochemistry* 36(17):5207-5211.

20. Caldecott KW, Aoufouchi S, Johnson P, & Shall S (1996) XRCC1 Polypeptide Interacts with DNA Polymerase β and Possibly Poly (ADP-Ribose) Polymerase, and DNA Ligase III Is a Novel Molecular 'Nick-Sensor' In Vitro. *Nucleic Acids Res.* 24(22):4387-4394.

21. Caldecott KW, Tucker JD, Stanker LH, & Thompson LH (1995) Characterization of the XRCC1-DNA ligase III complex in vitro and its absence from mutant hamster cells. *Nucleic Acids Res.* 23(23):4836-4843.

22. Caldecott KW, McKeown CK, Tucker JD, Ljungquist S, & Thompson LH (1994) An interaction between the mammalian DNA repair protein XRCC1 and DNA ligase III. *Mol. Cell. Biol.* 14(1):68-76.

23. Taylor RM, Whitehouse J, Caldecott KW, Cappelli E, & Frosina G (1998) Role of the DNA ligase III zinc finger in polynucleotide binding and ligation. *Nucleic Acids Res.* 26(21):4804-4810.

24. Taylor RM, Whitehouse CJ, & Caldecott KW (2000) The DNA ligase III zinc finger stimulates binding to DNA secondary structure and promotes end joining. *Nucleic Acids Res.* 28(18):3558-3563.

25. Cotner-Gohara E, Kim I-K, Tomkinson AE, & Ellenberger T (2008) Two DNA-binding and Nick Recognition Modules in Human DNA Ligase III. *J. Biol. Chem.* 283(16):10764-10772.

26. Kukshal V, *et al.* (2015) Human DNA ligase III bridges two DNA ends to promote specific intermolecular DNA end joining. *Nucleic Acids Res.* 43(14):7021-7031.

27. Kulczyk AW, Yang J-C, & Neuhaus D (2004) Solution Structure and DNA Binding of the Zinc-finger Domain from DNA Ligase IIIα. *J. Mol. Biol.* 341(3):723-738.

28. Cherepanov AV & de Vries S (2003) Kinetics and thermodynamics of nick sealing by T4 DNA ligase. *Eur. J. Biochem.* 270(21):4315-4325.

Appendix B

Additional figures to support Chapter 3

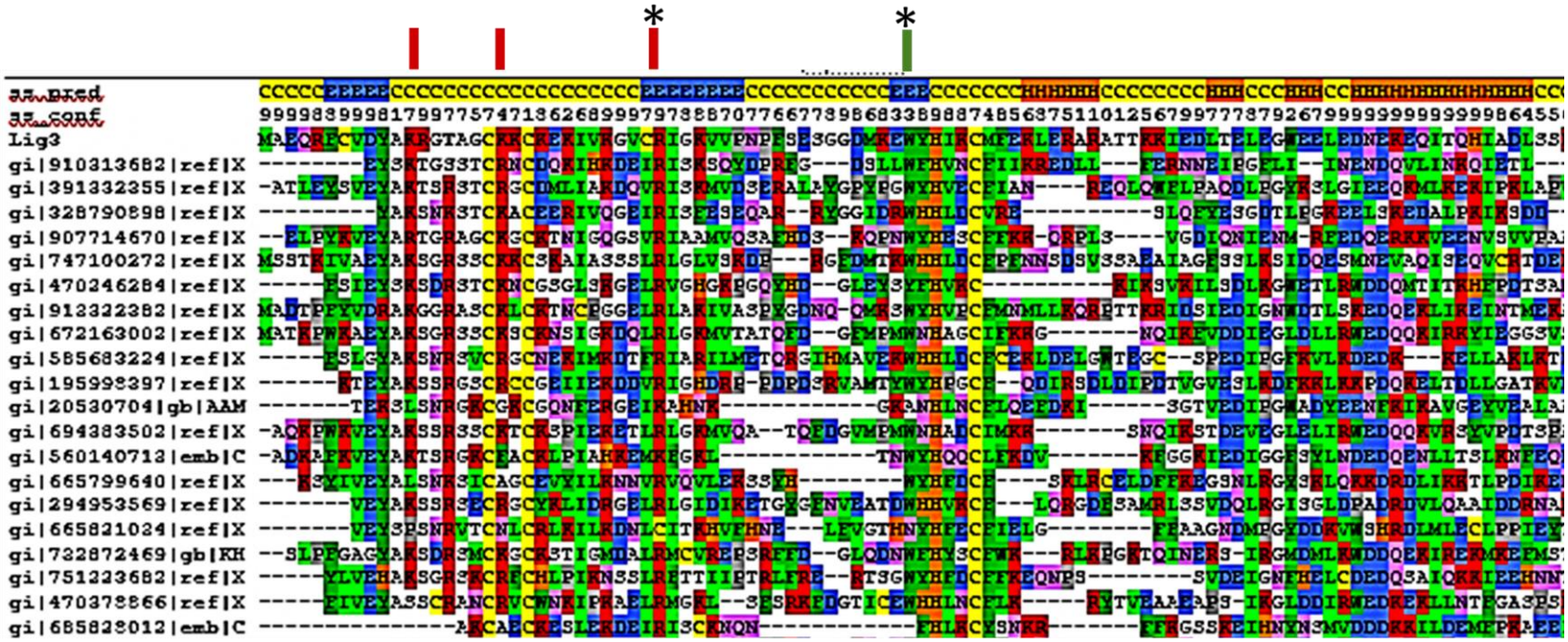

Figure B.1. Multiple sequence alignment of LIG3 N-terminal ZnF. Conserved residues of LIG3 N-terminal ZnF were identified by alignment of ZnF homologs possessing low sequence identity to the LIG3 ZnF sequence. Sequences (obtained via NCBI) were aligned using the Clustal Omega multiple sequence alignment tool online. Highly conserved residues are those indicated with red and green markings indicate residues of interest. Markings with an asterisk (*) indicate residues mutagenized and used throughout this study. Conserved cysteine and histidine residues participate in zinc coordination and were not considered for mutagenesis.

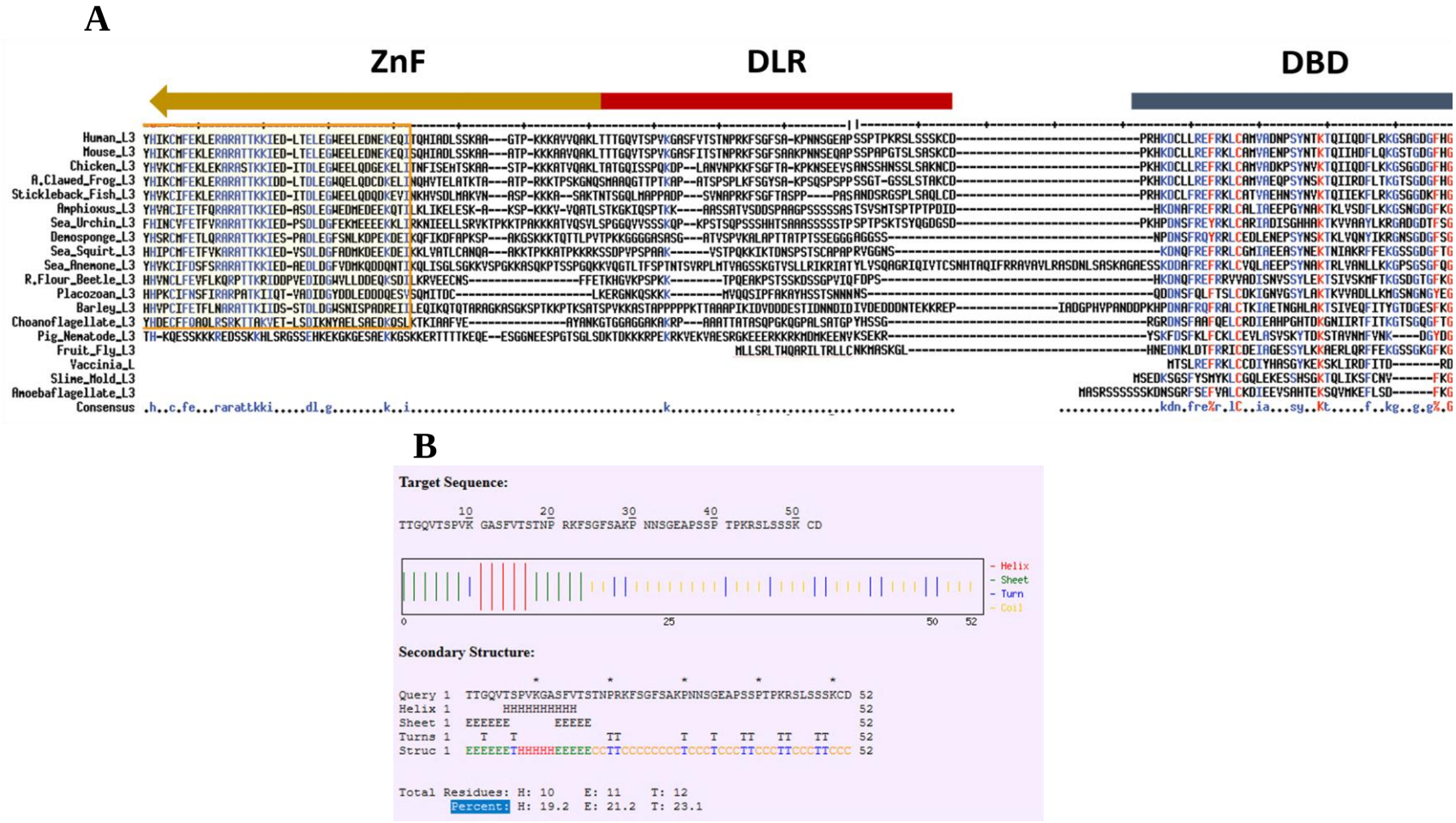

Figure B.2. Sequence alignments and secondary structure predictions of LIG3 DLR. A, Multiple sequence alignment adapted from Simsek *et al*, (2011) (5). Yellow arrow indicates residues within the ZnF domain. Red bar indicates residues within the LIG3 DLR. Blue arrow indicates residues within the DBD. B, Secondary structure prediction from the Chou & Fasman Secondary Structure Prediction Server (CFSSP). CFSSP predicts secondary structure within the first 16 residues of the 50 residue DLR.

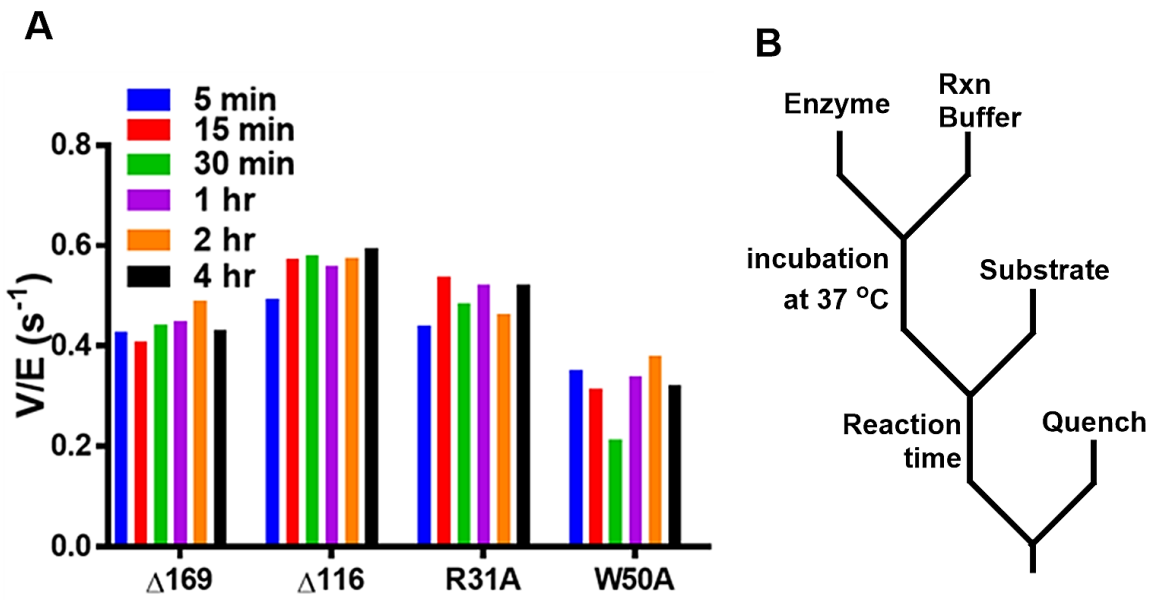

Figure B.3. LIG3 mutants are stable under standard reaction conditions. A, stability of LIG3 variants as a function of preincubation time. B, Experimental work flow to investigate the stability of LIG3 variants. Briefly, 5 nM enzyme was incubated at 37 ̊C in the absence of DNA substrate in standard reaction buffer containing 1 mM ATP and 20 mM $MgCl_2$ 150 mM ionic strength. Activities were determined by the addition of nicked DNA to determine initial rates of reaction as a function of preincubation time. Ligation rates remained unchanged as a function of preincubation time. This experiments was not performed in duplicate.

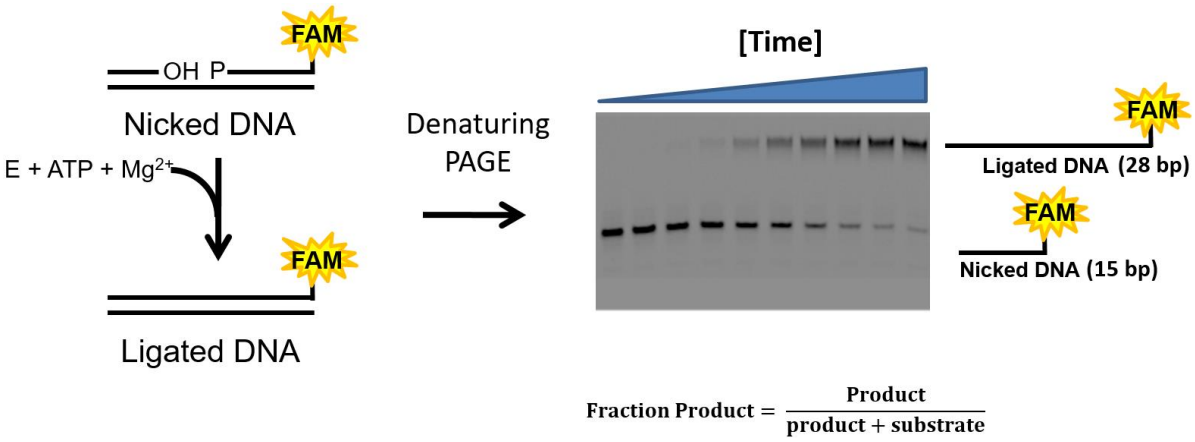

Figure B.4. Gel based ligation assay used for the characterization of LIG3 N-terminal mutants. A synthetic 28 base paired duplex DNA was generated by annealing three complementary oligonucleotides. The synthetic DNA substrate contained an unlabeled upstream 13-mer oligonucleotide containing a 3'-hydroxyl, and a downstream 5'-phosphorylated, 3'-fluorescein (FAM) labeled 15-mer oligonucleotide. Both upstream and downstream oligonucleotides were annealed to an unlabeled 28-mer template DNA strand as described (Methods). The fluorescent 28-mer DNA substrate was reacted with LIG3 under various assay conditions. Reactions were stopped with quenching solution (Methods) and analyzed via DNA denaturing PAGE (*Right*). 3'-FAM labeled substrate enabled the detection of product species. Fluorescent bands were quantified and fraction products were determined.

Name	Sequence 5' → 3'	Tm ˚C
Lig3K12AFP	GTGGACTATGCC**GCG**CGTGGCACAGCTG	78.1
Lig3K12ARP	CAGCTGTGCCACG**CGC**GGCATAGTCCAC	78.1
Lig3K12MFP	GTGTGGACTATGCC**ATG**CGTGGCACAGC	78.7
Lig3K12MRP	GCTGTGCCACG**CAT**GGCATAGTCCACAC	78.7
Lig3K12EFP	GTGGACTATGCC**GAG**CGTGGCACAGC	78.5
Lig3K12ERP	GCTGTGCCACG**CTC**GGCATAGTCCAC	78.5
Lig3K19AFP	GTGGCACAGCTGGCTGC**GCA**AAATGCAAGGAAAAG	78.8
Lig3K19ARP	CTTTTCCTTGCATTT**TCG**GCAGCCAGCTGTGCCAC	78.8
Lig3K19MFP	CGTGGCACAGCTGGCTGC**ATG**AAATGCAAGGAAAAG	78.8
Lig3K19MRP	CTTTTCCTTGCATTT**CAT**GCAGCCAGCTGTGCCACG	78.8
Lig3K19EFP	GGCACAGCTGGCTGC**GAA**AAATGCAAGGAAAAG	79.1
Lig3K19ERP	CTTTTCCTTGCATTT**TTC**GCAGCCAGCTGTGCC	79.1
Lig3R31AFP	GTGAAGGGCGTATGC**GCA**ATTGGCAAAGTGGTGC	78.7
Lig3R31ARP	GCACCACTTTGCCAAT**TGC**GCATACGCCCTTCAC	78.7
Lig3R31MFP	GATTGTGAAGGGCGTATGC**ATG**ATTGGCAAAGTGGTGCCC	78.7
Lig3R31MRP	GGGCACCACTTTGCCAAT**CAT**GCATACGCCCTTCACAATC	78.7
Lig3R31EFP	GTGAAGGGCGTATGC**GAA**ATTGGCAAAGTGGTGCC	78.8
Lig3R31ERP	GGCACCACTTTGCCAAT**TTC**GCATACGCCCTTCAC	78.8
Lig3W50AFP	CTGGGGGTGATATGAAAGAG**GCG**TACCACATTAAATGCATG	79.2
Lig3W50ARP	CATGCATTTAATGTGGTA**CGC**CTCTTTCATATCACCCCCAG	79.2
Lig3W50EFP	CTGGGGGTGATATGAAAGAG**GAG**TACCACATTAAATGCATG	78.2
Lig3W50ERP	CATGCATTTAATGTGGTA**CTC**CTCTTTCATATCACCCCCAG	78.2

FORWARD PRIMERS	***BAMHI*** + SEQUENCE	Tm ˚C
LIG3_BAMHI_Δ116	*CCAC**GGATCC***ACTGGCCAGGTGACTTCTCC	59
LIG3_BAMHI_ Δ169	*CCAC**GGATCC***CATAAGGACTGTCTGCTACGGGAGTTTCG	63
REVERSE PRIMERS	***SALI*** + SEQUENCE	
LIG3A_SALI	*GCAG**GTCGAC***TTAGCAGGGAGCTACCAG	58
LIG3B_SALI	*GCAG**GTCGAC***TATCTCCTGCCTGCTGGC	62

Figure B.5. Primers used for mutagenesis of LIG3α and LIG3β. "RP" refers to reverse primer. "FP" refers to forward primer. *BAMHI* and *SALI* refer to restriction endonuclease sites required for sub-cloning the truncation constructs into the destination vector. The lysine and arginine residues were each mutagenized to alanine, methionine and glutamate whereas the tryptophan residue was mutagenized to alanine and glutamate in both LIG3α and LIG3β. The creation of the various ZnF point mutants enabled alanine screening, the utilization of residues occupying a similar volume (lysine and arginine vs methionine), or oppositely charged residues to disrupt the ZnF•DNA interactions without perturbing the tertiary ZnF domain structure, or Zn^{2+} coordination. LIG3α proteins were not expressed or purified, for the analysis of LIG3α•XRCC1 complex and the role of the N-terminal plays in this complex will be the subject of future study.

Chapter 4

Comparative end-joining by human DNA ligases I and III[4]

Introduction

The human genome is continuously assaulted by endogenous and exogenous sources of DNA damage. DNA replication, repair, and recombination pathways work together to maintain and safeguard the stability of the genome from these insults. Human DNA ligases I (LIG1), III (LIG3) and IV (LIG4) catalyze the ultimate step in the aforementioned pathways by rejoining DNA molecules to restore continuous genomic DNA strands. DNA ligases employ a three-step chemical mechanism that is amendable to joining single- or double-strand DNA breaks (SSBs and DSBs, respectively). During a single round of catalysis, ligases catalyze self-adenylylation with ATP to form a high-energy intermediate. This activated enzyme intermediate binds to a 5'-phosphorylated SSB or DSB DNA and transfers AMP from the active site lysine to the 5'-phosphate to form an adenylylated DNA intermediate (Figure 4.1A). During SSB ligation, the 3'-hydroxyl adjacent to the adenylylated 5'-phoshate is appropriately positioned for efficient sealing

[4]Amanda Ames helped with trouble shooting and establishment of the double-strand DNA break repair assay described within this chapter. Jeremy Day-Storms performed initial experiments identifying the ability of LIG1 to catalyze EJ. Thomas Jurkiw gifted purified Δ232 LIG1 and APTX to this study. I performed the study and wrote the chapter.

of the phosphodiester DNA backbone, completing the final chemical step of ligation with the release of AMP and the repaired DNA molecule. The ligation activities of LIG1 and LIG3 have already been reported for the repair of SSBs (1-5). In the case of DSBs that lack cohesive ends, there is an additional challenge to orienting two DNA molecules to catalyze the formation of the phosphodiester bond without the aid of a bridging DNA strand (Figure 4.1A). Many studies have reported on the EJ activity of human LIG3 (3, 4, 6-10), but we are not aware of any previous efforts to investigate potential EJ by human LIG1.

LIG1 and LIG3 possess a structurally conserved three-domain architecture of 22% sequence identity that completely encircles a SSB (3, 5, 11). These proteins differ structurally in their N- and C-termini, suggesting these regions flanking the conserved three-domain ligase core direct biological activities. LIG3 contains an N-terminal zinc finger (ZnF) domain homologous to those of poly (ADP-ribose) polymerase 1 (PARP-1) tethered to the DNA-binding domain via a ~50 residue linker region (Figure 4.1B) (12, 13). This N-terminal region of LIG3 has been described as dynamic and proposed to serve as a nick sensor for SSB ligation, contain non-specific DNA binding properties, and play an essential role in LIG3 catalyzed EJ (3, 4, 6, 8, 12-15). In contrast, the N-terminal region of LIG1 (~260 residues) does not contribute to the kinetic parameters of the enzyme (1). In the cell, this region is important for targeting LIG1 to the nucleus as well as facilitating protein-protein interactions in a post-translational modification dependent manner (5, 16). The differences in the N-termini of LIG1 and LIG3 have fueled the consensus that LIG1 is incapable of performing EJ reactions due to the lack of an additional DNA interacting domain outside of its three-domain architecture.

The extent to which LIG1 performs EJ reactions is unknown. Recently, two independent genetic studies using cultured mouse B-cells indicated that EJ can occur during class switch recombination (CSR) in the absence of LIG3 and LIG4 (17, 18). These data implicate LIG1 as the

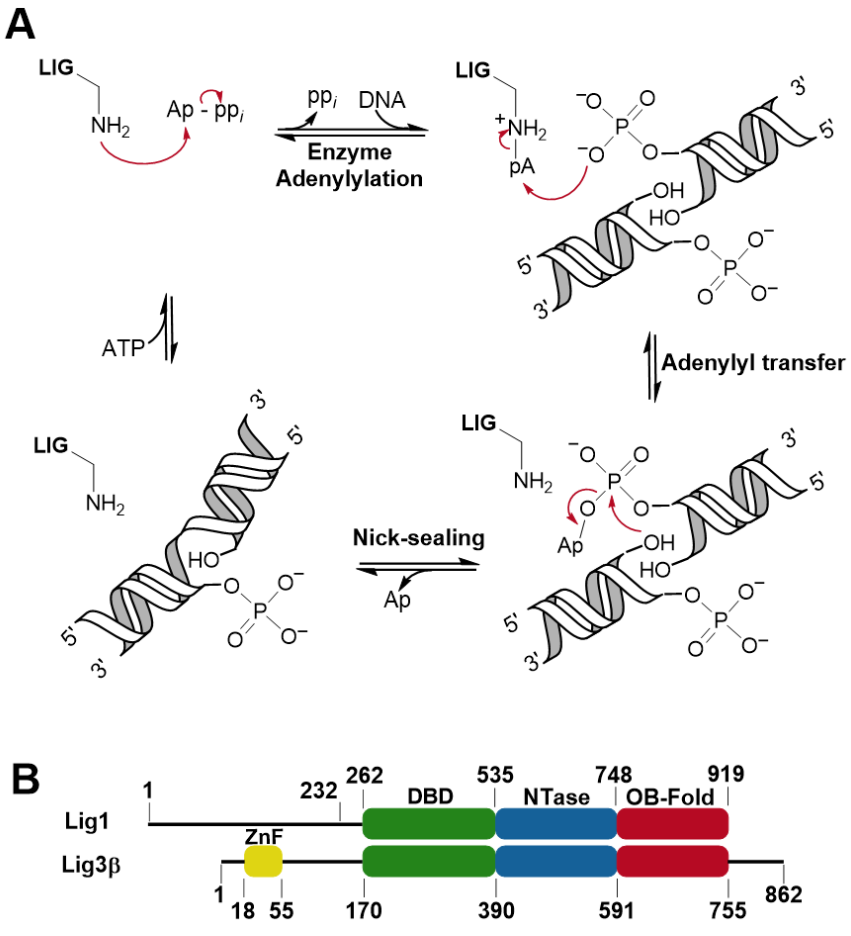

Figure 4.1. Human LIG1 and LIG3 share structural and mechanistic characteristics. A, chemical mechanism of blunt end ligation by ATP-dependent DNA ligases. The end-joining reaction produces a nicked DNA product (single ligation product) that must undergo a second round of catalysis to join the opposite side of the DNA molecule. B, simplistic schematic of LIG1 and LIG3 domains and their corresponding boundaries (*numbers*). B, LIG1 and LIG3β possess conserved DNA binding (DBD, *green*), nucleotidyltransferase (NTase, *blue*), and oligonucleotide-binding (OB-fold, *red*) domains. LIG3 has an additional DNA binding N-terminal zinc finger domain (ZnF, *yellow*).

source of the EJ activity, but there is no mechanistic information regarding how LIG1-mediated EJ may occur. Roughly three decades prior to these studies, two research groups reported that rat and calf thymus LIG1 are capable of catalyzing EJ *in vitro* (19, 20). Together, these studies suggest that LIG1 could participate in an undefined EJ pathway that overlaps with the EJ activities of LIG3 and LIG4.

We took a systematic biochemical approach to characterize the EJ activities of LIG1 and LIG3 on DNA ends of varying structure. We demonstrate that LIG1 is capable of performing EJ, highlighting the differences in end-joining efficiencies and substrate specificities of LIG1 and LIG3. Most notably, LIG3 efficiently joined all tested DSB substrates, whereas LIG1 shows a preference for 3'-overhangs over 5'-overhangs and blunt ends. To simulate the crowded conditions within the cell, we employed polyethylene glycol as an inert molecular crowding agent. Molecular crowding increased the catalytic efficiency of LIG1 by up to 100-fold, while also stabilizing the LIG3•substrate complex, enabling a transient kinetic characterization of EJ. Remarkably, we found that a single molecule of LIG3 was capable of performing the sequential ligation events required to completely repair double-strand DNA breaks in a single DNA binding encounter. This work highlights the similarities and differences of LIG1 and LIG3 mediated EJ and documents, for the first time, their catalytic efficiencies for *in vitro* EJ.

Results and Discussion

Previous structural and biochemical studies of single-strand break repair by LIG3 and LIG1 demonstrate many conserved mechanistic features (1-3, 5). Although numerous studies have qualitatively investigated the ability of LIG3 to catalyze end-joining *in vitro* (3, 4, 6-10), the specificity and mechanism by which LIG3 recognizes and ligates DNA ends remains in question.

Furthermore, there has been a strong dogma that LIG1 does not perform EJ, and that this characteristic sets it apart from LIG3 and LIG4 (16, 21, 22). EJ reactions can be complex if there are multiple ligatable ends, and therefore we developed a simplified assay with defined compatible ends to systematically characterize the activity and specificity of human DNA LIG1 and LIG3.

EJ assay development.

We designed synthetic DNA hairpin substrates containing GNA trinucleotide loop structures that are closed by 14-16 base-pairs of duplex DNA (Figure 4.2A). The resulting hairpin substrates were A•T rich to achieve melting temperatures between 61-64 ̊C. Hairpin lengths were optimized for the detection of abortive, single, and double ligation products via denaturing PAGE (Figure 4.2B). A 14-bp duplex DNA hairpin was found to be sufficient in length because blunt-end substrates of 14 and 18 bp showed similar rates of ligation by LIG1 and LIG3 (Figure C.2). These data are in agreement with a footprint of roughly 8 base pairs upstream and downstream of a SSB that can be inferred from crystal structures of LIG1 and LIG3 (3, 5). Hairpin substrates were designed with blunt ends or with either 3' or 5' overhangs with 3 nucleotides of complementarity (Figure 4.2A). The blunt-end substrate contained a terminal G•C base-pair, whereas the 3'- and 5'- 3 nucleotide overhang (henceforth referred to as 3'- or 5'-DSB) substrates contained A•T and G•C terminal base-pairs in the 16- and 14-bp duplex DNA hairpins, respectively. With the exception of the terminal base pair, all hairpin sequences were identical. Abortive, single, and double ligation products were verified by enzymatic digestion of the ligation products (Figure C.3) and by observing the banding patterns associated with the formation and decay of the single ligation product as a function of time (Figure C.4).

Catalytic efficiencies of LIG1- and LIG3-catalyzed end-joining.

To determine the catalytic efficiencies ($k_{cat}/K_{M,\ DNA}$) of LIG1 and LIG3 EJ, DNA substrate concentration dependences were measured in the presence of saturating (18 mM free) and physiological (1 mM free) Mg^{2+} on blunt-end and cohesive-end substrates. Initial rates of LIG1 EJ

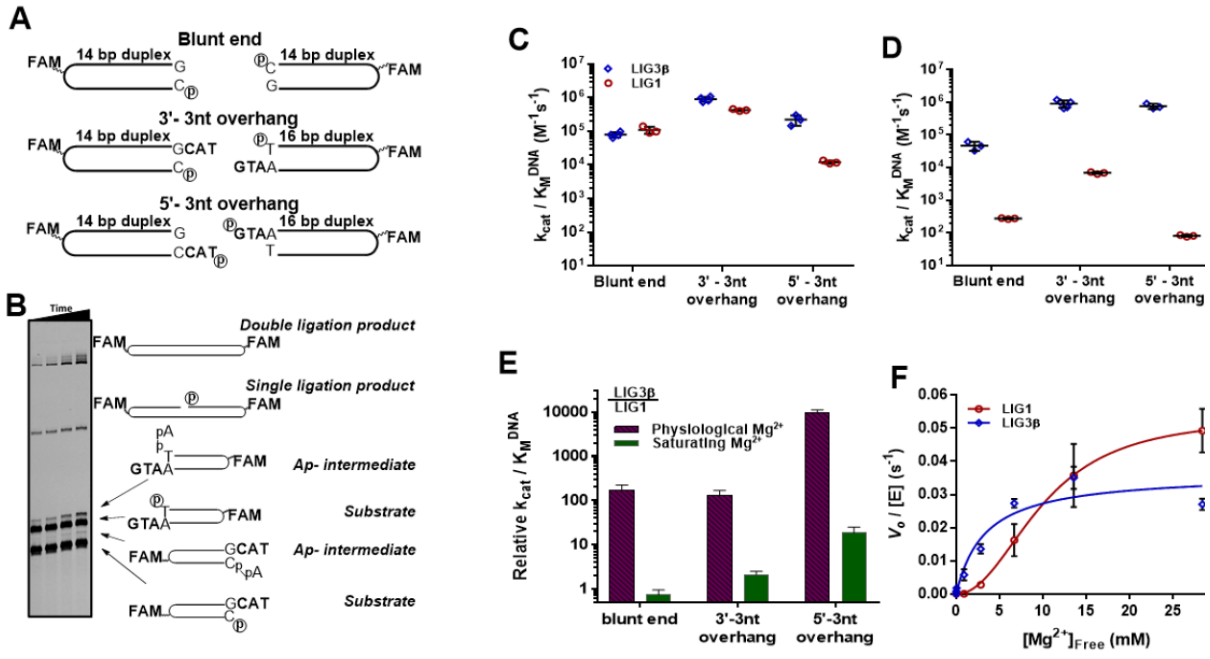

Figure 4.2. End-joining efficiencies of DNA LIG1 and LIG3β. A, schematic of hairpin substrates used to investigate end-joining of LIG1 and LIG3β. Oligonucleotides contain a centrally localized GTA tri-loop sequence containing dT-fluorescein (FAM). B. Representative DNA denaturing gel illustrating the banding pattern of substrates, adenylylated (Ap-) intermediates, single and double ligation products. C, end-joining efficiencies of LIG1 (red circles) and LIG3β (blue diamonds) determined under saturating Mg^{2+} concentrations (18 mM free Mg^{2+}). D, end-joining efficiencies of LIG1 and LIG3β determined under physiological Mg^{2+} conditions (1 mM free Mg^{2+}). E, relative catalytic efficiencies of LIG1 and LIG3β presented in *A and B* are represented as LIG3β/LIG1. F, Mg^{2+} concentration dependences for LIG1 and LIG3 catalyzed blunt-end DNA ligation. Catalytic efficiencies and $V_o/[E]$ values were determined in at least triplicate (mean ± S.D.).

were linearly dependent on substrate concentration (Figure C.5), indicating that the tested substrate concentrations were below the $K_{M,\ DNA}$ value. Strikingly, in the presence of saturating Mg^{2+}, LIG1 and LIG3 had remarkably similar k_{cat}/K_M values for the blunt-end and 3'-DSB substrates. The efficiency of LIG1-catalyzed EJ of 5'-DSB was 10-fold lower than that of LIG3 (Figures 4.2C and 4.2E). The $k_{cat}/K_{M,\ DNA}$ values determined for LIG1 and LIG3 EJ were achieved via different mechanisms: LIG1 efficiency was influenced by greater k_{cat} values than LIG3, whereas LIG3 had lower K_M values than LIG1 under the saturating Mg^{2+} condition (Figures C.5 and C.6). It is notable that the catalytic efficiencies of LIG1 EJ were reduced by 1.5-2 orders of magnitude for all substrates at upon reduction of Mg^{2+} to physiological concentrations. This large effect caused by the reduction of Mg^{2+} is particularly remarkable, because LIG1 had a 10-fold lower K_{Mg} value than LIG3 for SSB ligation (2). Equally surprising, LIG3 specificity remained unchanged for the blunt-end and 3'-DSB substrates at physiological Mg^{2+} concentration (Figure 4.2D). Under the reduced Mg^{2+} condition, LIG3 had a maximal turnover number (k_{cat}) of ~0.008 s^{-1} with the 3'- and 5'-DSB substrates (Figure C.6). This observation indicates that the steady-state rate of cohesive end ligation is limited by the Mg^{2+} cofactor availability at physiological levels, and this rate can be significantly increased by increasing the Mg^{2+} concentration. The k_{cat}/K_M values for LIG3 EJ of 5'- and 3'-DSB substrates were determined by Michaelis-Menten analysis and direct competition reactions, respectively, as the $K_{M,\ DNA}$ values were too low for accurate determination (Figures C.6). The striking differences in the catalytic efficiencies of LIG1- and LIG3-catalyzed EJ in the presence of physiological and saturating Mg^{2+} can be explained by large differences in their Mg^{2+} concentration dependences for EJ (Figure 4.2F). The hyperbolic and sigmoidal Mg^{2+} dependences of LIG3 and LIG1, respectively, highlight why LIG3 had 100-10,000-fold greater catalytic efficiencies than LIG1 at physiological Mg^{2+} concentrations. (Figure 4.2E and 4.2F). The reduced

specificity of LIG1 toward 5'-DSB may be due to the lack of available electrostatic interactions with the DNA backbone opposite the 5'-phosphorylated DNA strand, destabilizing the enzyme•substrate complex. These data indicate LIG1 and LIG3 are both capable of performing EJ reactions; however, the catalytic efficiencies of LIG1 EJ were highly sensitive to Mg^{2+} concentrations.

Abortive ligation by LIG1.

Previous studies indicated that LIG1 activity on SSBs is susceptible to accumulating abortive ligation products at low levels of Mg^{2+} (1, 2). Interestingly, LIG1 accumulated aborted EJ products with each DSB substrate at physiological Mg^{2+} (Figure C.7). LIG1 aborted the 5'-DSB cohesive end substrates to a greater extent than the 3'-DSB and blunt-end substrates, indicating that LIG1 possesses structural preferences for EJ substrates (Figures 4.3 and C.7). These observations indicate LIG1 can readily adenylylate DNA ends, allowing the accumulation of the toxic 5'-DNA-adduct. LIG1 abortive products were generated almost exclusively on A•T terminal base paired cohesive ended substrates (Figure C.7), suggesting the reduced stability of the terminal A•T base pair sufficiently destabilized the enzyme•Ap-DNA complex, thereby preventing the formation of a productive EJ complex (Figures 4.3A and 4.3B). The propensity of LIG1 to accumulate abortive intermediates was not dependent on substrate concentration; roughly 70% of all adenylyl transfer events failed to form productive end-joining complexes with the 3'-DSB substrate (Figure 4.3C). Likewise, the blunt-end and 5'-DSB substrates were aborted 75% and 90%, respectively, relative to successful end-joining events (Figure C.7). In contrast, LIG3 did not accumulate appreciable abortive products for any of the DSB substrates at either physiological or

saturating Mg^{2+} concentrations (Figure 4.3A). As observed with SSB ligation, abortive ligation by LIG1 was completely alleviated at saturating Mg^{2+} concentrations.

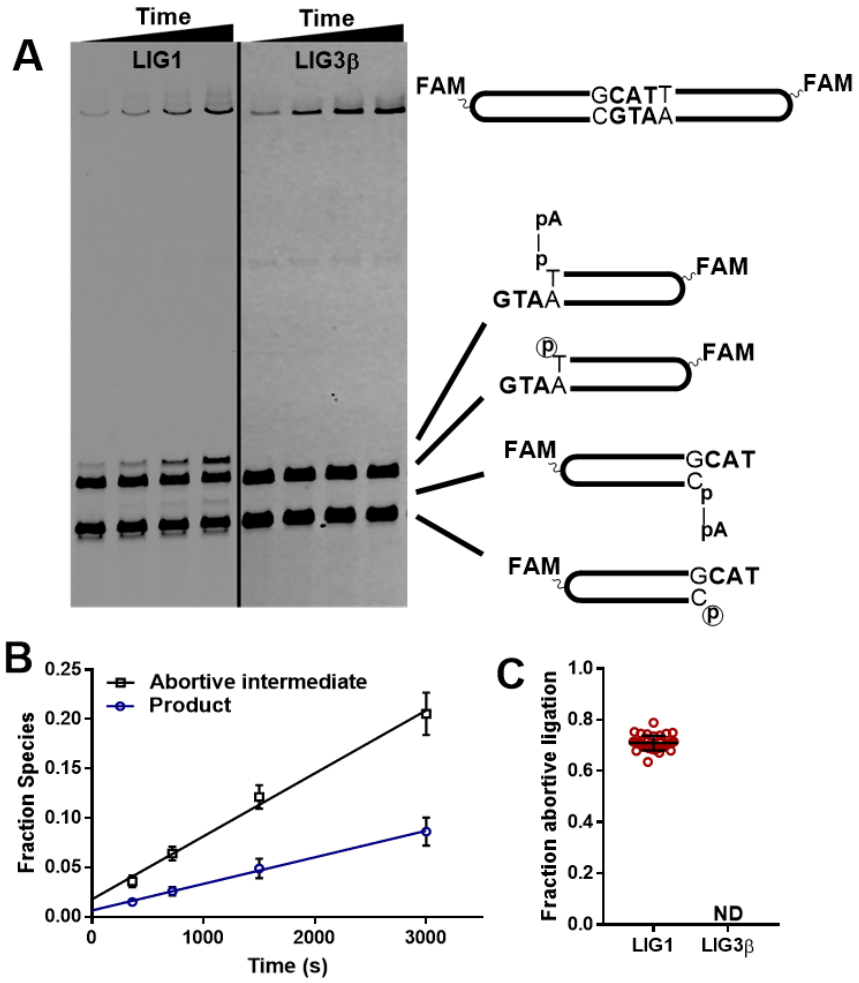

Figure 4.3. Abortive ligation by LIG1 is dependent on DNA sequence. A, DNA denaturing PAGE gel comparing LIG1 and LIG3β ligation of the 3'-3 nt overhang substrate under physiological Mg^{2+} in standard reaction buffer. LIG1 accumulates adenylylated terminal A•T base pairs to a greater extent than terminal G•C base pairs. Abortive ligation products generated by LIG3β are below the limit of detection (N.D.). B, comparison of fraction abortive EJ products and successful EJ products generated by LIG1. Partitioning between successful ligation and abortive ligation is independent of substrate concentration. Data averaged in *B* was acquired from reactions containing 50, 100 and 200 nM 3'-3nt DNA. Time points were taken at 360, 720, 1500 and 3000 seconds. C, Accumulation of adenylylated 3'-3nt DNA by LIG1. Greater than 70% of all adenylyl transfer events by LIG1 result in aborted ligation products (Figure C.8). Presented in (*B*) is the average of 9 independent experiments with error bars representing one standard deviation from the mean.

Influence of molecular crowding on EJ.

We next considered the impact that the crowded cellular environment would have on DNA EJ. Macromolecules occupy 20-30% of the intracellular volume and the sum of protein and oligonucleotide concentrations is ~300 mg/mL (23). Molecular crowding agents increase the effective viscosity of a solution thereby reducing translational diffusion, aiding in substrate capture and stabilization of the enzyme•substrate complex (24). To mimic the crowded environment of the cell, we employed the inert molecular crowding agent polyethylene glycol 6000 (PEG). Molecular crowding agents like PEG have been previously shown to increase ligase EJ activities (7, 20, 25, 26). To test the effect of molecular crowding on LIG1 mediated EJ, we determined that 10% PEG was suitable for EJ analysis by LIG1 and LIG3. PEG concentrations greater than 10% resulted in LIG3 inhibition, while LIG1 activity was equally stimulated within the 10% to 15% range (Figure 4.4A). Under physiological Mg^{2+} conditions, we found that the k_{cat}/K_M values of LIG1 EJ increased by 10- and 30-fold for the 3'-DSB and blunt-end substrates, respectively. Surprisingly, the catalytic efficiency of LIG1-catalyzed 5'-DSB EJ increased by two orders of magnitude in the presence of PEG (Figure 4.4B). The 10% PEG also reduced the accumulation of abortive ligation products by 20–30% (Figure C.7). Together, our studies indicate molecular crowding enhances the catalytic efficiency LIG1 EJ, suggesting that LIG1 is capable of catalyzing EJ reactions within the context of the crowded cellular environment. These findings corroborate prior observations that LIG1 is prone to abortive ligation, and may require the activity of aprataxin, an RNA/DNA polynucleotide deadenylase that can restore the 5' phosphate by hydrolyzing the 5'-5' AMP-DNA intermediate (27).

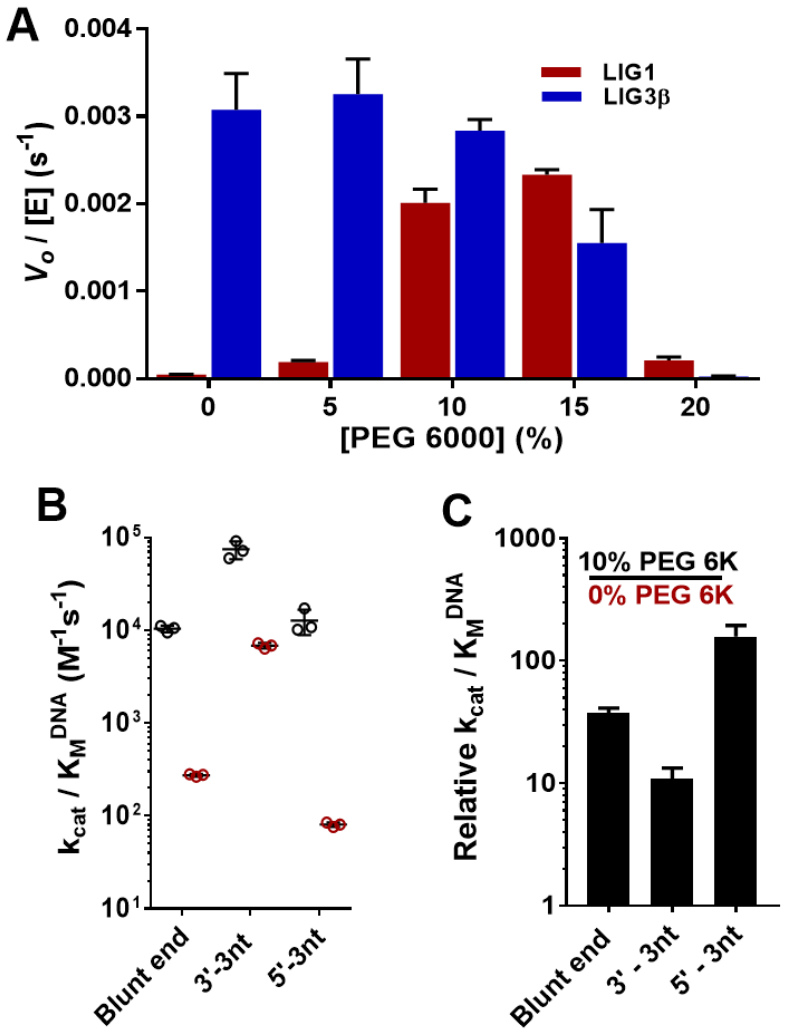

Figure 4.4. Molecular crowding enhances LIG1 end-joining activity. A, comparison of LIG1 and LIG3 ligation rates at various polyethylene glycol 6000 (PEG) concentrations in the presence of physiological Mg^{2+}. PEG concentrations in excess of 10% (w/v) reduced LIG3 blunt-end ligation rates. LIG1 maximal ligation rates were observed in the presence of 10 and 15% PEG. B, end-joining efficiencies of LIG1 in the presence (black circles) and absence (red circles) of 10% PEG and physiological Mg^{+2} as described in the methods. C, relative catalytic efficiencies of LIG1 in the presence and absence of PEG. Influence of PEG on end-joining rates and catalytic efficiencies were determined in at least triplicate (mean ± S.D.).

Pre-steady-state analysis of LIG3-catalyzed EJ.

Interestingly, molecular crowding agents enabled the pre-steady-state analysis of sequential ligation events by stabilizing LIG3 complexes and reducing the rate of product release. Under these conditions, LIG3 exhibited a pre-steady-state burst, followed by a slow steady-state ligation (Figure 4.5A). The k_{cat} values for blunt-end, 3'- and 5'-DSB ligation by LIG3 are within 2-fold as determined by analysis of the steady-state rates (Figure 4.5A, Table 4.1). To determine the observed rate constants of sequential ligation events by LIG3, optimized time courses enabled the detection of the first and second ligation products (Figure 4.5B). Pre-steady-state experiments were designed such that substrate concentration (40 nM) was in 2-fold excess of LIG3 (20 nM) to prevent competitive inhibition by LIG3 end-binding. Observed rate constants were determined by fitting the data to a two-step irreversible model using the kinetics simulation software Berkeley Madonna. The blunt-end and 5'-DSB substrates had similar observed rate constants for the first ligation event. The observed rate constants we report encapsulate multiple steps of the ligation mechanism. Following the first ligation event, LIG3 undergoes conformational changes to release AMP and sample adjacent sites on the DNA. During this time, LIG3 undergoes self-adenylylation while associated with DNA and is able to reposition, capture, and repair the nick on the opposing DNA strand (Figure 4.5D). This model, were it to operate in a cell, ensures faithful ligation of DSB with compatible ends. We note that many physiological breaks will only contain a single ligatable strand and additional processing steps would be required to generate the substrate for the second DNA ligation event.

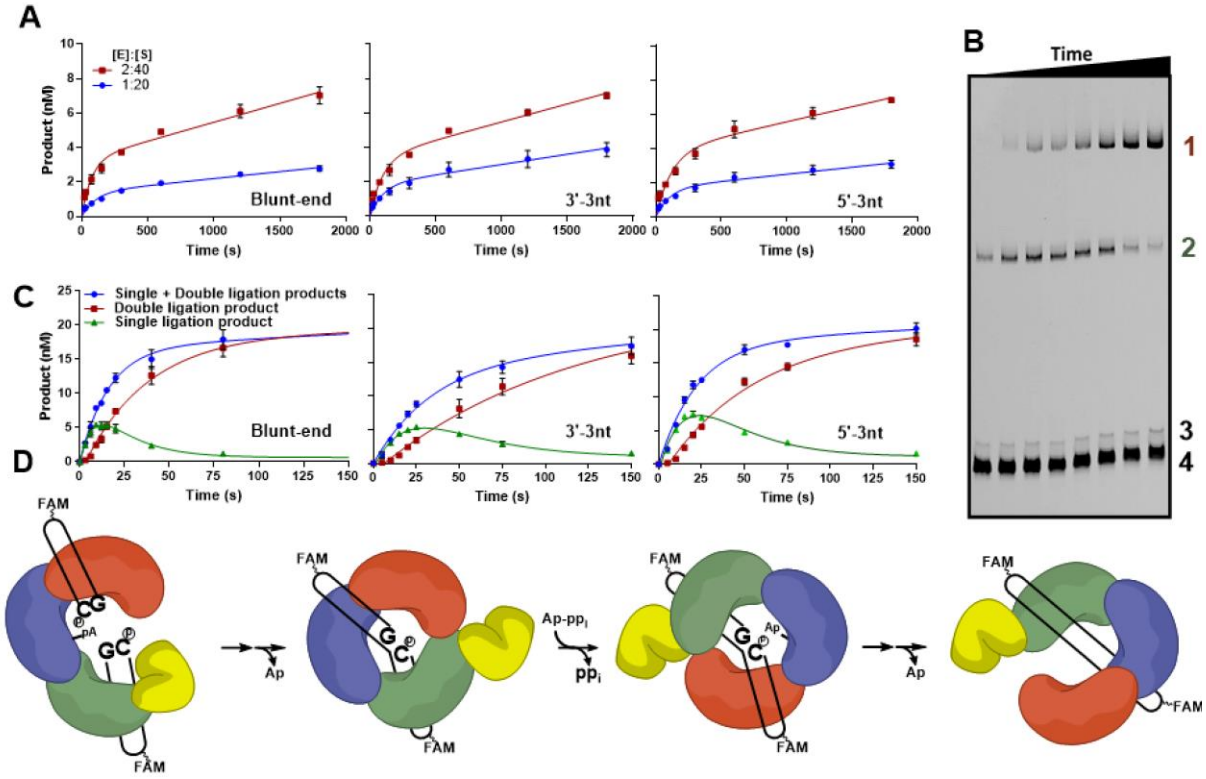

Figure 4.5. Molecular crowding enables the detection of sequential ligation events by LIG3β. A, burst analysis of 1 and 2 nM LIG3 in the presence of 20 and 40 nM EJ substrates, respectively. B, representative gel illustrating the formation and decay of the single ligation product (*labeled 2*) followed by the formation of the double ligation product (*labeled 1*) during blunt-end ligation at physiological Mg^{2+}. *3* and *4* indicate adenylylated substrate and substrate, respectively. C, pre-steady-state quantification of single (green) and double (red) blunt-end ligation products. Sum of both products presented in blue. D, simplified mechanism of sequential ligation events by LIG3β. Domains are color coded as follows: ZnF, *yellow*; DBD, *green*; NTase, *blue*; OB-fold, *red*. Experiments in *B* and *C* were performed in triplicate and are presented as mean ± S.D..

Table 4.1
Rate constants for sequential ligation by LIG3β[a]

k_{obs} (s^{-1})	Blunt end	3'-3nt	5'-3nt
First ligation	0.054 ± 0.004	0.027 ± 0.008	0.043 ± 0.005
Second ligation	0.082 ± 0.005	0.038 ± 0.004	0.040 ± 0.002
Steady-state[b]	0.00097 ± 0.00020	0.0021 ± 0.0002	0.0018 ± 0.0002

[a]Observed single-turnover rate constants obtained at physiological Mg^{2+} in the presence of 10% PEG (Figure 4.5C). Reactions contained 20 nM LIG3β and 40 nM substrate. Reactions were performed at 1 mM free Mg^{2+}.
[b]Values represent k_{cat} determined using 1 and 2 nM enzyme in the presence of 20 and 40 nM EJ substrates, respectively. Reactions were performed at 1 mM free Mg^{2+} in the presence of 10% PEG. Observed velocities were divided by the concentration of enzyme to yield k_{cat} (Figure 4.5B).

Conclusions

In response to the recent observations of LIG1 mediated EJ in mouse B-cells (17, 18), we pursued the first biochemical analysis of human DNA LIG1 catalyzed end-joining. We demonstrate that LIG1 and LIG3 are capable of joining various DNA ends. In the presence of artificially high Mg^{2+} cofactor concentrations, LIG1 EJ activity is similar to that of LIG3. Upon reduction of cofactor concentration to physiological levels, the catalytic efficiency of LIG1 EJ was reduced by 2-4 orders of magnitude, while LIG3 catalyzed EJ remained relatively unchanged. Strikingly, the catalytic efficiency of LIG1 EJ was partially restored in the presence of PEG, a molecular crowding agent, raising the possibility that LIG1 participates in EJ within the crowded environment of a cell. Notably, LIG1's weak affinity for DSB substrates resulted in a substantial accumulation of abortive EJ products at physiological Mg^{2+}. LIG1 abortive ligation was slightly reduced by the addition of PEG, and completely abolished in the presence high of Mg^{2+}

concentrations. Under all conditions tested, LIG3 shows higher affinity for DSBs, and no propensity to accumulate abortive EJ products. Furthermore, this greater affinity enabled the first transient kinetic analysis of LIG3 catalyzed DSB ligation. Our kinetic analysis of LIG1- and LIG3-catalyzed EJ sheds light on the similarities, differences and erroneous behaviors of the human DNA ligases, facilitating future investigations of these activities.

Experimental Procedures

Recombinant LIG1 and LIG3β.

Human DNA LIG1 N-terminal truncation mutant Δ232 was cloned into a pET19 vector containing an N-terminal His_6-PreScission protease cleavable tag and expressed in Rosetta2 (DE3) *E. coli* by auto induction in terrific followed by a three-step purification as described previously (28). Nuclear LIG3β was cloned into a pET28 vector containing an N-terminal His_6-SUMO protease cleavable tag and expressed in C41 pRare3 (DE3) cells by IPTG induction in Luria broth followed by the four step purification as previously described (2).

DNA substrates.

Oligonucleotides were purchased from KECK oligonucleotide Synthesis facilities and Integrated DNA Technologies. All oligonucleotides were further purified by 15% polyacrylamide, 8 M urea denaturing PAGE as previously described (1). SSB (nicked DNA) substrate was described previously (1, 2). End-joining DNA substrate concentrations were determined by absorbance of the internal dT-fluorescein fluorophore at 495 nm. DNA concentrations described

in assays refers to the amount of product capable of forming (e.g., 100 nM blunt-end substrate contains 200 nM of ligatable hairpin ends). The 14 bp blunt-end substrate sequence: pCATAGAATATTTACGFAGTAAATATTCTATG. The 3'-DSB overhang substrate consisted of two DNA hairpins of differing length (14 and 16 bp) containing complementary overhangs. The 14 bp hairpin (34 nt in length) sequence : pCATAGAATACTTACGFAGTAAGTATTCTATGCAT. And the 16 bp hairpin (38 nt in length) sequence: pAGAATACTTATTAATCGFAGATTAATAAGTATTCTATG. The 5'-DSB 14 bp hairpin contained the sequence: pTACCATAGAATACTTACGFAGTAAGTATTCTATG and the 16 bp: pGTAAGAATACTTATTAATCGFAGATTAATAAGTATTCT. The 10bp duplex hairpin and 18 bp duplex hairpins used to investigate substrate length dependences are pGAATATTTACGFAGTAAATATTC and pCATAGAATATTTATTAACGFAGTTAATAAATATTCTATG, respectively. Each of the above oligonucleotides were 5'-phosphorylated (p), and contained an internal dT-fluorescein (F). Hairpins were annealed as previously described (2). Digestion of oligonucleotide species observed via DNA denaturing PAGE was performed as described in Figure C.3.

Gel-based end-joining assay.

Ligation reactions were performed at 37 ˚C in standard reaction buffer (50 mM NaMOPS, pH 7.5, 10% glycerol, 1 mM ATP, 1 mM DTT, 100 µg/µL BSA) at 150 mM ionic strength, unless otherwise stated. Ionic strength was controlled using the Debye-Hückel theory of electrolytes. $Mg(OAc)_2$ and NaOAc concentrations were adjusted to achieve the desired reaction conditions. Reactions were stopped by the addition of reaction solutions into 1.2X quench solution (90% formamide, 50 mM EDTA, 0.006% bromophenol blue 0.006% xylene cyanol) at predetermined

times. Quenched samples were loaded directly onto a running 15% (w/v) polyacrylamide, 8 M urea, 1 × TBE DNA-denaturing gel. Gels were scanned using a typhoon 5 imaging system (GE) set to monitor emission at 525 (BP20) with excitation set to 488 nm. Separated DNA species were quantified using ImageQuant TL (GE) and plotted as a function of time using GraphPad Prism.

Effects of chloride on catalytic efficiency.

Multiple-turnover reactions were performed in standard reaction buffer with ionic strength maintained at 300 mM. All reactions contained 20 mM $Mg(OAc)_2$ while altering the Cl^- concentration by varying the ratios of NaCl to NaOAc. Cl^- concentrations ranged from 0 – 205 mM. Nicked DNA concentration dependences were performed to determine catalytic efficiencies ($k_{cat}/K_{M,\ DNA}$) under varying Cl^- concentrations. Reactions contained 0.5 nM enzyme while substrate ranged from 5 - 1,500 nM. Two methods were utilized to determine catalytic efficiency of LIG1 and LIG3. Linear regression of initial rates ($V_o/[E]$ (s^{-1})) at 5, 10, 20 and 40 nM DNA (LIG1) (Figure C.1B), and Michaelis-Menten analysis of rates (LIG3) (Equation 4.1, Figure C.1C). The catalytic efficiencies of LIG1 and LIG3β were plotted as a function of Cl^- concentration and fit well to a four parameter dose response curve (Figure C.1).

$$\frac{\boldsymbol{V_o}}{[\boldsymbol{E}]} = \frac{\boldsymbol{k_{cat}}\times[\boldsymbol{S}]}{(\boldsymbol{K_M}+[\boldsymbol{S}])} \qquad \text{(Eq. 4.1)}$$

Multiple-turnover kinetics of end-joining.

EJ efficiencies were determined using the discontinuous gel-based assay. reactions were performed in standard reaction buffer at 150 mM ionic strength at 37˚C. Initial rates of steady-state reactions were determined by linear regression of the first 10 % of product formation (product is the sum of singly and doubly ligated products). LIG1 EJ efficiencies were determined by reacting 5 nM enzyme with 25, 50, 100 and 200 nM DNA substrate at 2 and 20 mM $Mg(OAc)_2$. Free Mg^{2+} concentrations of 1 and 18 mM were estimated based on the K_d values for the ATP•Mg^{2+} and ATP•$2Mg^{2+}$ complexes (12 μM and 17 mM, respectively), as described previously (2). Plotting the initial rates of product formation as a function of substrate concentration yield catalytic efficiencies ($k_{cat}/K_{M,\ DNA}$) that report on successful end-joining events. Our reports of catalytic efficiency do not include the consumption of substrate that result in the formation of abortive ligation intermediates observed under physiological Mg^{2+} conditions. LIG1 experiments described above were repeated in the presence of 10% polyethylene glycol. The catalytic efficiencies of LIG3β EJ were determined by reacting 1 nM enzyme with 5, 10, 20, and 40 nM DNA substrate at 2 and 20 mM $Mg(OAc)_2$. Reactions in which EJ rates were linearly dependent on DNA concentration were fit using linear regression to determine k_{cat}/K_M values. Reactions in which DNA concentrations ranged from below to above K_M, were fit using the Michaelis-Menten equation to determine k_{cat} and K_M values. Substrates in which a k_{cat}/K_M value could not be determined were subjected to a direct competition reaction with the blunt-ended substrate to determine a relative k_{cat}/K_M value. Competition experiments contained 4 nM LIG3 with 30 nM + 200 nM as well as 30 nM + 400 nM of the blunt-end and 3'-DSB substrates, respectively, in the presence of 2 mM $Mg(OAc)_2$. The Mg^{2+} concentration dependences of LIG1 and LIG3β blunt-end ligation (0-30 mM $Mg(OAc)_2$) were conducted in standard reaction buffer containing 5 nM enzyme and 300 nM

blunt-end substrate. Plots of initial rates vs Mg^{2+} concentration fit well to a two metal random binding model (LIG1, Equation 4.3) and a hyperbolic curve (LIG3β, Equation 4.4). Determination of fraction abortive ligation was achieved using Equation 4.5. Initial rates of LIG1 and LIG3 in the presence of 0-20% polyethylene glycol 6000 (PEG) contained 5 nM enzyme and 200 nM blunt-end in the presence of 2 mM $Mg(OAc)_2$ in standard reaction buffer.

$$\frac{V_A}{V_B} = \frac{\left(k_{cat}/K_M\right)^A \times [A]}{\left(k_{cat}/K_M\right)^B \times [B]} \quad \text{(Eq. 4.2)}$$

$$\frac{V_o}{[E]} = \frac{V_o/[E]}{\frac{K_1 * K_2}{[Mg^{2+}]^2} + \frac{K_1 + K_2}{[Mg^{2+}]} + 1} \quad \text{(Eq. 4.3)}$$

$$\frac{V_{init}}{[E]} = \frac{k_{cat} \times [Mg^{2+}]}{(K_{Mg} + [Mg^{2+}])} \quad \text{(Eq. 4.4)}$$

$$\textbf{Fraction abortive ligation} = \frac{[I]}{([I]+[P])} \quad \text{(Eq. 4.5)}$$

Pre-steady-state analysis of LIG3β.

Burst and pre-steady-state analysis of LIG3β was performed in standard reaction buffer containing 10% PEG with 2 mM $Mg(OAc)_2$. Burst experiments contained 1 and 2 nM LIG3β with 20 and 40 nM DNA substrates, respectively. Reported bursts are the sum of the single and double ligation products. Time courses fit well to Equation 4.6 where *Ao* is the burst amplitude, *k* is the

pre-steady-state rate constant, V_{ss} is the steady-state velocity and t is time. Pre-steady-state reactions contained 20 nM LIG3β and 40 nM substrate. Single and double ligation products were plotted individually and observed rate constants (k_{obs}) determined using a two step-irreversible mechanism in the kinetics simulation program Berkeley Madonna.

$$[\boldsymbol{P}] = \boldsymbol{A_o}\left(\mathbf{1} - \boldsymbol{exp}^{-\boldsymbol{k}\times\boldsymbol{t}}\right) + \left(\boldsymbol{V_{ss}} \times \boldsymbol{t}\right) \quad \text{(Eq. 4.6)}$$

References

1. Taylor MR, Conrad JA, Wahl D, & O'Brien PJ (2011) Kinetic Mechanism of Human DNA Ligase I Reveals Magnesium-dependent Changes in the Rate-limiting Step That Compromise Ligation Efficiency. *J. Biol. Chem.* 286(26):23054-23062.

2. McNally JR & O'Brien PJ (2017) Kinetic analyses of single-stranded break repair by human DNA ligase III isoforms reveal biochemical differences from DNA ligase I. *J. Biol. Chem.* 292(38):15870-15879.

3. Cotner-Gohara E, *et al.* (2010) Human DNA Ligase III Recognizes DNA Ends by Dynamic Switching between Two DNA-Bound States. *Biochemistry* 49(29):6165-6176.

4. Cotner-Gohara E, Kim I-K, Tomkinson AE, & Ellenberger T (2008) Two DNA-binding and Nick Recognition Modules in Human DNA Ligase III. *J. Biol. Chem.* 283(16):10764-10772.

5. Pascal JM, O'Brien PJ, Tomkinson AE, & Ellenberger T (2004) Human DNA ligase I completely encircles and partially unwinds nicked DNA. *Nature* 432(7016):473-478.

6. Taylor RM, Whitehouse CJ, & Caldecott KW (2000) The DNA ligase III zinc finger stimulates binding to DNA secondary structure and promotes end joining. *Nucleic Acids Res.* 28(18):3558-3563.

7. Bauer RJ, *et al.* (2017) Comparative analysis of the end-joining activity of several DNA ligases. *PLoS One* 12(12):e0190062.

8. Kukshal V, *et al.* (2015) Human DNA ligase III bridges two DNA ends to promote specific intermolecular DNA end joining. *Nucleic Acids Res.* 43(14):7021-7031.

9. Chen X, *et al.* (2009) Distinct kinetics of human DNA ligases I, IIIa, IIIb and IV reveal direct DNA sensing ability and differential physiological functions in DNA repair. *DNA repair* 8(8):961-968.

10. Della-Maria J, *et al.* (2011) Human Mre11/Human Rad50/Nbs1 and DNA Ligase IIIα/XRCC1 Protein Complexes Act Together in an Alternative Nonhomologous End Joining Pathway. *J. Biol. Chem.* 286(39):33845-33853.

11. Simsek D & Jasin M (2011) DNA ligase III: A spotty presence in eukaryotes, but an essential function where tested. *Cell Cycle* 10(21):3636-3644.

12. Mackey ZB, *et al.* (1999) DNA Ligase III Is Recruited to DNA Strand Breaks by a Zinc Finger Motif Homologous to That of Poly(ADP-ribose) Polymerase Identification of Two Functionally Distinct DNA Binding Regions Within DNA Ligase III. *J. Biol. Chem.* 274(31):21679-21687.

13. Kulczyk AW, Yang J-C, & Neuhaus D (2004) Solution Structure and DNA Binding of the Zinc-finger Domain from DNA Ligase IIIα. *J. Mol. Biol.* 341(3):723-738.

14. Taylor RM, Whitehouse J, Caldecott KW, Cappelli E, & Frosina G (1998) Role of the DNA ligase III zinc finger in polynucleotide binding and ligation. *Nucleic Acids Res.* 26(21):4804-4810.

15. Tomkinson AE & Sallmyr A (2013) Structure and function of the DNA ligases encoded by the mammalian LIG3 gene. *Gene* 531(2):150-157.

16. Ellenberger T & Tomkinson AE (2008) Eukaryotic DNA Ligases: Structural and Functional Insights. *Annu. Rev. Biochem.* 77(1):313-338.

17. Masani S, Han L, Meek K, & Yu K (2016) Redundant function of DNA ligase 1 and 3 in alternative end-joining during immunoglobulin class switch recombination. *Proc. Natl. Acad. Sci. U. S. A.* 113(5):1261-1266.

18. Lu G, *et al.* (2016) Ligase I and ligase III mediate the DNA double-strand break ligation in alternative end-joining. *Proc. Natl. Acad. Sci. U. S. A.* 113(5):1256-1260.

19. Elder RH, Montecucco A, Ciarrocchi G, & Rossignol JM (1992) Rat liver DNA ligases. Catalytic properties of a novel form of DNA ligase. *Eur. J. Biochem.* 203(1-2):53-58.

20. Teraoka H & Tsukada K (1987) Influence of polyethylene glycol on the ligation reaction with calf thymus DNA ligases I and II. *J. Biochem.* 101(1):225-231.

21. Tomkinson AE, Vijayakumar S, Pascal JM, & Ellenberger T (2006) DNA Ligases: Structure, Reaction Mechanism, and Function. *Chem. Rev.* 106(2):687-699.

22. Sallmyr A & Tomkinson AE (2018) Repair of DNA double-strand breaks by mammalian alternative end-joining pathways. *J. Biol. Chem.* 293(27):10536-10546.

23. Ellis RJ (2001) Macromolecular crowding: obvious but underappreciated. *Trends Biochem. Sci.* 26(10):597-604.

24. Cravens SL, *et al.* (2015) Molecular crowding enhances facilitated diffusion of two human DNA glycosylases. *Nucleic Acids Res.* 43(8):4087-4097.

25. Shuman S & Ru XM (1995) Mutational analysis of vaccinia DNA ligase defines residues essential for covalent catalysis. *Virology* 211(1):73-83.

26. Pheiffer BH & Zimmerman SB (1983) Polymer-stimulated ligation: enhanced blunt- or cohesive-end ligation of DNA or deoxyribooligonucleotides by T4 DNA ligase in polymer solutions. *Nucleic Acids Res.* 11(22):7853-7871.

27. Rass U, Ahel I, & West SC (2007) Actions of aprataxin in multiple DNA repair pathways. *J. Biol. Chem.* 282(13):9469-9474.

28. Maffucci P, *et al.* (2018) Biallelic mutations in DNA ligase 1 underlie a spectrum of immune deficiencies. *J. Clin. Invest.* 128(12):5489-5504

Appendix C

Additional figures to support Chapter 4

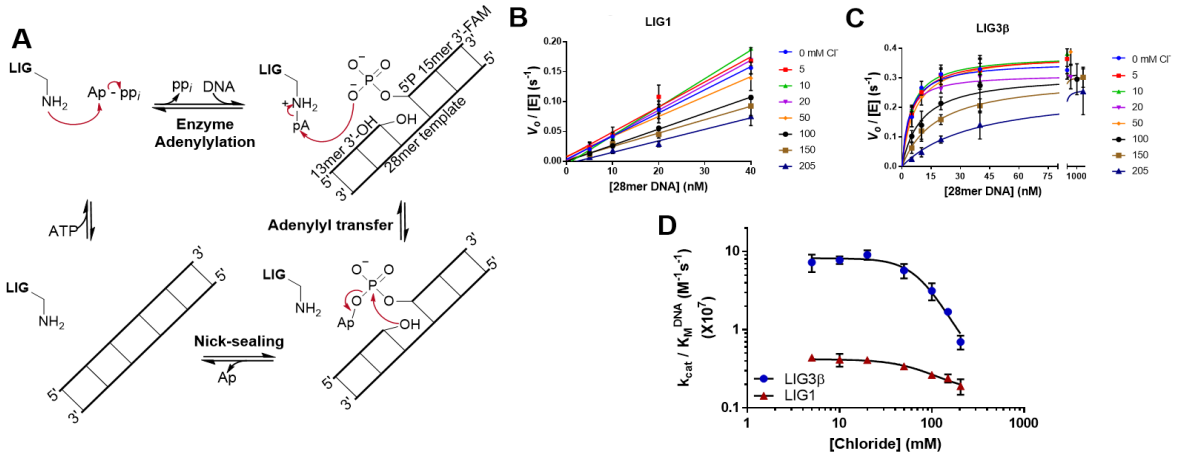

Figure C.1. Influence of chloride on the catalytic efficiencies of LIG1 and LIG3β. A, chemical mechanism for nicked DNA ligation. 28mer nicked DNA substrate (2) was used to determine k_{cat}/K_M values. Catalytic efficiencies were determined by (B) linear regression of V/E values at numerous subsaturating DNA concentrations or by (C) obtaining k_{cat} and K_M values. Reactions were performed at 300 mM ionic strength with 20 mM $Mg(OAc)_2$ used in all reactions. Desired chloride concentrations were achieved by varying NaCl:NaOAc ratios. 0.5 nM LIG3β and LIG1 were assayed in the presence of 5-1500 nM DNA in standard reaction buffer containing 1 mM ATP and 1 mM DTT. D, catalytic efficiencies vs chloride concentrations illuminate differential inhibitory effects of chloride on the ligases. Experiments were completed in duplicate (mean ± S.D.).

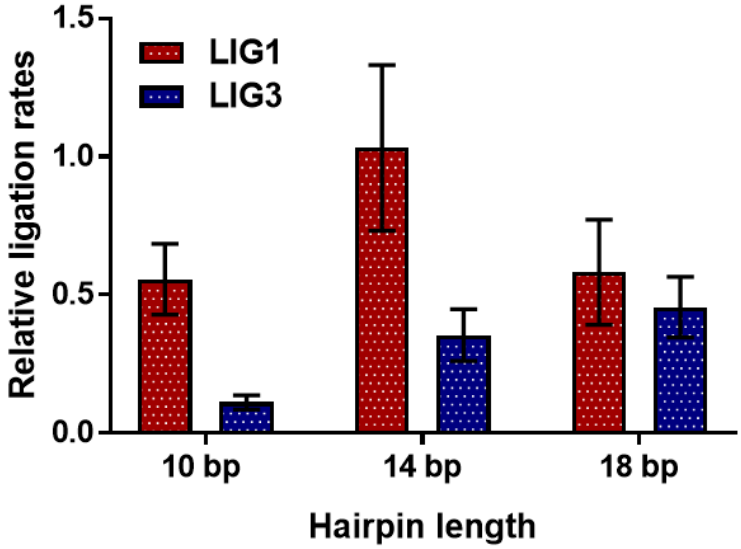

Figure C.2. Hairpin length dependence on LIG1 and LIG3β end-joining. End-joining rates of LIG1 and LIG3 were investigated in the presence of 5 nM enzyme, 300 nM DNA (600 nM ligatable ends), saturating Mg^{2+} in standard reaction buffer with ionic strength maintained at 150 mM using NaCl. Ligation rates were within 2-fold for LIG1 on all tested blunt-end substrate lengths. Ligation rates were within 3-fold for of all tested hairpin lengths. Reaction rates were normalized to the LIG1 end-joining reactions with14bp duplex DNA. Data suggests the 14 bp hairpin was sufficient in length for end-joining analysis of DNA LIG1 and LIG3. 10bp and 18bp DNA sequences can be found it the *Materials and Methods.* Reactions were performed in duplicate (mean ± S.D.).

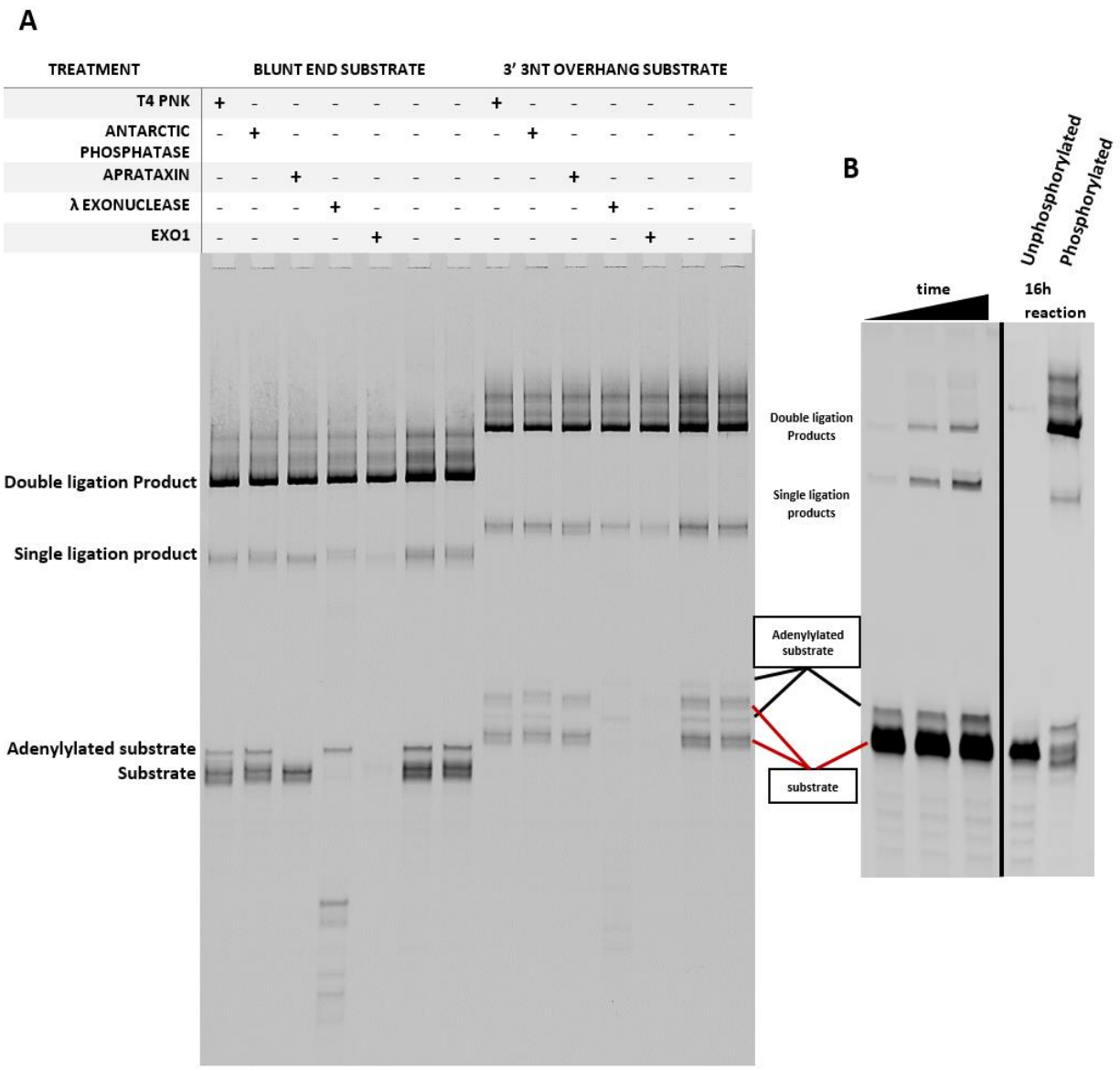

Figure C.3. Identification of substrate, intermediate and product bands of DSB analysis. Product and intermediate species generated from an overnight ligation reaction containing 300 nM DNA, 20 nM LIG3β in standard reaction buffer were subject to analysis by various enzymes for band identification. Ligation products were investigated at a final solution volume of 20 uL containing 150 nM of DSB ligation products. A. Enzymatic analysis of products proceeded for 4 hours at 37℃ in the presence of 10 U of T4 PNK, 5 U Antarctic phosphatase, 5 nM aprataxin, 5 U lambda exonuclease, 10 U EXO1. Reactions were incubated at 95℃ to stop reactions and analyzed by DNA denaturing PAGE. B. Identification of mid-sized product band. Left, 50:50 mixture of unphosphorylated (Antarctic phosphatase treated) and phosphorylated (T4 PNK treated) blunt end substrates generate 50:50 mixture of singly and doubly ligated product species. right, 16 hour ligation reaction of unphosphorylated and phosphorylated blunt end products confirms efficient dephosphorylation and phosphorylation of blunt end DNA substrates.

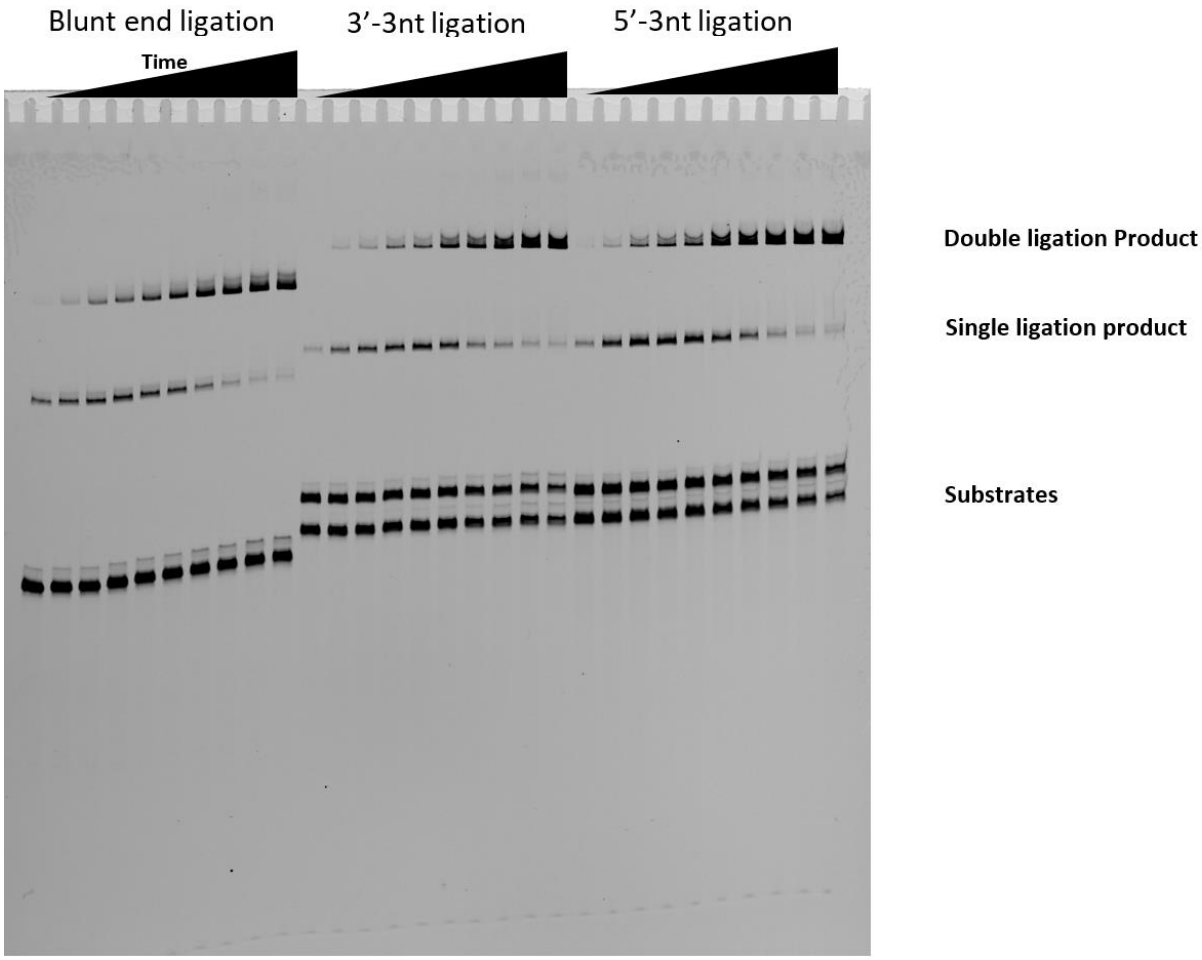

Figure C.4. transient kinetic analysis of sequential ligation events by LIG3β. Representative gel of quantified DNA species and time courses used to determine sequential ligation rates by LIG3β on blunt, 3’-3nt, and 5’-3nt overhang substrates. Experiments investigating the sequential ligation events of LIG3 mediated end-joining contained 20 nM LIG3β, 40 nM DNA (80 nM ends), 1 mM ATP, 2 mM $Mg(OAc)_2$, in standard reaction buffer with ionic strength maintained at 150 mM using NaOAc. Data were acquired from 2 – 150 seconds. Experiments were completed in triplicate and are represented as mean ± S.D..

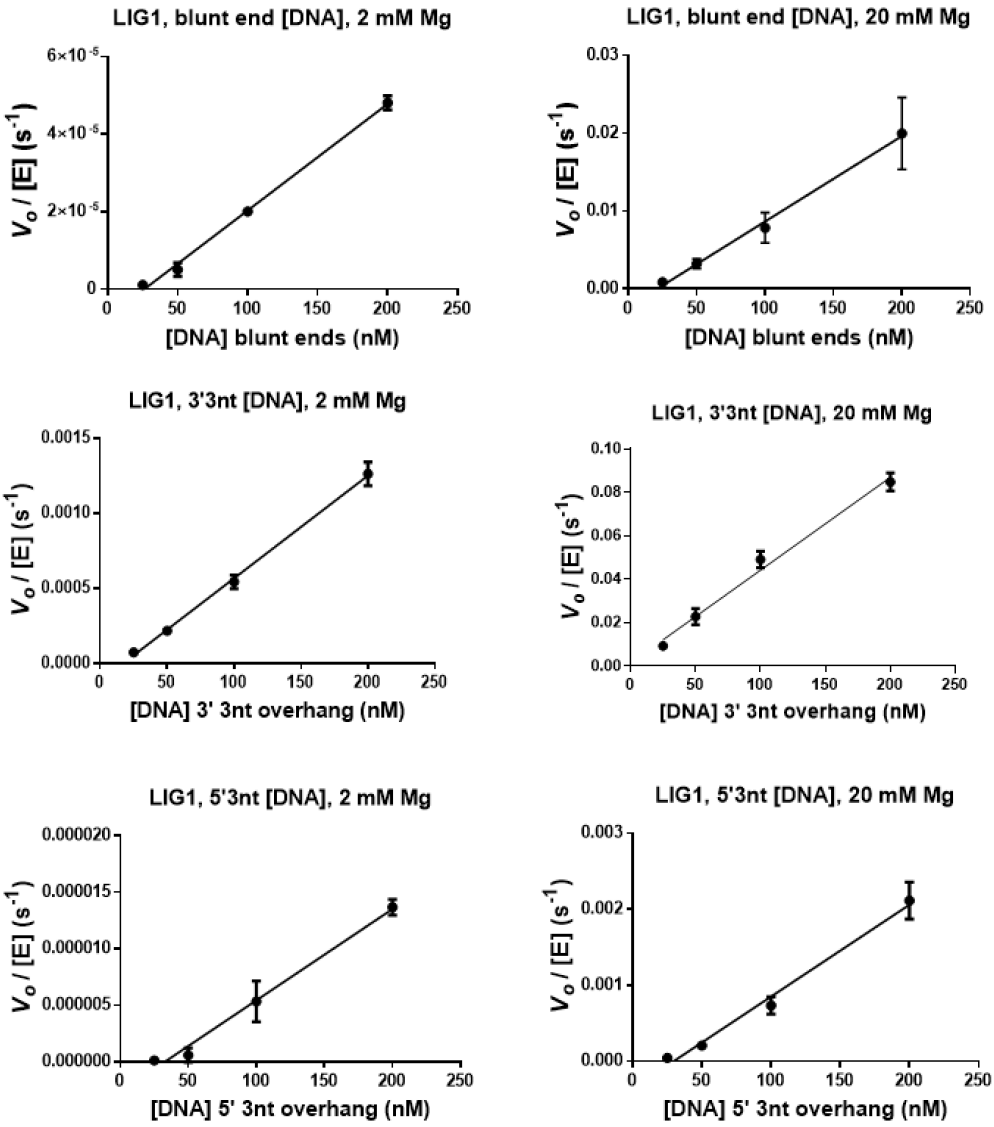

Figure C.5. Determination of LIG1 specificity constants. DNA concentration dependences were conducted in the presence of 5 nM LIG1, 2 and 20 mM Mg^{2+}, 1 mM ATP and 25-200 nM DNA. Ligatable ends tested include: blunt ends, 3' and 5' cohesive ends, 3 nucleotides in length. Reported catalytic efficiencies were calculated using linear regression of the DNA concentration dependence reactions. Experiments were repeated 3 times with error bars representing on standard deviation from the mean. Catalytic efficiencies values were calculated using the rates of successful ligation events.

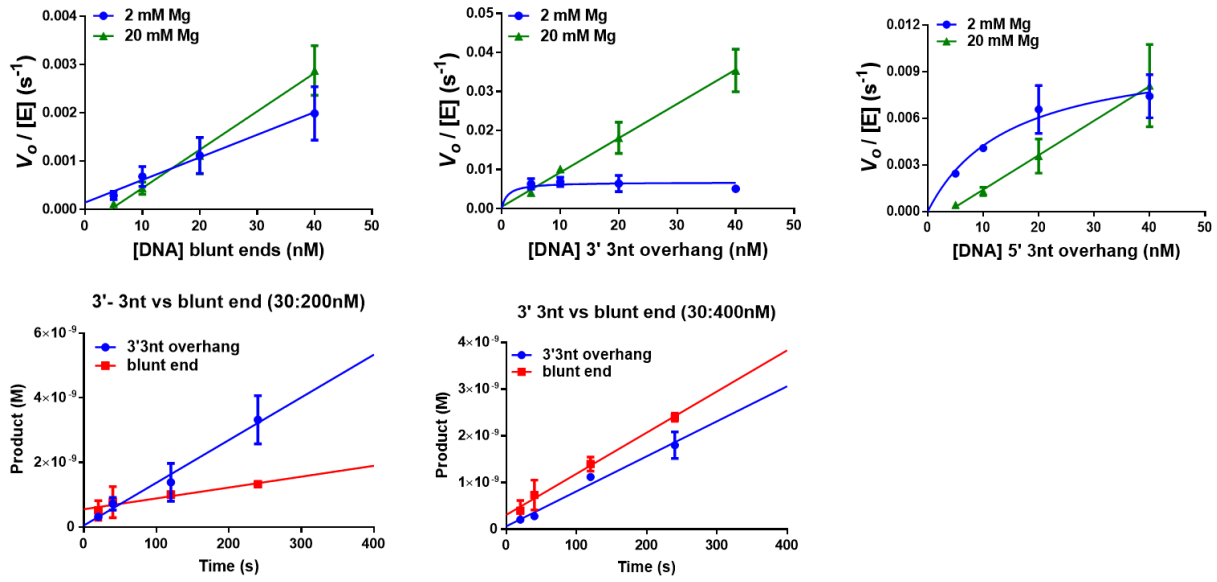

Figure C.6. Determination of LIG3β specificity constants. DNA concentration dependences were conducted in the presence of 1 nM LIG3β, 2 and 20 mM Mg^{2+}, 1 mM ATP and 5-40 nM DNA. ligatable ends tested include: blunt ends, 3' and 5' cohesive ends, 3 nucleotides in length. All substrate concentration dependences were linear at high Mg^{2+} concentrations. Cohesive ended substrates at 2 mM Mg^{2+} saturate at low mM Mg^{2+} range due to a maximal ligation rate of roughly 0.007 s^{-1}. Reported catalytic efficiencies were calculated using linear regression of the DNA concentration dependence reactions. The 5' 3nt cohesive end substrate was calculated using the estimated k_{cat} and K_M values determined using the Michaelis-Menten equation. To determine the catalytic efficiency of the 3' 3nt overhang substrate, direct competition studies (3' 3nt vs blunt end ligation) were performed in the presence of 4 nM LIG3β, 2 mM Mg^{2+}, 1 mM ATP in standard reaction buffer in the presence of 30:200 or 30:400 nM of 3'3nt:blunt end substrates, respectively.

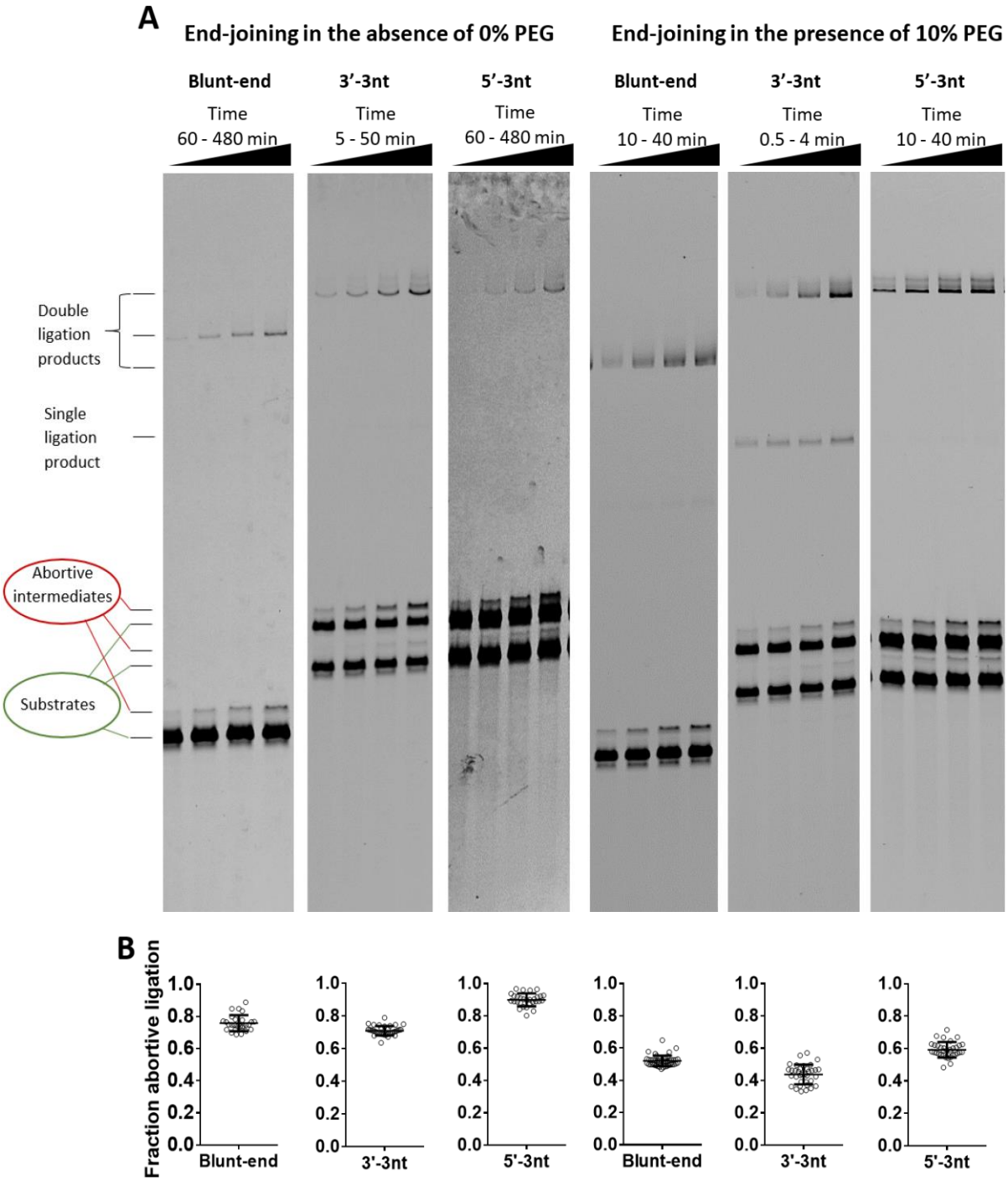

Figure C.7. Polyethylene glycol increases LIG1 reaction rates while reducing abortive ligation at physiological Mg^{2+}. A, representative gels illustrate the accumulation of abortive intermediates and products generated during LIG1 catalyzed end-joining in the absence (*left*) and presence (*right*) of 10% PEG at 1 mM free Mg^{2+}. Reactions contained 5 nM LIG1 and 100 nM of designated DNA in standard reaction buffer. B, LIG1 abortive ligation is reduced by 20 - 30% in the presence of 10% PEG. Fraction abortive ligation was calculated as previously described (1).

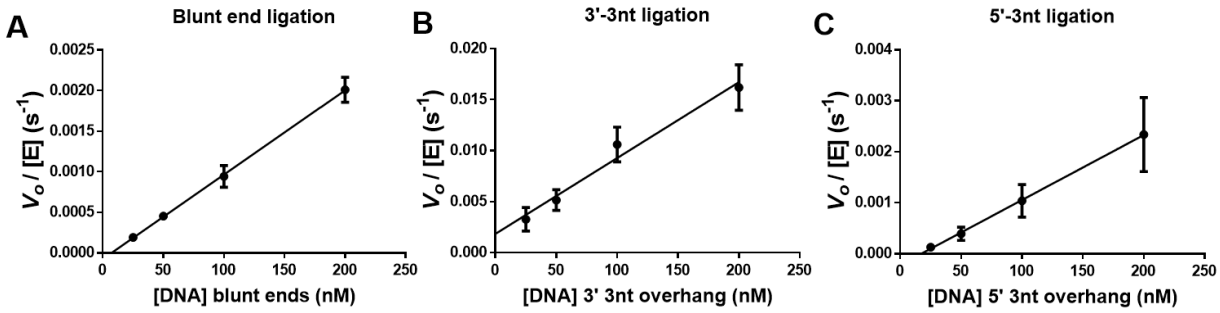

Figure C.8. Determination of LIG1 catalytic efficiencies in the presence of PEG 6K with physiological Mg^{2+}. DNA concentration dependence was measured with 5 nM LIG1, 2 and 20 mM Mg^{2+}, 1 mM ATP and 25-200 nM DNA. Ligatable ends tested include: blunt ends, 3' and 5' cohesive ends, 3 nucleotides in length. Reported catalytic efficiencies were calculated using linear regression of the DNA concentration dependence reactions. Experiments were repeated 3 times with error bars representing on standard deviation from the mean. Catalytic efficiencies values were calculated using the rates of successful ligation events.

Appendix C References

1. McNally JR & O'Brien PJ (2017) Kinetic analyses of single-stranded break repair by human DNA ligase III isoforms reveal biochemical differences from DNA ligase I. J. Biol. Chem. 292(38):15870-15879.

Chapter 5

A real-time DNA ligase assay suitable for high throughput screening[5,6]

Introduction

The mammalian DNA ligases catalyze the formation of phosphodiester bonds in DNA thereby repairing single- and double-strand DNA breaks, and completing DNA replication, repair, and recombination pathways (1). DNA ligation proceeds through an ATP-dependent three-step chemical mechanism. During the first step of catalysis, an active site lysine reacts with the alpha phosphate of ATP resulting in enzyme adenylylation with a loss of inorganic pyrophosphate. Upon encountering the 5' phosphate of a nicked DNA fragment, ligase transfers the adenylyl group from the active-site lysine to the 5' phosphate, forming an adenylylated DNA intermediate. During the final chemical step of ligation, the 3' hydroxyl nucleophile of the adjacent DNA strand attacks the 5' adenylylated phosphate, forming the phosphodiester bond with the release of AMP (1). This three-step chemical mechanism is conserved among the human DNA ligases (Figure 5.1A).

---

[5]Emily Overway helped trouble shoot and validate the robustness of the real-time fluorescence based assay by performing some of the kinetics experiments described in this chapter. Michael Baldwin aided in substrate design. Thomas Jurkiw generously gifted purified Δ232 LIG1 to this study. Justin McNally planned all of the experiments, assisted in and performed all of the experiments described and wrote the chapter. Patrick O'Brien provided insightful guidance and feedback on this work. [6]This chapter was submitted to the Department of Pharmacology Master's Program as a thesis to fulfill the requirements for the Master's in Pharmacology.

Human DNA ligases 1 (LIG1) and 3 (LIG3) share only 22 % sequence identity (2), but have a high degree of structural conservation in their three conserved domains (3,4) (Figure 5.1B). LIG1 and LIG3 differ in their N- and C-terminal regions, which contribute to their specialized biological activities (1). LIG3 has an N-terminal zinc finger (ZnF) domain that contributes to the efficiency of single- and double-strand DNA break ligation (4,5). Recent studies have reported that the erroneous ligation activity of nuclear LIG3 can contribute to telomere fusions and reciprocal chromosomal translocations (6-9). Furthermore, observations of LIG3 overexpression in various cancers that are reliant on LIG3 activity suggest that LIG3 may be a promising pharmacological target (10,11). To better understand the biology and chemistry of the DNA ligases, gel-based ligation assays have been used to characterize the activities of these enzymes on both single- and double-strand DNA breaks (3-5,12-15). Although gel-based ligation assays can be very quantitative, this method is laborious and is not amenable to high-throughput data acquisition. Observation of ligation products is difficult in the absence of DNA denaturing conditions or separation techniques. Interestingly, several approaches have been reported to efficiently measure ligase activity by utilizing FRET to detect conformational changes in DNA structure or detect the joining of two DNA molecules as a product of DNA ligation. Molecular beacons (MBs) report on DNA ligation by the observation of FRET signal change caused by a ligation induced conformational change in DNA structure (16). FRET has also been used to efficiently observe DNA double-strand break ligation by reporting the joining of two labeled DNA molecules (17). Oddly, the authors of this assay did not display any real-time data, suggesting this method used to monitor end-joining activity was best used discontinuously. Likewise, if real-time monitoring of DNA ligation is not important to the experimentalist, efficient methods to detect nicked DNA ligation in a discontinuous format have been developed. Chemical denaturants have

been used to denature nicked DNA substrates to observe a measurable FRET signal (18). In an attempt to create a simple assay that monitors ligase activity in real-time and is also conducive to high-throughput screening of small-molecule libraries (in discontinuous mode), we developed a reporter of nicked-DNA ligation that is not dependent on conformational changes to distinguish between substrate and product species, does not require a ligase capable of DNA double-strand break ligation, and does not require DNA denaturing agents (Figure 5.2A).

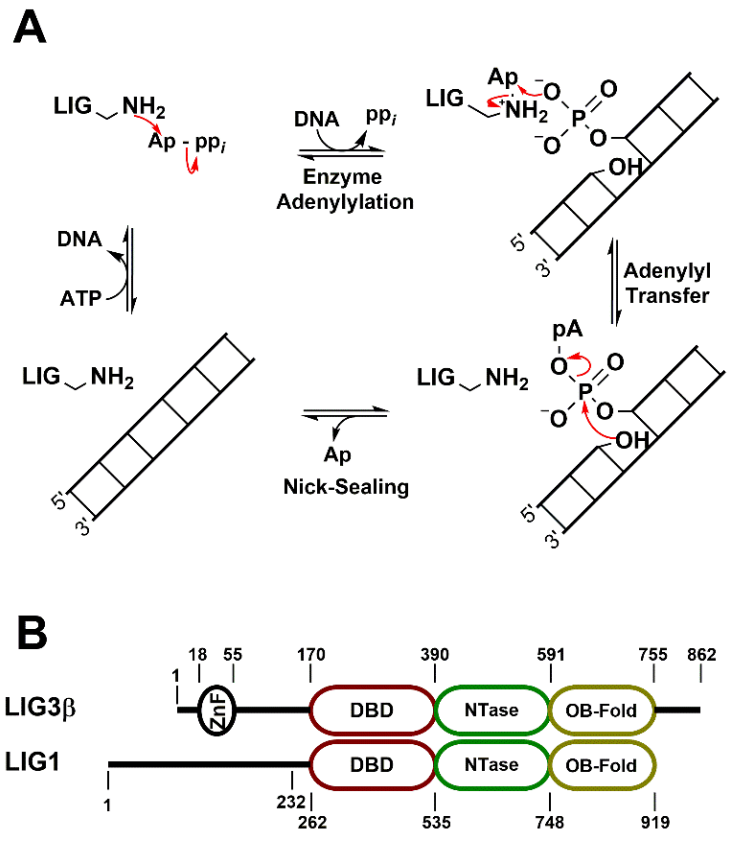

Figure 5.1. DNA ligase mechanism and structure. A, conserved three step reaction mechanism of ATP-dependent DNA ligases. B, Schematic representation of DNA LIG1 and LIG3β. The *numbers* indicate domain boundaries of the two ligases. Ligase domains are color-coded; DNA binding Domain (DBD), *red*; Nucleotidyltransferase domain (NTase), *green*; Oligonucleotide binding domain (OB-fold), *yellow*; zinc finger (ZnF), *black*.

We developed a fluorescence-based ligation assay capable of monitoring steady-state DNA ligation in real-time. Using this assay, we characterized the activities of LIG1 and LIG3β and obtained similar Mg^{2+} cofactor and ATP dependences as previously reported using a traditional gel-based DNA ligation assay (12,13). In addition to defining the kinetic parameters of LIG1 and LIG3β under continuous monitoring mode, we adapted the assay to function in a discontinuous format, enabling efficient screening of small-molecule libraries to identify inhibitors of the human DNA ligases. We statistically validated the discontinuous assay screening conditions and investigated the inhibition characteristics of the human ligases using the inhibitor L67. Our data suggests that this assay could be a viable option for conducting large scale high-throughput screens to identify and characterize DNA ligase inhibitors.

Materials and Methods

Expression and purification of human DNA ligases

Human DNA ligase 1 (Δ232 LIG1) and 3 (full-length nuclear LIG3β) were expressed and purified as previously described (13,19).

DNA substrates

Synthetic DNA oligonucleotides were acquired from Integrated DNA Technologies (IDT) or Keck Oligonucleotide Synthesis facilities and purified by denaturing PAGE as previously described (12). The real-time fluorescence substrate is composed of three DNA strands; 5'TET-CATAGTA, 5'GGTCCATGAAGTACTATG-D, and 5'P-CTTCATGGACC where TET indicates the presence of a 5'-tetrachlorofluoroscein, D indicates the presence of a 3' quencher (3'-TTdT-

dabcyl), and P indicates the presence of a 5'-phosphate. The three oligonucleotides were annealed at 1:1.5:2 molar equivalents, respectively, in annealing buffer (10 mM NaMES pH 6.5, 50 mM NaCl) by heating the solution to 95 ℃ and cooling to 4 ℃ at a rate of 12 ℃ min^{-1}.

Real-time fluorescence assay

Reactions were performed in black 96-well half-area non-binding flat bottom plates (Corning). Reaction buffer for protein characterization contained 50 mM NaMOPS, pH 7.5, 10% glycerol, 1 mM TCEP, 100 μg mL^{-1} BSA with ionic strength maintained at 150 mM using NaCl for all reported reactions. Ionic strength was calculated using the Debye-Hückel theory of electrolytes. Enzyme concentration dependences of LIG1 and LIG3 were tested independently over the 20-fold range of 0.2 – 4 nM. Enzyme concentration dependences were conducted in reaction buffer containing 1 mM $MgCl_2$, 100 μM ATP and 500 nM DNA substrate. The LIG1 DNA concentration dependence reactions contained 10 nM ligase, 0.4 – 4 μM DNA, 1 mM $MgCl_2$, and 100 μM ATP in reaction buffer. The LIG3 DNA concentration dependence was determined using 1 nM ligase, 20 – 800 nM DNA, 1 mM $MgCl_2$, and 100 μM ATP in reaction buffer. The Mg^{2+} concentration dependences for multiple-turnover ligation were conducted in reaction buffer containing 1 nM ligase, 0-25 mM $MgCl_2$, 1 mM ATP, and 400 nM DNA. ATP concentration dependences were determined in the presence of 1 nM enzyme, 20 mM $MgCl_2$, and 400 mM DNA, and 0 – 150 μM ATP in reaction buffer.

Data acquisition and analysis

Fluorescence measurements were performed using Tecan GeniosPro or Tecan Safire2 plate readers set to 30 ℃. The plate readers were configured to monitor TET emission at 550 nm (BP20)

using an excitation wavelength of 510 nm (BP20). Reaction progress traces were analyzed by a series of steps. Data underwent background subtraction, followed by fluorescence normalization to a scale of 0 – 1.0. To do so, fluorescence reaction progression curves were divided by the no enzyme control fluorescence values, enabling the conversion of fluorescence units (A.U.) to fraction substrate. Normalized plots were fit using linear regression to obtain slopes required to determine reaction rates. Reaction progress curves were linear for the first 50% of the reaction. Reaction rates were determined by multiplying the slope by the reacting substrate concentration to obtain reaction velocities (V_{max}). Reaction velocities were normalized to enzyme concentration to obtain $V_{max}/[E]$ with units of $time^{-1}$. Initial rates (represented as V/[E]) were plotted as a function of the tested variable to determine the kinetic parameters of the tested enzyme. ATP and DNA substrate dependences were analyzed using the Michaelis-Menten equation (Equation 5.1). The Mg^{2+} cofactor dependences were analyzed using a hyperbolic single-site binding model (Equation 5.2).

$$\frac{V}{[E]} = \frac{k_{cat} \times [S]}{(K_M + [S])} \qquad \text{(Eq. 5.1)}$$

$$\frac{V}{[E]} = \frac{k_{cat} \times [MgCl_2]}{\left(K_{Mg} + [MgCl_2]\right)} \qquad \text{(Eq. 5.2)}$$

Discontinuous high-throughput screen and Z' score analysis

The real-time fluorescence assay can be modified for discontinuous activity measurements to enable efficient high-throughput screening using automated platforms. The high-throughput screening reaction buffer contained 50 mM NaMOPS, pH 7.5, 112 mM NaCl, 1 mM $MgCl_2$, 1

mM TCEP, 100 µg/mL BSA, 100 µM ATP, DMSO control (5% v/v) or dissolved L67 in DMSO (5% v/v). LIG1 reactions possessed 10 nM LIG1 and 500 nM DNA, whereas LIG3β reactions contained 2 nM LI3β and 50 nM DNA. Positive controls were performed in the absence of enzyme. For both enzymes, the DNA concentration was maintained at or below their respective $K_{M,\ DNA}$ values. 50 µL reactions were incubated at ambient temperature for 50 minutes prior to quenching with 0.5 M EDTA to achieve a final EDTA concentration of 45 mM. Reactions quenched via metal chelation did not destabilize DNA products or alter the fluorescence properties of the substrate/product species. The Z' score analysis was calculated as previously described (Equation 5.3) (20). σ represents 1 standard deviation from the mean for the positive ($_{c+}$) and negative ($_{c-}$) controls. µ represents the mean values for positive ($_{c+}$) and negative ($_{c-}$) controls.

$$Z' = 1 - \frac{3\sigma_{c+} + 3\sigma_{c-}}{|\mu_{c+} - \mu_{c-}|} \qquad \text{(Eq. 5.3)}$$

Ligase inhibition by L67

L67 was determined greater than 98% pure by HPLC (MedKoo Biosciences). L67 was dissolved in 100% DMSO to a concentration of 10 mM. The L67 concentration dependence on enzyme activity was investigated while maintaining DMSO concentrations at 5% (v/v) in all reactions. L67 concentration dependences on ligase activities were performed as described in *Discontinuous high-throughput screen and Z' score analysis*. Briefly, reactions were performed at ambient temperature for 50 minutes prior to being stopped by the addition of 0.5 M EDTA to achieve a final EDTA concentration of 45 mM. Reactions were scanned as described above. Raw fluorescence values underwent baseline subtraction, followed by normalization to a scale of 0 –

1.0 with 0 representing completely inhibited reactions and 1.0 representing uninhibited reactions. These normalized values were plotted as a function of L67 concentration and fit to a four-variable dose response curve using GraphPad Prism software.

Gel based ligation assay

To confirm the occurrence of ligation during the real-time fluorescence assay, ligation reactions were analyzed using denaturing polyacrylamide electrophoresis. Briefly, discontinuous ligation reactions containing 50 mM NaMOPS, pH 7.5, 112 mM NaCl, 1 mM $MgCl_2$, 1 mM TCEP, 100 µg/mL BSA, 100 µM ATP, 2 nM LIG3β, 50 nM DNA were conducted in parallel to real-time ligation reactions but were stopped at 10 min intervals using a DNA denaturing quench solution (90% formamide, 50 mM EDTA, 0.006% bromophenol blue, 0.006% xylene cyanol). Quenched samples were incubated at 95 ℃ for 3 minutes, snap-cooled in ice water, then loaded onto a 20% polyacrylamide, 6.6 M Urea, 1X TBE DNA denaturing gel. Gels were imaged using a Typhoon 5 imaging system (GE Healthcare) set to monitor emission at 525 (BP20) while exciting at 488 nm. DNA substrates and products were quantified using ImageQuant TL (GE Healthcare) and analyzed using GraphPad Prism softwares.

Results

Real-time fluorescence assay

We previously characterized the substrate and cofactor dependences of human DNA ligases 1 and 3 using a discontinuous gel-based ligation assay (12,13). The gel-based system is not optimal for small-molecule screening due to significant time investment and material costs. We designed an oligonucleotide substrate suitable for measuring DNA ligase activity in real-time (Figure 5.2A and Materials and Methods). A 7-mer acceptor strand and a 5'-phosphorylated 11-mer donor strand were designed to anneal to an 18-mer DNA template to form a ligatable nick. The 7-mer was labeled at the 5' terminus with tetrachlorofluorescein. The template strand was designed with a 3' overhang containing a dT-dabcyl quencher. The 7-mer only transiently anneals to the template strand at room temperature, with equilibrium favoring the dissociated, highly fluorescent state. Ligation greatly increases the stability of the fluorophore-labeled DNA, locking it in the annealed and low-fluorescence (quenched) state. We confirmed that the loss in fluorescence signal correlates with ligation by monitoring the reaction using the gel-based assay, in which substrate and product can be identified unambiguously (Figure 5.2B). To validate the robustness of this real-time ligation assay, the steady-state kinetic parameters of LIG1 and LIG3 were determined.

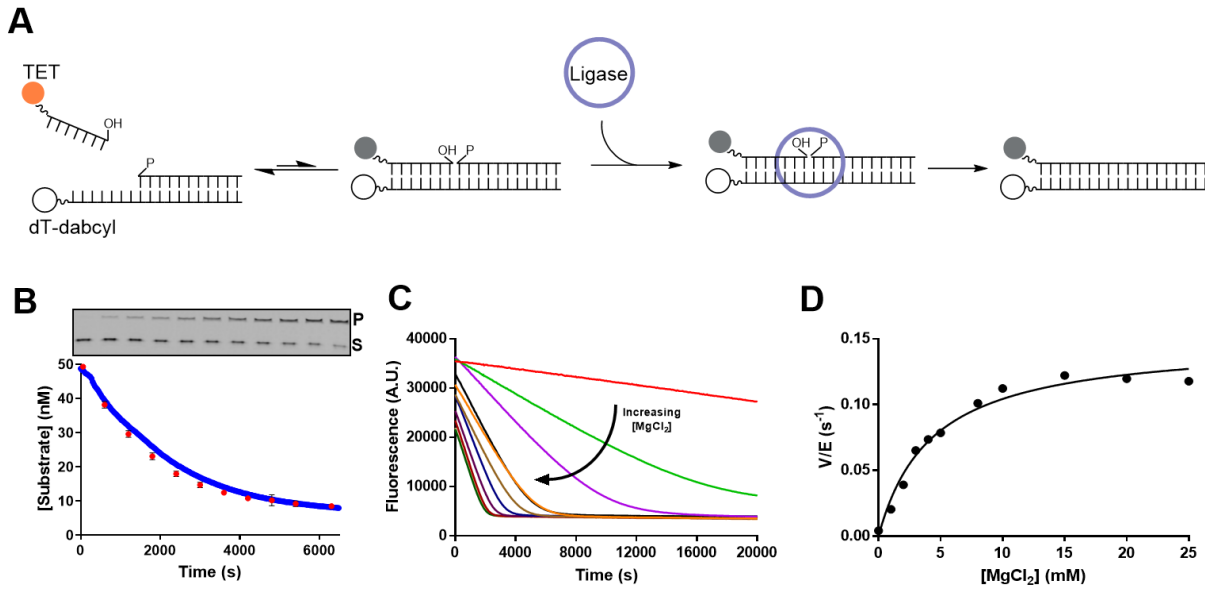

Figure 5.2. Real-time fluorescence assay monitors DNA ligation. A, description of the real-time fluorescence-based ligation assay. Tetrachlorofluorescein (TET) labeled 7-mer oligonucleotide fluoresces in the absence of a quencher. The 7-mer oligonucleotide transiently anneals to the dabcyl-containing complementary oligonucleotide, forming a ligatable complex. Upon ligation, the stabilized DNA duplex brings the TET in proximity of the dabcyl, resulting in decreased fluorescence. B, representative reaction progress curve monitoring substrate consumption by real-time fluorescence (blue trace), and discontinuous gel-based ligation assay (red circles) under identical reaction conditions. Inset representative gel shows product (upper bands labeled *P*) and substrate (lower bands labeled *S*) of the real-time assay performed discontinuously and analyzed by denaturing PAGE. C, representative reaction progress curves used to determine LIG3β $MgCl_2$ concentration dependence on ligation. D, representative $MgCl_2$ dependence of LIG3β determined from rates of substrate consumption followed by a normalization of DNA and enzyme concentrations, represented by V/E (s^{-1}). Values reported using the gel-based ligation assay in B are the mean ± S.D.; n = 3. Real-time ligation traces in B and C are representative data from individual experiments.

Substrate and metal dependence of human DNA LIG1

We first investigated the LIG1 concentration dependence on reaction rate. Over a 20-fold concentration range (0.2-4 nM), LIG1 activity was linearly proportional to its concentration, indicating that the reaction conditions were suitable for a detailed kinetic analysis (Figure 5.3A). The DNA concentration dependence of LIG1 was measured with 1 mM $MgCl_2$ and gave a $K_{M,\,DNA}$ value of 800 nM (Figure 5.3B). We next determined the Mg^{2+} dependence and found a K_{Mg} value

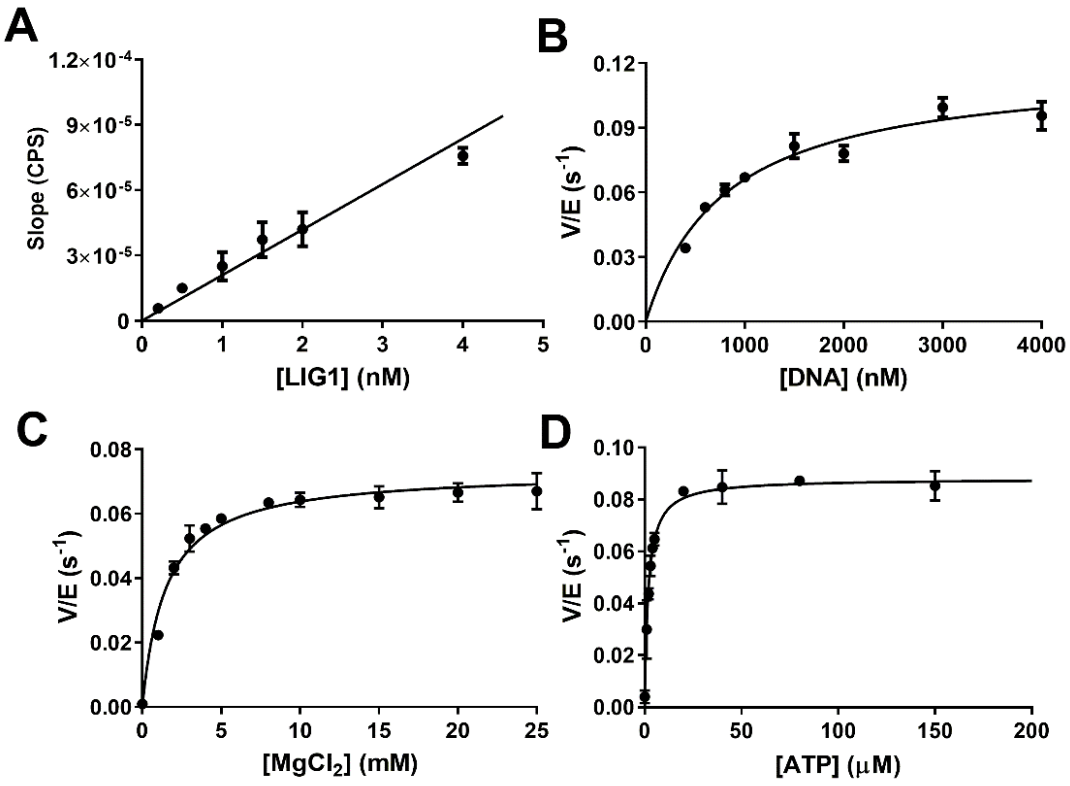

Figure 5.3. Kinetic parameters of LIG1 determined using the real-time ligation assay. *A*, Multiple-turnover ligation rate of LIG1 is linearly dependent on enzyme concentration. *B*, DNA concentration dependence measured using 10 nM LIG1 in the presence of 1 mM $MgCl_2$ and 100 μM ATP. LIG1 has a $K_{M,DNA}$ value of 800 nM. *C*, $MgCl_2$ concentration dependence of LIG1 was measured in the presence of 1 mM ATP and 400 nM DNA with ionic strength maintained at 150 mM. LIG1 has a K_{Mg} value of 1.5 mM. *D*, ATP concentration dependence was measured in the presence of 20 mM $MgCl_2$ and 400 nM DNA. LIG1 possess a $K_{M,ATP}$ value of 1.5 μM. Each experiment was completed in triplicate (mean ± S.D.).

of 1.5 mM (Figure 5.3C). The multiple-turnover ATP concentration dependence of LIG1 indicated $K_{M,\ ATP}$ was equal to 1.9 μM (Figure 5.3D). The ATP and Mg^{2+} dependences of LIG1 were similar to previous observations using the gel-based assay (Table 5.1) (12). The maximal rates of reaction with this real-time assay were greatly reduced when compared to previous reports using an optimal nicked DNA substrate (Table 5.1). The reduced rate of ligation of the real-time substrate was likely attributed to the unfavorable annealing of the TET-7-mer oligonucleotide that limits the formation of a productive enzyme complex.

Substrate and metal dependence of human DNA LIG3β

We next determined the steady-state kinetic parameters of LIG3β. The rate of LIG3β mediated ligation was proportional to enzyme concentration, also indicating that LIG3β was well-behaved under reaction conditions (Figure 5.4A). The DNA concentration dependence of LIG3β was measured within the range of 20 – 800 nM DNA yielding a $K_{M,DNA}$ of 50 nM (Figure 5.4B). Mg^{2+} and ATP concentration dependences report K_{Mg} and $K_{M,ATP}$ values of 4.3 mM and 9.6 μM, respectively (Figures 5.4C and 5.4D). The DNA concentration dependence of LIG3β cannot be directly compared to previous reports of nicked DNA ligation due to the different reaction conditions, but the enzyme had a markedly lower $K_{M,DNA}$ value compared to LIG1, as previously described (13). Importantly, K_{Mg} and $K_{M,ATP}$ values were similar to previously reported values, suggesting this assay reliably reported cofactor and substrate dependences (Table 5.1) (13).

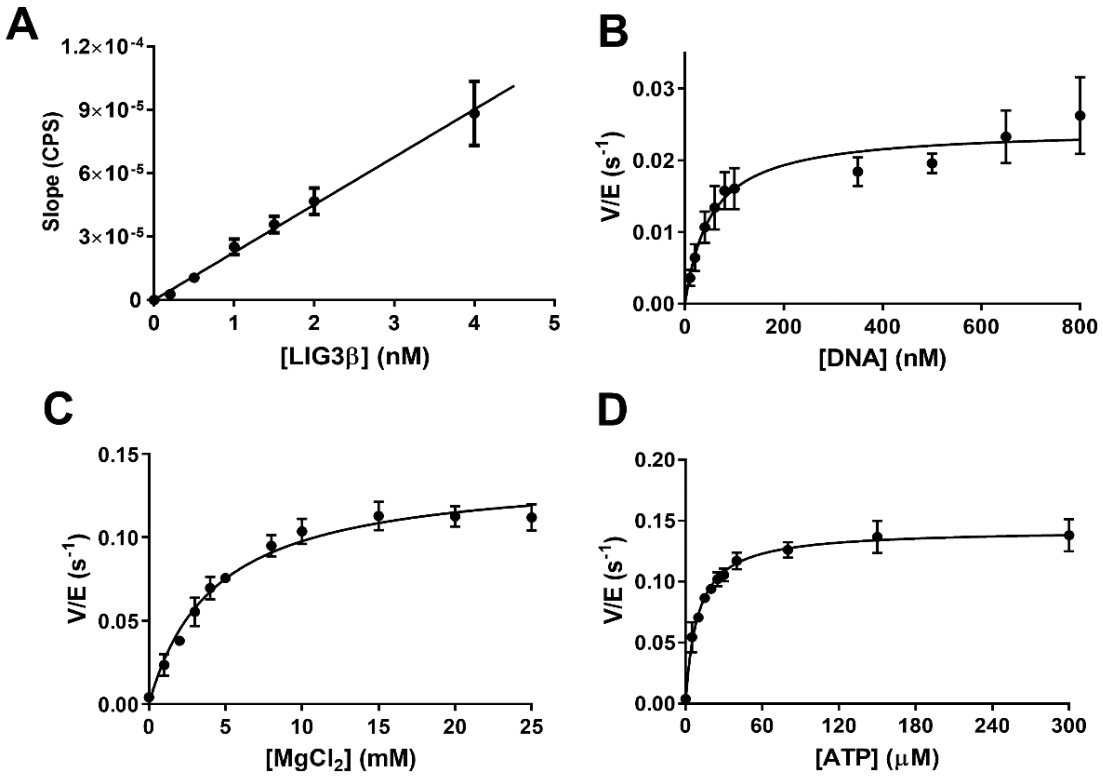

Figure 5.4. Kinetic parameters of LIG3β determined using the real-time ligation assay. *A*, Multiple-turnover ligation rate of LIG3β is linearly dependent on enzyme concentration. *B*, DNA concentration dependence measured in the presence of 1 mM $MgCl_2$ and 100 μM ATP. LIG3β has a $K_{M,DNA}$ value of 50 nM. *C*, $MgCl_2$ concentration dependence of LIG3β was measured in the presence of 1 mM ATP and 400 nM DNA with ionic strength maintained at 150 mM. LIG3β possesses a K_{Mg} value of 4.3 mM. *D*, ATP concentration dependence was measured in the presence of 20 mM $MgCl_2$ and 400 nM DNA. LIG3β possess a $K_{M,ATP}$ value of 9.6 μM. Each experiment was completed in triplicate (means ± S.D.).

High-throughput discontinuous assay

Although high-throughput screening could be performed in continuous kinetic mode, it is often advantageous to quench samples at a set time for subsequent scanning and analysis. We optimized sample handling such that reactions could be incubated at ambient temperature and quenched using concentrated EDTA. We directly compared reaction progress curves for the continuous and discontinuous assays, which were in good agreement with each other (Figure

5.5A). The absolute fluorescence values were slightly reduced for the quenched assay, presumably due to the dilution of the reaction mixture from the addition of EDTA to the reaction solution to stop catalysis. Under the selected conditions, a 50 minute incubation time provided optimal signal to noise ratio (Figure 5.5A). To determine the influence of DMSO on LIG3β activity, we followed the real-time ligation activity of LIG3β in the presence of 0 –15% (v/v) DMSO (Figure 5.5B). LIG3β tolerated DMSO up to 15% v/v and exhibited a ~50% increase in activity at 5% DMSO. Fluorescence intensities remained consistent at all DMSO concentrations, demonstrating that

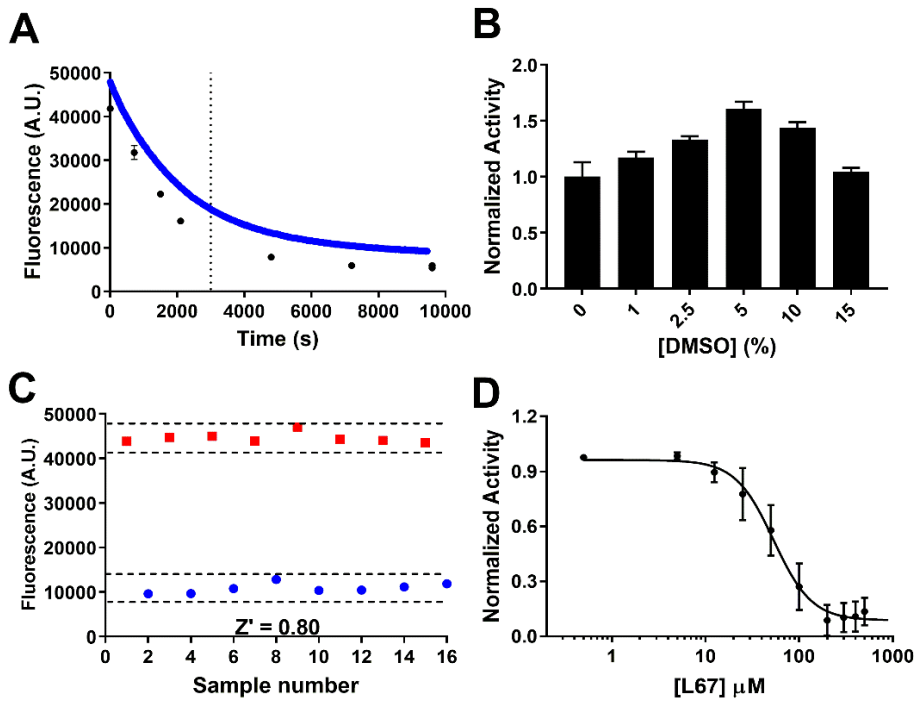

Figure 5.5. Discontinuous fluorescence ligation assay optimization for high-throughput screening of small-molecule inhibitors of LIG3β. *A.* comparison of a real-time fluorescence progress curve (blue) with EDTA quenched reactions confirm sufficient ligation within 50 minutes (3000 seconds, marked with dashed line) for small-molecule screening. *B*, DMSO concentration dependence on LIG3β activity. Rate of LIG3β mediated ligation is minimally impacted by the presence of high DMSO concentrations. *C*, scatterplot of the relative fluorescence units of control reactions (8 positive (no enzyme), *red*; and 8 negative, *blue*) for inhibition. dashed lines represent three S.D. from the mean. *D*, dose response curve of ligase inhibitor, L67, possessing an IC50 of 50 μM. Dose response data were fit to a four-variable dose response curve. Each experiment was completed in at least triplicate (mean ± S.D.).

DMSO did not interfere with fluorescence or annealing of the DNA strands (data not shown). After optimizing conditions for small-molecule screening, we evaluated the ligation assay protocol using negative controls (uninhibited ligation reaction) and positive controls (reactions representing

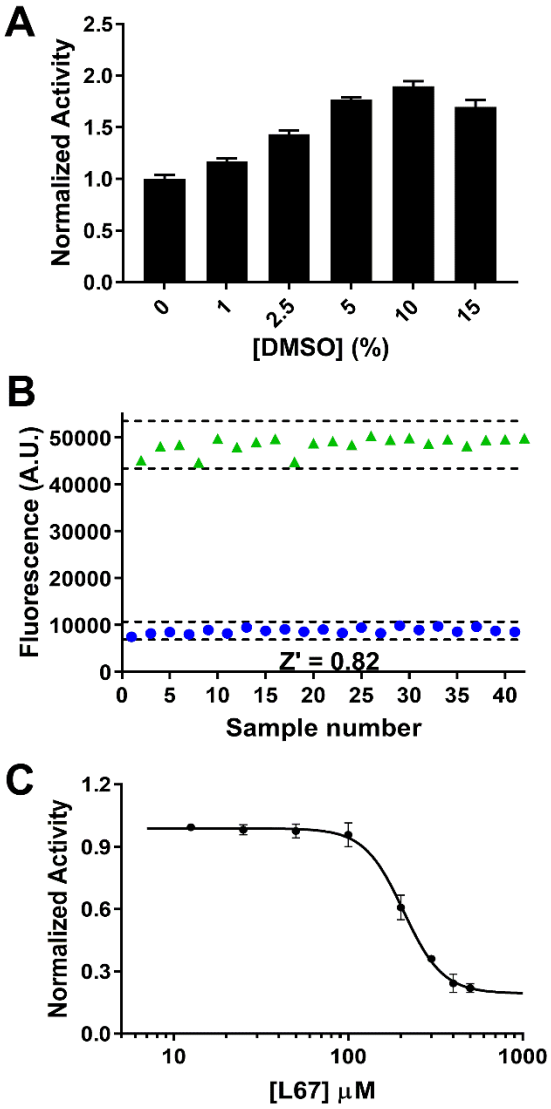

Figure 5.6. Discontinuous fluorescence ligation assay for LIG1. *A*, DMSO concentration dependence on LIG1 activity. *B*, scatterplot of the relative fluorescence units of control reactions (20 positive, *green*; and 20 negative, *blue*) for inhibition. Dashed lines represent three S.D. from the mean. *C*, dose response curve of L67 yielded an IC50 value of 200 μM. Data were fit to a four-variable dose response curve. Each experiment was completed in at least triplicate (mean ± S.D.).

idealized inhibition by omitting LIG3β). The LIG3β control data yielded a Z' score of 0.80 indicating the assay was suitable for high-throughput screening (Figure 5.5C). For further assay validation, we performed a concentration dependence of the reported mammalian DNA ligase inhibitor L67 (21). We found that L67 inhibited LIG3β with an IC50 of 50 μM, (Figure 5.5D).

The high-throughput discontinuous assay was next optimized for LIG1, which could be used to screen for inhibitors of LIG1, or to counter screen for compounds specific to LIG3β. The DNA concentration was chosen to be 500 nM, which was below the determined $K_{M,\,DNA}$ value of 800 nM. For convenience, LIG1 concentration was increased to 10 nM to achieve a similar incubation time as LIG3β. Varying DMSO concentrations had modest effect on LIG1 activity, tolerating 15% (v/v) DMSO. As with LIG3β, DMSO increased ligation rates of LIG1 in a concentration dependent manner, with maximal ligation rates observed in the presence of 10% DMSO (Figure 5.6A). We evaluated the LIG1-catalyzed discontinuous assay by comparing negative and positive controls, which yielded a Z' value of 0.82 (Figure 5.6B). To further validate these conditions as a viable counter screen, an L67 dose response curve indicated the compound had an IC50 of 200 μM under the tested conditions. By using the real-time fluorescence assay to determine the kinetic parameters of the human DNA ligases, we were able to exploit their DNA and Mg^{2+} binding characteristics to define suitable conditions to perform high-throughput screening and/or investigate the binding properties of ligase inhibitors.

Table 5.1
Comparison of multiple turnover kinetic parameters determined by real-time fluorescence assay and reported values.[a]

	Fluorescence-based ligation of 18-mer transient nicked DNA substrate		Gel-based ligation of 28mer stably nicked DNA substrate	
Parameter	**LIG3β**	**LIG1**	**LIG3β[b]**	**LIG1[c]**
k_{cat}				
ATP (s^{-1})	0.14 ± 0.003	0.088 ± 0.001	0.55 ± 0.02	0.74 ± 0.09
Mg^{2+} (s^{-1})	0.14 ± 0.001	0.074 ± 0.001	0.69 ± 0.03	0.81 ± 0.10
DNA (s^{-1})	0.024 ± 0.001	0.12 ± 0.01	0.51 ± 0.03*****	0.87 ± 0.10*****
K_M				
ATP (μM)	9.6 ± 0.8	1.9 ± 0.1	31 ± 3	11 ± 3
Mg^{2+} (mM)	4.3 ± 0.4	1.5 ± 0.1	7.4 ± 0.7	0.71 ± 0.2
DNA (nM)	52 ± 9	800 ± 80	49 ± 8*****	570 ± 170*****
k_{cat}/K_M				
ATP ($M^{-1}s^{-1}$)	$1.5 \pm 0.1 \times 10^4$	$4.6 \pm 0.2 \times 10^4$	$1.8 \pm 0.2 \times 10^4$	6.7×10^4
Mg^{2+}($M^{-1}s^{-1}$)	33 ± 3	49 ± 3	93 ± 10	$1.1 \pm 0.4 \times 10^3$
DNA ($M^{-1}s^{-1}$)	$4.6 \pm 0.8 \times 10^5$	$1.5 \pm 0.2 \times 10^5$	$1.0 \pm 0.2 \times 10^7$*****	$1.5 \pm 0.5 \times 10^6$*****

[a]Multiple-turnover kinetic parameters were all determined at 150 mM ionic strength. ATP concentration dependences were conducted at fixed DNA (400 nM) and Mg^{2+} (20 mM) concentrations. Likewise, Mg^{2+} concentration dependences were conducted at fixed DNA (400 nM) and ATP (1 mM) concentrations. DNA concentration dependences were performed at fixed ATP (100 μM) and Mg^{2+} (1 mM) concentrations.

[b] The LIG3β values (excluding *****) were previously determined using a gel-based ligation assay with a nicked DNA substrate at 150 mM ionic strength (13).

[c] The LIG1 values (excluding *****) were previously determined by a gel-based ligation assay using a nicked DNA substrate at 150 mM ionic strength (12).

***** Values of LIG1 and LIG3β nicked DNA concentration dependences were obtained at 300 mM ionic strength using a gel-based ligation assay (13).

Discussion

Human DNA LIG1 and LIG3 play important and overlapping roles catalyzing the DNA ligation reactions required for successful completion of the DNA replication, repair, and recombination pathways. LIG1 has been suggested to primarily catalyze single-strand DNA break ligation, whereas LIG3 has been reported to catalyze single- and double-strand DNA break ligation (1). The double-strand break ligation activity attributed to LIG3 is reported to erroneously generate chromosomal translocations (7) and telomere fusions (8,9). Moreover, patient-derived cancer cells overexpress LIG3 and are reliant on this LIG3 activity for survival, making LIG3 an attractive pharmacological target (10,11). A major obstacle restricting the discovery of inhibitors targeting the human DNA ligases is the lack of a robust, high-throughput methodology necessary for identifying such compounds.

A number of DNA ligation assays have been developed to increase the efficiency of monitoring ligase activity. Molecular beacons (MBs) are an attractive method for investigating nicked DNA ligation in real-time. These substrates utilize two oligonucleotides adjacently-annealed to the loop region of a hairpin structured oligonucleotide. Upon ligation of the nick, the MB undergoes a conformational change that disrupts the hairpin structure thereby generating a fluorescence signal (16,22). MBs may be an elegant approach for monitoring DNA ligase activity in theory; however, it is unclear if they are suitable substrates for a wide variety of DNA ligases that function under a wide range of conditions. Analysis of T4 DNA ligase using MBs indicate that these substrates may be sensitive to changes in ionic strength. Monovalent cation concentrations upwards of 300 mM, and Mg^{2+} concentrations of more than 20 mM either inactivate T4 DNA ligase, or the MB does not report on DNA ligation at these elevated ionic strengths due

to stabilization of the hairpin (22). Furthermore, MBs may not be suitable substrates for all DNA ligases due to their conformationally restricted DNA structure. T4 DNA ligase, unlike the human DNA ligases, has a relatively small DBD, bringing into question whether the human DNA ligases (and other DNA ligases with highly homologous domain structures) can physically engage with and encircle the nick in a physiologically relevant mode to perform catalysis (23). Human DNA LIG3 is suggested to have a ~14 nucleotide footprint as determined by DNase I digestions (24) and X-ray crystallography (4). This binding footprint is a substantial percentage of the MB loop structure (~20-nt that adopt a circular structure). An alternative DNA substrate proposed to be used as an efficient discontinuous assay for high-throughput screening of DNA ligases is based on DNA end-joining ligase activity. A double-strand DNA break substrate comprised of 5' 4 – nucleotide overhangs generates a FRET signal upon ligation (17). This substrate design has inherent complexities since it requires double-strand break ligation to achieve a signal, and due to this style of substrate, may not be appropriate for all DNA ligases. Alternatively, Shapiro *et al.* developed a discontinuous ligation assay utilizing a nicked-DNA substrate that requires chemical denaturation prior to observation of the FRET signal (18). This method, although unable to report on ligation in real-time, was shown to be amenable to high-throughput screening. Each of the described approaches have been described as efficient methods to monitor DNA ligation. Each of these assays, however, have limitations that disallow the experimental flexibility and simplicity that is desired for efficient small-molecule screening, counter-screening, and characterization of compounds of interest.

In an attempt to overcome the limitations of the previous FRET-based assays, we strove to generate a substrate that reports on nicked DNA ligation in real-time and is adaptable to efficient screening of small-molecule libraries. The three oligonucleotide architecture of the substrate

(Figure 5.1) resembles a simple nicked DNA substrate previously used for the characterization of human DNA LIG1 and LIG3 (12,13). The DNA substrate was engineered such that the upstream TET labeled 7-mer oligonucleotide would be transiently annealed to the dabcyl-containing 18-mer DNA template strand under a broad spectrum of assay conditions. Importantly, fluorescence quenching was not observed in the presence of high (25 mM) Mg^{2+} concentrations, indicating that the increased divalent metal concentration did not shift the equilibrium of the free (fluorescent) 7-mer to the annealed (quenched) state. Investigation of the Mg^{2+} concentration dependences of LIG1 and LIG3 confirmed that the changes in metal cofactor concentrations directly influenced DNA ligase activity. LIG1 and LIG3 both reported K_{Mg} values within 2-fold of previously reported values. Likewise, we report that the $K_{M,\ ATP}$ values obtained using this fluorescence-based assay are similar to those previously described using a gel-based ligation assay under nearly identical reaction conditions (Table 5.1) (12,13). Interestingly, LIG3 was reported to have $K_{M,\ DNA}$ values roughly 12-fold lower than that of LIG1 (13). A comparison of $K_{M,DNA}$ values acquired using the real-time assay indicates LIG3 $K_{M,\ DNA}$ values were 15-fold lower than that of LIG1, a difference strikingly similar to those reported on a stably annealed nicked DNA substrate (13). Importantly, due to the transient nature of the 7-mer DNA strand, rates of DNA ligation (k_{cat}) were greatly reduced when compared to those of a stably nicked DNA species. (Table 5.1). In general, the DNA, ATP and Mg^{2+} concentration dependences of both LIG1 and LIG3β are consistent with previously reported values, confirming that this assay may be used as an efficient biochemical method to quantify DNA ligase activity (Table 5.1) (12,13).

This study describes and validates a real-time fluorescence based ligation assay capable of determining steady-state kinetic parameters of DNA ligases that is adaptable to high-throughput screening for ligase inhibitors. Small-scale analysis of positive and negative controls indicates Z’

scores of 0.82 and 0.80 for LIG1 and LIG3β, respectively. As proof-of-principle, we confirmed that a previously characterized inhibitor, L67, was effective at inhibiting both LIG3β and LIG1, with modestly greater efficacy against LIG3β.

References

1. Ellenberger, T., and Tomkinson, A. E. (2008) Eukaryotic DNA Ligases: Structural and Functional Insights. *Annu. Rev. Biochem.* **77**, 313-338

2. Simsek, D., and Jasin, M. (2011) DNA ligase III: A spotty presence in eukaryotes, but an essential function where tested. *Cell Cycle* **10**, 3636-3644

3. Pascal, J. M., O'Brien, P. J., Tomkinson, A. E., and Ellenberger, T. (2004) Human DNA ligase I completely encircles and partially unwinds nicked DNA. *Nature* **432**, 473-478

4. Cotner-Gohara, E., Kim, I.-K., Hammel, M., Tainer, J. A., Tomkinson, A. E., and Ellenberger, T. (2010) Human DNA Ligase III Recognizes DNA Ends by Dynamic Switching between Two DNA-Bound States. *Biochemistry* **49**, 6165-6176

5. Cotner-Gohara, E., Kim, I.-K., Tomkinson, A. E., and Ellenberger, T. (2008) Two DNA-binding and Nick Recognition Modules in Human DNA Ligase III. *J. Biol. Chem.* **283**, 10764-10772

6. Lu, G., Duan, J., Shu, S., Wang, X., Gao, L., Guo, J., and Zhang, Y. (2016) Ligase I and ligase III mediate the DNA double-strand break ligation in alternative end-joining. *Proc Natl Acad Sci U S A* **113**, 1256-1260

7. Simsek, D., Brunet, E., Wong, S. Y.-W., Katyal, S., Gao, Y., McKinnon, P. J., Lou, J., Zhang, L., Li, J., Rebar, E. J., Gregory, P. D., Holmes, M. C., and Jasin, M. (2011) DNA Ligase III Promotes Alternative Nonhomologous End-Joining during Chromosomal Translocation Formation. *PLoS Genetics* **7**

8. Badie, S., Carlos, A. R., Folio, C., Okamoto, K., Bouwman, P., Jonkers, J., and Tarsounas, M. (2015) BRCA1 and CtIP promote alternative non-homologous end-joining at uncapped telomeres. *EMBO J.* **34**, 828

9. Jones, R. E., Oh, S., Grimstead, J. W., Zimbric, J., Roger, L., Heppel, N. H., Ashelford, K. E., Liddiard, K., Hendrickson, E. A., and Baird, D. M. (2014) Escape from telomere-driven crisis is DNA ligase III dependent. *Cell Rep* **8**, 1063-1076

10. Newman, E. A., Lu, F., Bashllari, D., Wang, L., Opipari, A. W., and Castle, V. P. (2015) Alternative NHEJ Pathway Components Are Therapeutic Targets in High-Risk Neuroblastoma. *Mol. Cancer Res.* **13**, 470-482

11. Tomkinson, A. E., Howes, T. R., and Wiest, N. E. (2013) DNA ligases as therapeutic targets. *Transl Cancer Res* **2**

12. Taylor, M. R., Conrad, J. A., Wahl, D., and O'Brien, P. J. (2011) Kinetic Mechanism of Human DNA Ligase I Reveals Magnesium-dependent Changes in the Rate-limiting Step That Compromise Ligation Efficiency. *J. Biol. Chem.* **286**, 23054-23062

13. McNally, J. R., and O'Brien, P. J. (2017) Kinetic analyses of single-stranded break repair by human DNA ligase III isoforms reveal biochemical differences from DNA ligase I. *J. Biol. Chem.* **292**, 15870-15879

14. Taylor, R. M., Whitehouse, J., Caldecott, K. W., Cappelli, E., and Frosina, G. (1998) Role of the DNA ligase III zinc finger in polynucleotide binding and ligation. *Nucleic Acids Res.* **26**, 4804-4810

15. Taylor, R. M., Whitehouse, C. J., and Caldecott, K. W. (2000) The DNA ligase III zinc finger stimulates binding to DNA secondary structure and promotes end joining. *Nucleic Acids Res.* **28**, 3558-3563

16. Huang, J. H., Wu, J. Q., and Li, Z. G. (2015) Biosensing using hairpin DNA probes. *Rev Anal Chem* **34**, 1-27

17. Chen, X. C., Hentz, N. G., Hubbard, F., Meier, T. I., Sittampalam, S., and Zhao, G. (2002) Development of a fluorescence resonance energy transfer assay for measuring the activity of Streptococcus pneumoniae DNA ligase, an enzyme essential for DNA replication, repair, and recombination. *Anal. Biochem.* **309**, 232-240

18. Shapiro, A. B., Eakin, A. E., Walkup, G. K., and Rivin, O. (2011) A high-throughput fluorescence resonance energy transfer-based assay for DNA ligase. *J Biomol Screen* **16**, 486-493

19. Maffucci, P., Chavez, J., Jurkiw, T. J., O'Brien, P. J., Abbott, J. K., Reynolds, P. R., Worth, A., Notarangelo, L. D., Felgentreff, K., Cortes, P., Boisson, B., Radigan, L., Cobat, A., Dinakar, C., Ehlayel, M., Ben-Omran, T., Gelfand, E. W., Casanova, J. L., and Cunningham-Rundles, C. (2018) Biallelic mutations in DNA ligase 1 underlie a spectrum of immune deficiencies. *J. Clin. Invest.* **12**, 5489-5504.

20. Zhang, J. H., Chung, T. D., and Oldenburg, K. R. (1999) A Simple Statistical Parameter for Use in Evaluation and Validation of High Throughput Screening Assays. *J Biomol Screen* **4**, 67-73

21. Chen, X., Zhong, S., Zhu, X., Dziegielewska, B., Ellenberger, T., Wilson, G. M., MacKerell, A. D., Jr., and Tomkinson, A. E. (2008) Rational design of human DNA ligase inhibitors that target cellular DNA replication and repair. *Cancer Res.* **68**, 3169-3177

22. Tang, Z., Wang, K., Tan, W., Li, J., Liu, L., Guo, Q., Meng, X., Ma, C., and Huang, S. (2003) Real-time monitoring of nucleic acid ligation in homogenous solutions using molecular beacons. *Nucleic Acids Res.* **31**, e148

23. Shi, K., Bohl, T. E., Park, J., Zasada, A., Malik, S., Banerjee, S., Tran, V., Li, N., Yin, Z., Kurniawan, F., Orellana, K., and Aihara, H. (2018) T4 DNA ligase structure reveals a

prototypical ATP-dependent ligase with a unique mode of sliding clamp interaction. *Nucleic Acids Res.* **46**, 10474-10488

24. Mackey, Z. B., Niedergang, C., Murcia, J. M.-d., Leppard, J., Au, K., Chen, J., Murcia, G. d., and Tomkinson, A. E. (1999) DNA Ligase III Is Recruited to DNA Strand Breaks by a Zinc Finger Motif Homologous to That of Poly(ADP-ribose) Polymerase Identification of Two Functionally Distinct DNA Binding Regions Within DNA Ligase III. *J. Biol. Chem.* **274**, 21679-21687

25. von Ahsen, N., Wittwer, C. T., and Schutz, E. (2011) Monovalent and divalent salt correction algorithms for Tm prediction--recommendations for Primer3 usage. *Brief Bioinform* **12**, 514-517

Chapter 6

Conclusions and Future Directions

Summary of conclusions

This thesis provides the first systematic kinetic characterization of two human DNA ligase 3 isoforms catalyzing ligation of single- and double-strand DNA breaks (SSB and DSB, respectively). To complete this body of work I developed methods to express and purify nuclear LIG3α and LIG3β to homogeneity and investigate their kinetic parameters. The LIG3 isoforms are markedly more efficient at ligating SSBs than LIG1; however, the LIG3 isoforms have weaker magnesium affinities than LIG1. Interestingly, this reduced Mg^{2+} affinity does not increase the susceptibility of LIG3 to accumulate potentially toxic abortive ligation intermediates, in contrast to what was seen with LIG1 (1, 2). To better understand how the structural characteristics unique to the LIG3 isozymes contribute to their kinetic parameters, we performed a systematic analysis of numerous N-terminal variants under steady-state reaction conditions. These studies were performed using SSBs and indicate that the ZnF domain and a previously uncharacterized disordered linker region (DLR) both contribute to the efficiency of LIG3-catalyzed SSB ligation.

Recently LIG1 and LIG3 were both suggested to perform the ligation reactions required for successful class-switch recombination mouse B-cells (3, 4). These genetic experiments suggest LIG1 has end-joining capabilities; however, the biochemistry of LIG1-catalyzed end-joining has never been reported. To fill this void, we investigated the kinetics of LIG1 and LIG3 catalyzed

DSB ligation. The observation that LIG1 can ligate DSBs with similar efficiency as LIG3 under optimal conditions challenges the longstanding belief that LIG1 is poorly suited to catalyze end-joining reactions and supports the genetic studies that find comparable contributions of LIG1 and LIG3 to the end-joining behavior required for class-switch recombination. Although LIG1 may contribute to DSB repair, LIG3 is central to the relatively minor error-prone alternative end-joining pathway (5). Observations that LIG3 activity is required in cancer cells over expressing the enzyme, and the fact that the enzyme has erroneous ligation activity (6-10), make LIG3 an attractive pharmacological target for anti-cancer therapies (11). With this in mind, we developed a rapid and reliable method to monitor DNA ligation that is adaptable to high-throughput small-molecule screening of DNA ligase inhibitors.

Kinetic characterization of the nuclear LIG3 isoforms

The first goal of this thesis project was to determine the kinetics and thermodynamics of SSB ligation by LIG3α and LIG3β, and to compare these characteristics to those of the nuclear replicative DNA ligase, LIG1. The kinetic parameters of the LIG3 isoforms are nearly identical under all tested conditions, indicating that the BRCA1 C-terminal (BRCT) domain specific to LIG3α does not alter ligation kinetics in the absence of its interacting protein XRCC1. Although LIG3 is only 22% identical to LIG1 across their conserved domains (12), the two enzymes had very similar maximal ligation rates. Comparison of the rate and equilibrium constants for LIG3 and LIG1 nevertheless revealed important differences. The LIG3 isoforms were 7-fold more efficient than LIG1 at ligating nicked DNA under optimal conditions. The increased ligation efficiency attributed to LIG3 is due to decreased $K_{M,DNA}$ values, possibly explaining why LIG3 is less prone to abortive ligation than LIG1. Surprisingly, LIG3 binds Mg^{2+} 10-fold weaker than

LIG1. We suggest that Mg^{2+} availability may regulate DNA ligation *in vivo* because Mg^{2+} levels are higher in the mitochondria than in the nucleus (13). The similarities and differences between the LIG3 isoforms and LIG1 presented here provide the first direct biochemical comparison of the enzymes, enhancing our understanding of their unique and overlapping biological roles.

Role of the LIG3 N-terminus in single-strand break ligation

LIG3 is the only human DNA ligase to possess an N-terminal ZnF domain and the degree by which the ZnF domain contributes to catalysis is poorly understood. Numerous efforts have been made to establish mechanisms by which LIG3 utilizes the ZnF domain for nicked DNA binding affinity and DNA end-binding characteristics (14-19). Due to experimental design, these studies do not indicate the degree by which the ZnF domain contributes to the kinetics of nicked DNA ligation, nor do they invite the possibility that regions outside of the enzyme's structured domains (ZnF, DBD, NTase, OB-fold domains) may contribute to catalysis. Using LIG3β as a surrogate for both nuclear isozymes, we investigated the role of the LIG3β ZnF domain by performing a systematic kinetic analysis of numerous N-terminal variants using a nicked DNA substrate. Highly conserved residues localized to the putative DNA binding interface of the ZnF domain were identified via multiple sequence and structural alignments. These candidate residues were targeted for mutagenesis with the intention of disrupting the ZnF•DNA interaction. Truncation mutants were also generated to identify degree by which the ZnF domain and DLR contribute to LIG3 ligation efficiency. The resulting modifications had minimal effects on maximal ligation rates (k_{cat}), and steady-state requirements for ATP. However, Mg^{2+} affinities were strengthened by the disruption and removal of the ZnF domain. Removal of the ZnF reduced ligation efficiency ($k_{cat}/K_{M,DNA}$) by 3-fold. A similar 3-fold reduction was observed among the

enzymes containing point mutations along the ZnF•DNA binding interface, suggesting the point mutations drastically reduced the DNA binding affinity of the ZnF domain. Strikingly, removal of the DLR reduced LIG3 catalytic efficiency by an additional 3-fold, suggesting that this linker region contributes to DNA binding. This kinetic analysis indicates that the N-terminal region of LIG3, in its entirety, contributes to the ligation efficiency of nicked DNA substrates.

Kinetic analysis of LIG1 and LIG3 double-strand break ligation

LIG3 and LIG4 have long been accepted as the enzymes responsible for repairing DNA DSBs by rejoining the phosphodiester backbone (5). Recent genetic experiments in LIG4 deficient B cells have revealed surprising similarities when either LIG1 or LIG3 is deleted, suggesting LIG1 is capable of DSB ligation (3, 4). To follow up on these observations, we investigated the DSB repair activities of LIG1 and LIG3 using *in vitro* biochemical assays. We reported that LIG1 has robust end-joining efficiency on blunt-end and 3'-overhang breaks that approaches the efficiency of LIG3 under optimal conditions. Surprisingly, the activity of LIG1 is attenuated at physiological Mg^{2+} concentrations. LIG1 end-joining efficiency was enhanced by molecular crowding agent polyethylene glycol, a polymer commonly used to simulate the crowded environment of a cell. Interestingly, LIG3 has similar efficiencies on 3' or 5' overhang substrates whereas LIG1 has a strong preference for 3'-overhang substrates. Under all conditions tested, LIG3 shows greater affinity for DSB substrates than LIG1. Remarkably, LIG3 was capable of ligating both strands of a DSB in a single binding encounter and we report the first transient kinetic analysis for DSB ligation by a DNA ligase. Due to the weaker DNA binding affinity of LIG1, we observed significant abortive ligation that varies depending on polarity and sequence context of the cohesive

end. Taken together, these results redefine our understanding of the substrate specificity of human LIG1 and LIG3 and broaden our understanding of alternative end-joining.

A Real-Time DNA Ligase Assay Suitable for High Throughput Screening

The ATP-dependent mammalian DNA ligases catalyze the formation of a single phosphodiester bond between adjacent DNA molecules via a conserved three-step chemical mechanism. Historical approaches used to monitor DNA ligation activity to obtain kinetic parameters are not conducive to high-throughput screening of small-molecule libraries. We reported the development and validation of a robust real-time fluorescence-based ligation assay that is amendable to high-throughput screening of small-molecule libraries. To test the sensitivity and reliability of the assay, steady-state kinetic parameters of LIG1 and LIG3β were measured in parallel and report ATP and Mg^{2+} concentration dependences in close agreement to those previously reported (1, 2). The assay was also converted to a discontinuous format, facilitating the screening of chemical libraries to identify novel ligase inhibitors. During the writing of this thesis, I have had the opportunity to collaborate with the Newman laboratory to perform a high-throughput screen of >100,000 small-molecule compounds at the University of Michigan's Center for Chemical Genomics (CCG) at the Life Sciences Institute. Employment of the assay (with slight modifications) has reproducibly yielded Z' scores of at least 0.8.

Future directions

Characterization of the LIG3α•XRCC1 complex

LIG3α is constitutively bound to XRCC1 outside of the mitochondria (20), suggesting the interaction between the two proteins is essential for the enzyme's stability (21). Our current characterization of LIG3α in the absence of XRCC1 reflects on the essential mitochondrial activity of the protein, as XRCC1 is not localized to the mitochondria (2, 22, 23). We are perfectly poised to determine how the presence of XRCC1 influences LIG3 single- and double-strand break ligation parameters. Since XRCC1 is known to interact with numerous DNA repair proteins, including polymerase beta (Polβ) (24), we are interested in determining how LIG3α activity may be coupled to the activity of Polβ in an XRCC1 dependent manner. Investigating the protein-protein interactions relevant for the base excision repair pathway may reveal functional advantages to protein-protein interactions during DNA repair.

Mechanistic analysis of LIG1 and LIG3 catalyzed end-joining

An interesting area of research would entail the elucidation of the mechanism(s) by which LIG1 and LIG3 perform DSB ligation. The data presented in Chapter 4 provided new insights, but also leaves several key mechanistic questions unanswered. For example, is there a preferred order of substrate binding and to what extent do ligases stabilize a synapse between ends? In addition to better understanding the mechanism(s) by which the enzymes engage DNA ends to catalyze DSB ligation faithfully, it is of interest to investigate their fidelity during DSB ligation. The design of various DSB substrates that result on the formation of gaps and mismatches upon ligation is needed to understand similarities and differences in LIG1 and LIG3 catalyzed end-joining fidelity. A

recent study has claimed the presence of ribonucleotides at a DNA break increased the end-joining activity of LIG4 (25). It is unclear whether this observation is unique to the LIG4 dependent nonhomologous end-joining pathway or conserved among the human DNA ligases. Further investigation of the double-strand DNA break ligation characteristics of LIG1 and LIG3 will provide insight into the degree by which the enzymes participate in the alternative end-joining pathway. Although the alternative end-joining pathway repairs relatively few double-strand DNA breaks when compared to the LIG4-dependent nonhomologous pathway, the mechanisms by which DNA is repaired is poorly understood. Interestingly, cancers exhibiting deficiencies in the nonhomologous end-joining and/or homologous recombination pathways become increasingly dependent on the alternative end-joining pathways within the cell (5, 26). Understanding the capabilities of the enzymes required for alternative end-joining will be invaluable for characterizing and defining the various mechanisms that drive carcinogenesis.

Influence of the N-terminal ZnF domain on SSB and DSB ligation

As described in Chapter 4, chloride anions differentially influenced LIG1 and LIG3 catalytic efficiency in a concentration dependent manner. We established that an alternative salt anion (acetate) does not have the inhibitory effects of chloride, suggesting acetate is better suited for measuring enzyme activity under various salt concentrations. Our initial analysis of the LIG3 N-terminal variants was conducted in the presence of chloride anions (Chapter 3) to directly compare these proteins to the previously reported values of the LIG3 isoforms and LIG1 (Chapter 2) (1, 2). However, comparing SSB ligation characteristics of the LIG3 N-terminal variants to their respective DSB ligation characteristics (discussed below) will require that SSB ligation be

characterized in the absence of chloride. Complete datasets under both conditions will enable continuity in experimental conditions, minimizing the possibility of data misinterpretation.

It is currently believed that the N-terminal ZnF domain is essential for LIG3 catalyzed end-joining (14, 15, 19). Experiments investigating the contributions of these N-terminal regions on the kinetic parameters of DSB ligation are of interest for elucidating the mechanism by which LIG3 binds to and coordinates DNA ends prior to ligation. A complete kinetic analysis of the LIG3 N-terminal variants may shed light on the mechanism by which LIG3 performs the end-joining. Further mutagenesis and the generation of alternative LIG3 N-terminal truncation variants could be useful in identifying the mechanism by which the DLR is contributing to the catalytic efficiency of LIG3.

Utilization of metal cofactors by LIG3

Initial analysis of LIG1- and LIG3-catalyzed SSB and DSB ligation indicates that the two enzymes possess different Mg^{2+} cofactor binding affinities (Chapters 2 and 4). Expanding upon the observation of LIG3 possessing weaker magnesium affinity than LIG1 during SSB ligation invites the possibility that LIG3 may be more promiscuous in utilizing alternative activating metal cofactors than LIG1. In fact, preliminary experiments indicate LIG3 can catalyze multiple-turnover ligation while utilizing calcium as the activating metal cofactor, a capability not shared with LIG1. Furthermore, LIG3 possesses vastly different manganese concentration dependences than LIG1 for the adenylyl transfer and nick-sealing chemical steps of nicked DNA ligation. The increased promiscuity for metal cofactors and different metal binding profiles of LIG3 suggest the enzyme is an ideal candidate for metal mixing experiments that could help elucidate the stoichiometry and roles of the metal cofactors utilized during catalysis.

Identification and characterization of ligase specific inhibitors

Currently, the reported ligase inhibitors have poor chemical characteristics (reactive alkene moieties, low solubility and high IC50 values) (7, 27). Completion of a high-throughput small-molecule inhibitor screen by the University of Michigan's Center for Chemical Genomics at the Life Sciences Institute may lead to the identification of novel ligase inhibitors with better chemical characteristics. We initiated a high throughput screen of > 100,000 small-molecule compounds. After identifying compounds of interest, the inhibitors will need to be systematically evaluated to determine their IC50 values and modes of inhibition. Our interests in identifying LIG3-specific inhibitor are two-fold. Firstly, we would like to utilize ligase-specific inhibitors as tools to guide our understanding of their independent roles in the nucleus since the *LIG3* gene is not found in genetically tractable organisms. Secondly (but not less importantly), the identification of LIG3-specific inhibitors with promising pharmacological properties may establish a starting point for the development and treatment of cancer cells that are dependent on LIG3 activity for carcinogenesis (8).

References

1. Taylor MR, Conrad JA, Wahl D, & O'Brien PJ (2011) Kinetic Mechanism of Human DNA Ligase I Reveals Magnesium-dependent Changes in the Rate-limiting Step That Compromise Ligation Efficiency. *J. Biol. Chem.* 286(26):23054-23062.

2. McNally JR & O'Brien PJ (2017) Kinetic analyses of single-stranded break repair by human DNA ligase III isoforms reveal biochemical differences from DNA ligase I. *J. Biol. Chem.* 292(38):15870-15879.

3. Lu G, *et al.* (2016) Ligase I and ligase III mediate the DNA double-strand break ligation in alternative end-joining. *Proc. Natl. Acad. Sci. U. S. A.* 113(5):1256-1260.

4. Masani S, Han L, Meek K, & Yu K (2016) Redundant function of DNA ligase 1 and 3 in alternative end-joining during immunoglobulin class switch recombination. *Proc. Natl. Acad. Sci. U. S. A.* 113(5):1261-1266.

5. Sallmyr A & Tomkinson AE (2018) Repair of DNA double-strand breaks by mammalian alternative end-joining pathways. *J. Biol. Chem.* 293(27):10536-10546.

6. Sallmyr A, Tomkinson AE, & Rassool FV (2008) Up-regulation of WRN and DNA ligase IIIalpha in chronic myeloid leukemia: consequences for the repair of DNA double-strand breaks. *Blood* 112(4):1413-1423.

7. Chen X, *et al.* (2008) Rational design of human DNA ligase inhibitors that target cellular DNA replication and repair. *Cancer Res.* 68(9):3169-3177.

8. Newman EA, *et al.* (2015) Alternative NHEJ Pathway Components Are Therapeutic Targets in High-Risk Neuroblastoma. *Mol. Cancer Res.* 13(3):470-482.

9. Simsek D, *et al.* (2011) DNA Ligase III Promotes Alternative Nonhomologous End-Joining during Chromosomal Translocation Formation. *PLoS Genetics* 7(6).

10. Badie S, *et al.* (2015) BRCA1 and CtIP promote alternative non-homologous end-joining at uncapped telomeres. *EMBO J.* 34(6):828.

11. Tomkinson AE, Howes TR, & Wiest NE (2013) DNA ligases as therapeutic targets. *Transl Cancer Res* 2(3).

12. Simsek D & Jasin M (2011) DNA ligase III: A spotty presence in eukaryotes, but an essential function where tested. *Cell Cycle* 10(21):3636-3644.

13. Gout E, Rebeille F, Douce R, & Bligny R (2014) Interplay of Mg2+, ADP, and ATP in the cytosol and mitochondria: unravelling the role of Mg2+ in cell respiration. *Proc. Natl. Acad. Sci. U. S. A.* 111(43):E4560-4567.

14. Cotner-Gohara E, *et al.* (2010) Human DNA Ligase III Recognizes DNA Ends by Dynamic Switching between Two DNA-Bound States. *Biochemistry* 49(29):6165-6176.

15. Cotner-Gohara E, Kim I-K, Tomkinson AE, & Ellenberger T (2008) Two DNA-binding and Nick Recognition Modules in Human DNA Ligase III. *J. Biol. Chem.* 283(16):10764-10772.

16. Taylor RM, Whitehouse CJ, & Caldecott KW (2000) The DNA ligase III zinc finger stimulates binding to DNA secondary structure and promotes end joining. *Nucleic Acids Res.* 28(18):3558-3563.

17. Taylor RM, Whitehouse J, Caldecott KW, Cappelli E, & Frosina G (1998) Role of the DNA ligase III zinc finger in polynucleotide binding and ligation. *Nucleic Acids Res.* 26(21):4804-4810.

18. Caldecott KW, Aoufouchi S, Johnson P, & Shall S (1996) XRCC1 Polypeptide Interacts with DNA Polymerase β and Possibly Poly (ADP-Ribose) Polymerase, and DNA Ligase III Is a Novel Molecular 'Nick-Sensor' In Vitro. *Nucleic Acids Res.* 24(22):4387-4394.

19. Kukshal V, *et al.* (2015) Human DNA ligase III bridges two DNA ends to promote specific intermolecular DNA end joining. *Nucleic Acids Res.* 43(14):7021-7031.

20. Lakshmipathy U & Campbell C (2000) Mitochondrial DNA ligase III function is independent of Xrcc1. *Nucleic Acids Res.* 28(20):3880-3886.

21. Taylor RM, Moore DJ, Whitehouse J, Johnson P, & Caldecott KW (2000) A Cell Cycle-Specific Requirement for the XRCC1 BRCT II Domain during Mammalian DNA Strand Break Repair. *Mol. Cell. Biol.* 20(2):735-740.

22. Lakshmipathy U & Campbell C (2001) Antisense-mediated decrease in DNA ligase III expression results in reduced mitochondrial DNA integrity. *Nucleic Acids Res.* 29(3):668-676.

23. Lakshmipathy U & Campbell C (1999) The Human DNA Ligase III Gene Encodes Nuclear and Mitochondrial Proteins. *Mol. Cell. Biol.* 19(5):3869-3876.

24. Ellenberger T & Tomkinson AE (2008) Eukaryotic DNA Ligases: Structural and Functional Insights. *Annu. Rev. Biochem.* 77(1):313-338.

25. Pryor JM, *et al.* (2018) Ribonucleotide incorporation enables repair of chromosome breaks by nonhomologous end joining. *Science* 361(6407):1126-1129.

26. Pannunzio NR, Watanabe G, & Lieber MR (2018) Nonhomologous DNA end-joining for repair of DNA double-strand breaks. *J. Biol. Chem.* 293(27):10512-10523.

27. Howes TRL, *et al.* (2017) Structure-activity relationships among DNA ligase inhibitors: Characterization of a selective uncompetitive DNA ligase I inhibitor. *DNA Repair (Amst)* 60:29-39.